HAL open science

Modélisation de la compaction dynamique avec dérive des vitesses

Richard Saurel, Marie-Hélène Lallemand, Nicolas Favrie, Fabien Petitpas, Sergey Gavrilyuk

To cite this version:

Richard Saurel, Marie-Hélène Lallemand, Nicolas Favrie, Fabien Petitpas, Sergey Gavrilyuk. Modélisation de la compaction dynamique avec dérive des vitesses. [Research Report] RR-7347, INRIA. 2010, pp.73. inria-00505292

HAL Id: inria-00505292

https://inria.hal.science/inria-00505292v1

Submitted on 23 Jul 2010

HAL is a multi-disciplinary open access archive for the deposit and dissemination of scientific research documents, whether they are published or not. The documents may come from teaching and research institutions in France or abroad, or from public or private research centers.

L'archive ouverte pluridisciplinaire **HAL**, est destinée au dépôt et à la diffusion de documents scientifiques de niveau recherche, publiés ou non, émanant des établissements d'enseignement et de recherche français ou étrangers, des laboratoires publics ou privés.

INSTITUT NATIONAL DE RECHERCHE EN INFORMATIQUE ET EN AUTOMATIQUE

Modélisation de la compaction dynamique avec dérive des vitesses

Richard Saurel — Marie-Hélène Lallemand — Nicolas Favrie — Fabien Petitpas — Sergey Gavrilyuk

N° 7347

July 2010

Thème NUM

Rapport de recherche

ISSN 0249-6399

Modélisation de la compaction dynamique avec dérive des vitesses

Richard Saurel * † ‡, Marie-Hélène Lallemand* , Nicolas Favrie*, Fabien Petitpas * , Sergey Gavrilyuk *

Thème NUM — Systèmes numériques
Projet Smash

Rapport de recherche n° 7347 — July 2010 — 73 pages

Résumé : Dans ce rapport, on présente un modèle hyperbolique d'écoulement multiphasique incluant la compaction dynamique irréversible de poudres. Ce modèle doit être capable de remplir quatre principaux objectifs. Le premier objectif concerne le caractère irréversible de la compaction des poudres. Quand un lit de poudres est soumis à un cycle de charge-décharge, le volume final est plus petit que le volume initial. Afin de traiter ce problème d'hystérésie, on construit un modèle avec relaxation. Durant la phase de charge, on suppose que l'équilibre mécanique a lieu, ce qui correspond à une relaxation instantanée des pressions. Dans la phase de décharge, on suppose au contraire qu'une transformation mécanique a lieu, conduisant à un état mécanique hors équilibre. Par conséquent, durant chacun de ces cycles, les vitesses du son des modèles limites sont très différentes. Ces différences dans les propriétes acoustiques sont la cause justement du caractère irréversible du processus de compaction. Le second objectif est relié aux effets dynamiques, là où la pression et les ondes de chocs jouent un rôle important. La dynamique des ondes est assurée par l'hyperbolicité du modèle et l'on tient compte aussi bien de la compressibilité des phases que des énergies de configuration. Le troisième objectif concerne les effets multidimensionnels aux interfaces matérielles. En effet, la plupart des processus de compaction font intervenir des *surfaces libres*. Par conséquent, le modèle doit être capable de traiter de problèmes d'interfaces entre des fluides purs et des mélanges granulaires. Enfin, le quatrième objectif concerne la perméation des gaz qui peut jouer un rôle important dans certains cas spécifiques de compaction de poudres. Se pose alors la question délicate de description de ces vitesses multiples.
Ces quatre points sont considérés dans un modèle unique appartenant à la classe des modèles des interfaces diffuses. La capacité du modèle a traiter ces phénomènes est validée dans des situations où chaque effet est considéré séparément. En particulier, le caractère irréversible de la compaction est considéré et validé sur plusieurs exemples : expérience sur un matériel énergétique (HMX granulaire), compaction granulaire de NaCl. À part les équations d'état des matériaux (pressions granulaires et hydrodynamiques, et les énergies associées), le modèle est de plus exempt de paramètre ajustable. On reproduit enfin les effets de perméation des gaz à l'aide d'un modèle de dérive des vitesses, et une analyse sur la production d'entropie. Le modèle résultant est validé sur un cas test de tube à choc où une onde de choc traverse un lit granulaire de forte densité et montre un accord parfait avec l'expérience.

∗ E.P.I. SMASH – Polytech'Marseille/IUSTI – 5 rue E. Fermi – 13 453 Marseille Cédex 13
† University Institute of France, same address
‡ Richard.Saurel@polytech.univ-mrs.fr

Mots-clés : Interfaces solides, compaction de poudres, écoulements compressibles multiphasiques, analyse asymptotique, équations hyperboliques, équation d'état

Dynamic Powder Compaction Model with Velocity Drift Effects

Abstract: A multiphase hyperbolic model for dynamic and irreversible powder compaction is built. Four important points have to be addressed in this aim. The first one is related to the irreversible character of powder compaction. When a granular media is subjected to a loading-unloading cycle the final volume is lower than the initial one. To deal with this hysteresis phenomenon a multiphase model with relaxation is built. During loading, mechanical equilibrium is assumed corresponding to stiff mechanical relaxation, while during unloading non-equilibrium mechanical transformation is assumed. Consequently, the sound speeds of the limit models are very different during loading and unloading. These differences in acoustic properties are responsible for irreversibility in the compaction process. The second point is related to dynamic effects where pressure and shock waves play an important role. Wave dynamics is guaranteed by the hyperbolic character of the equations. Phase compressibility well as configuration energy are taken into account. The third point is related to multidimensional situations that involve material interfaces. Indeed, most processes with powder compaction entail *free surfaces*. Consequently the model has to be able to solve interfaces separating pure fluids and granular mixtures. Finally, the fourth point is related to gas permeation that may play important role in some specific powder compaction situations. This poses the difficult question of multiple velocities description. These four points are considered in a unique model fitting the frame of multiphase theory of diffuse interfaces. The ability of the model to deal with these various effects is validated on basic situations, where each phenomenon is considered separately. Special attention is paid to the validation of the hysteresis phenomenon that occurs during powder compaction. Basic experiments on energetic material (granular HMX) and granular NaCl compaction are considered and are perfectly reproduced by the model. Except for the material equations of state (hydrodynamic and granular pressures and energies) that are determined on the basis of separate experiments found in the literature, the model is free of adjustable parameter. Gas permeation effects are then restored in the two-phase flow model on the basis of velocity drift and entropy production analysis. It is validated against shock tube experiments involving shock interaction with dense granular bed, showing excellent agreement.

Key-words: Material interfaces, powder compaction, compressible multiphase flows, asymptotic analysis, hyperbolic equations, equation of state

1 Introduction

When a granular bed is subjected to mechanical loading, local deformations occur resulting in rearranged deformed grains that form a compact porous solid. Such a process is irreversible. As a matter of fact, if the loading stress is removed, the porous solid slightly expands but never turns back to its initial volume. The main difficulty in modelling such effect relies on its irreversible character. The literature on powder compaction provides at least three types of models :

– the first class is connected to quasi-static plasticity modelling in solids ([9, 23, 2, 20]). This approach usually considers powder mixture compressibility but neglects solid phase one. This restricts these models to weak compression waves, excluding strong shocks.
– The second one considers granular media at the discrete level where a large number of particles is simulated by considering contact forces between them ([21]).
– The third one deals with multiphase flow modelling of granular media ([3, 31, 4, 15, 5, 22]).

In the present work, irreversible compaction of powders is addressed in the context of multiphase flow theory of granular materials. There are some advantages with this approach. First, large scale experiments and engineering applications are easier to address with a continuous model of heterogeneous media. Second, wave dynamics is of fundamental importance in many applications dealing with shocks and explosions. Some success has been reached in this area with Baer and Nunziato ([3]) type model, except for the two following issues :

1. First, this type of model is unable to predict compacted powder zones after loading-unloading cycles that may occur, for example, after compression and expansion of a given granular sample. Progress in this direction has been done by Gonthier ([10, 11]).
2. Second, the original formulation is unable to solve interface problems, or material interfaces such as those separating a fluid and a granular mixture. Methods to solve interface conditions in the context of compressible fluids governed by different equations of state have been built during the last two decades with the pioneer works of Karni (1994) [16], and Abgrall (1996) [1]. Multiphase flow models have been used in this aim [31] in order to solve interface conditions with correct thermodynamics at interfaces, but in the context of fluid–fluid interfaces only.

The aim of the present work is to build a multiphase flow model able to deal with irreversible compaction and to solve interfaces separating fluids and granular mixtures, in the presence of pressure waves.

To do so, we first build a mechanical equilibrium model, with a single velocity and a single stress. For that purpose, we assume that the energy of the system is the sum of the hydrodynamic energy plus a configuration (or granular) energy that depends on other variables, such as volume fractions, particle radius, specific volumes and entropies. The concept of configuration pressure, or granular pressure, is introduced in particular in Passman et al. (1984) [24]. We then ask the flow model to respect conservation of mass, mixture momentum, mixture energy and to be adiabatic. From these constraints, the pressure definition that appears in the momentum equation is obtained, as well as the mechanical equilibrium condition. This analysis is carried out in section 2. However, this mechanical equilibrium model, already presented by Kapila et al. (2001) [15] is reversible. It is therefore unable to predict the hysteresis phenomenon such as compaction. In order to model irreversibility

the following phenomenon is observed : consider a loading–unloading cycle as depicted in figure 1.1 in the plane (stress : P)–(mixture specific volume : $\nu = 1/\rho$).

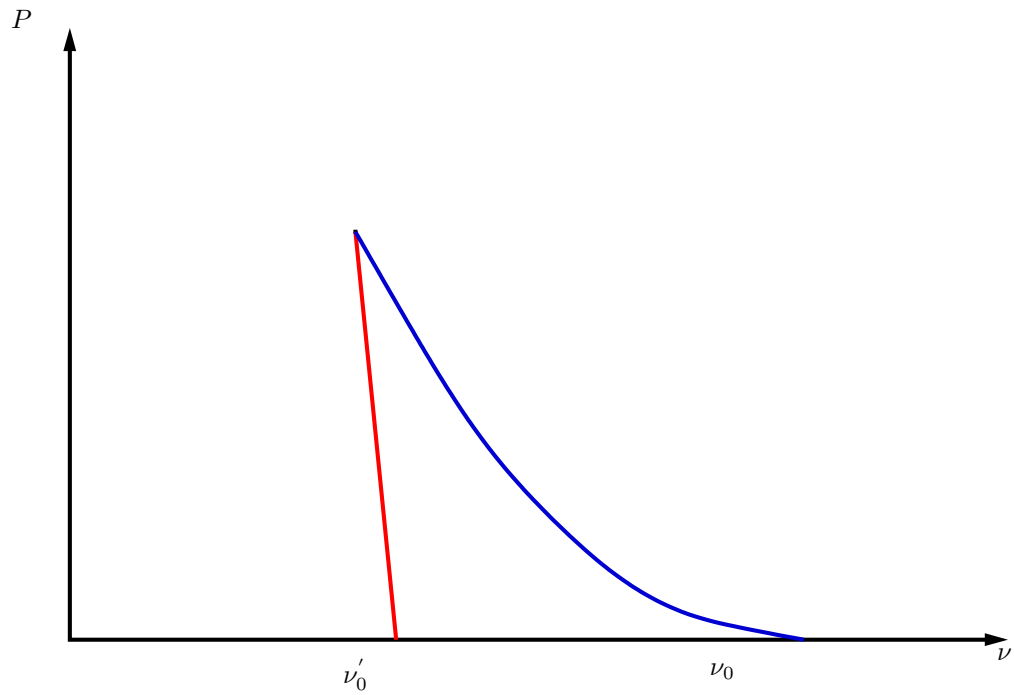

FIG. 1.1: *Schematic representation of a loading–unloading cycle for a powder sample, in the plane P–ν*

During the compression stage, the mixture specific volume decreases and reaches its minimum value for the applied stress. During unloading, the pressure variation is stiff for a small specific volume variation. It means hat the mixture sound speed

$$c^2 = -\nu^2 \left.\frac{\partial P}{\partial \nu}\right|_s ,$$

in the compression stage is much lower than the one involved in the expansion stage. Based on this observation we are going to build a non-equilibrium model that possesses two limit sound speeds :

- an *equilibrium* sound speed that will be the one of the mechanical equilibrium model. This sound speed will be the lowest one and will show up during the compression stage;
- a *frozen* sound speed, larger than the preceding one that will show up during the expansion stage.

The general model will be thus a non-equilibrium model with relaxation. The relaxation term expresses the degree of local stress disequilibrium. When the relaxation time tends to infinity, the

frozen sound speed is recovered and used during the expansion stage, while when the relaxation time tends to zero, the asymptotic limit of the non-equilibrium model corresponds to the mechanical equilibrium one. This model, with low sound speed, will be used during compression. Then the non-equilibrium model couples two limit models : with frozen sound speed on the one hand and equilibrium sound speed on the other hand, by using a unique formulation. The switch from one limit model to the other one is achieved by means of the relaxation parameter. Before examining the details of this relaxation *switch*, the non-equilibrium model with relaxation is studied in section 3. Thermodynamic closure of both models is addressed in section 4, where thermodynamic equations of state (EOS) are presented, as well as a new granular EOS. To solve the flow model, a numerical method is needed. The system consists in a non-conservative hyperbolic set of equations with relaxation. A similar system has been studied in the context of fluid mixtures by Saurel et al. (2009) [34]. Extension of this method to the granular flow model is detailed in section 5. Validations are then addressed in section 6. The ability of the model to propagate compression and expansion waves is demonstrated, as well as its capabilities to capture fluid-granular mixture interfaces. Comparisons with several experiments are done, in particular regarding successive hysteresis-type loading-unloading cycles. In section 7, discussion about the relaxation parameter switch is given on the basis of basic plasticity theory arguments, combined with an analysis of the various non-equilibrium stages that occur during the compaction process. That discussion intends to justify that switch. We show, in particular, that the model is free of parameters. In section 8, the flow model is extended to gas permeation effects. A Darcy type law, obtained from the asymptotic analysis of the Baer and Nunziato (1986) [3] model in the limit of stiff mechanical relaxation is obtained, following Guillard and Duval (2007) [12]. Corresponding drift effects are thus restored in the Kapila et al. (2001) [15] mechanical equilibrium model in a thermodynamically consistent manner, based on entropy production analysis (Saurel et al., 2008 [33]). Consistency is also achieved with respect to the parent model from which this reduced model is derived. The corresponding velocity non-equilibrium model is validated against shock tube experiments, involving shock interaction with dense granular beds, showing excellent agreement in section 9. Conclusions are given in section 10.

2 Mechanical equilibrium model

A granular medium is different from a fluid mixture by several aspects, one of them being the presence of intergranular contacts. Due to grain contacts, the medium presents resistance to compression related to efforts that exert in the grains around each contact point. At the macroscopic scale, these efforts can be summarized with an additional equation of state that expresses the compression resistance, with the help of a *granular pressure* or *configuration pressure*. The configuration energy associated with that configuration pressure can be derived. It can be understood as the energy stored in elasto-plastic layers around each contact point. *Granular pressure* as a function of solid volume fraction can be determined easily by experimental means. An excellent description of experimental facility and corresponding measurements are given in Kuo et al. (1980) [18].

There are some advantages with this thermodynamic approach based on *configuration* pressure and energy. The effects occurring at grain scale, such as rearrangements and plastic deformations are summarized in simple functions, linking macroscopic variables. Therefore the difficulty of solving

complex multidimensional effects at grain scale is replaced by the experimental determination of *granular* EOS parameters.

The aim of this section is to develop a flow model involving these physical effects specific to granular media. The model building method consists in taking the total system energy as a function of the various problem variables and to obtain :

– the mechanical equilibrium condition,

– the form of the pressure term that exerts in the momentum equation.

The mechanical equilibrium condition is then differentiated along a particle trajectory and therefore provides the volume fraction evolution equation that closes the system of classical balance equations : mass conservation for each phase, momentum and energy conservation for the mixture, entropy conservation for each phase and conservation of the number of particles per unit volume.

Let us assume that the total energy of the system is the sum of the classical thermodynamic internal energy e, augmented by the configuration (or granular) energy B plus the kinetic energy :

$$E = \mathcal{E} + \frac{1}{2}\, u^2 \ , \tag{2.1}$$

with

$$\mathcal{E} = e + B \ , \tag{2.2}$$

and

$$e = \sum_k Y_k\, e_k \ , \quad B = \sum_k Y_k\, B_k \ . \tag{2.3}$$

Here, for example, $k = 1$ stands for the solid phase and $k = 2$ corresponds to the gas phase; so, in that case $B_2 = 0$. However, we keep that general formulation as it is more convenient to get symmetrized relations in what follows.

The internal energy $e_k = e_k(\nu_k,s_k)$ of phase k depends on the specific volume ν_k and the specific entropy s_k. The configuration energy B_k associated with the solid deformed layers around each grain surface is assumed to be a function of five variables : $B_k = B_k(\alpha_k,R_k,\nu_k,s_k,Y_k)$ where

– α_k is the volume fraction of phase k, the dependence on which is obvious, since it is well known the energy to transfer into a granular bed is a function of the volume fraction at the end of the compaction process;

– R_k is the particle radius of the grains. Dependence on that variable cannot be excluded a priori;

– the thermodynamic pair of variables (ν_k,s_k) may also influence the value of B_k;

– $Y_k = (\alpha\rho)_k/\rho$ is the mass fraction, $\rho_k = 1/\nu_k$ is the density and $\rho = \sum_k \alpha_k\, \rho_k$ is the mixture density.

It is more convenient for the calculations to replace the dependence on R_k by the dependence on the number of particles per unit mass n_k, defined by $n_k = N_k/\rho$, where N_k is the number of particles per unit volume. The particle radius R_k, considered as spherical for simplicity, is linked to the preceding variables by the relation :

$$\nu_k\, Y_k = \frac{4}{3}\, \pi\, R_k^3\, n_k \ . \tag{2.4}$$

Define $\dfrac{\mathrm{D}}{\mathrm{D}t} = \dfrac{\partial}{\partial t} + u\,\dfrac{\partial}{\partial x}$, then the classical balance laws are given hereafter :

$$\frac{\partial \rho}{\partial t} + \frac{\partial (\rho\, u)}{\partial x} = 0\,, \qquad \text{mixture mass conservation}\,, \tag{2.5}$$

$$\frac{\mathrm{D}Y_k}{\mathrm{D}t} = 0\,, \qquad \text{mass conservation for phase } k\,, \tag{2.6}$$

$$\frac{\mathrm{D}s_k}{\mathrm{D}t} = 0\,, \qquad \text{entropy conservation for phase } k\,, \tag{2.7}$$

$$\frac{\partial (\rho\, u)}{\partial t} + \frac{\partial (\rho\, u^2 + P)}{\partial x} = 0\,, \qquad \text{mixture momentum conservation}\,, \tag{2.8}$$

$$\frac{\partial (\rho\, E)}{\partial t} + \frac{\partial}{\partial x}\left[(\rho\, E + P)\; u\right] = 0\,, \qquad \text{mixture total energy conservation}\,. \tag{2.9}$$

In the absence of both coalescence and fracture, we may write

$$\frac{\partial N_k}{\partial t} + \frac{\partial (N_k\, u)}{\partial x} = 0\,,$$

and therefore get

$$\frac{\mathrm{D}n_k}{\mathrm{D}t} = 0\,. \tag{2.10}$$

2.1 Definitions of P and configuration pressures and energies

In equation (2.8), the mixture pressure P is an unknown function which needs to be defined. Note that the phase entropies are assumed to be constant along their trajectory, therefore the transformations (loding–unloading) are considered as reversible with this model. The irreversible feature of the compaction process will be addressed later on with the non-equilibrium model.

By combining the momentum and total energy equations, we get the following mixture total internal energy equation

$$\frac{\mathrm{D}\mathcal{E}}{\mathrm{D}t} + P\,\frac{\mathrm{D}\nu}{\mathrm{D}t} = 0\,, \tag{2.11}$$

with $\mathcal{E} = e + B$ and $\nu = 1/\rho$. Using relations (2.5)–(2.10), and definitions of both e and B, we get

$$\frac{\mathrm{D}\mathcal{E}}{\mathrm{D}t} = \sum_k Y_k \left[\left.\frac{\partial e_k}{\partial \nu_k}\right|_{s_k} \frac{\mathrm{D}\nu_k}{\mathrm{D}t} + \left.\frac{\partial B_k}{\partial \alpha_k}\right|_{n_k,\nu_k,s_k,Y_k} \frac{\mathrm{D}\alpha_k}{\mathrm{D}t} + \left.\frac{\partial B_k}{\partial \nu_k}\right|_{\alpha_k,n_k,s_k,Y_k} \frac{\mathrm{D}\nu_k}{\mathrm{D}t} \right]\,. \tag{2.12}$$

In order to enlight the notations, we will simply denote by $\dfrac{\partial B}{\partial \xi_k}$ for all $\xi_k \in \{\alpha_k, n_k, \nu_k, s_k, Y_k\}$ to define the partial derivative of B_k w.r.t. ξ_k, where all variables but ξ_k from which B_k depends on are

set constant. Since the thermodynamic pressure P_k is defined by

$$P_k = -\left.\frac{\partial e_k}{\partial \nu_k}\right|_{s_k} ,$$

and the specific volume of phase k may be expressed as

$$\nu_k = \frac{\alpha_k}{Y_k}\,\nu ,$$

then, using (2.6) we have

$$\frac{\mathrm{D}\nu_k}{\mathrm{D}t} = \frac{\alpha_k}{Y_k}\frac{\mathrm{D}\nu}{\mathrm{D}t} + \frac{\nu}{Y_k}\frac{\mathrm{D}\alpha_k}{\mathrm{D}t} ,$$

and (2.12) can therefore be rewritten by

$$\frac{\mathrm{D}\mathcal{E}}{\mathrm{D}t} + \left[\sum_k \alpha_k \left(P_k - \frac{\partial B_k}{\partial \nu_k}\right)\right]\frac{\mathrm{D}\nu}{\mathrm{D}t} = -\nu\left[\sum_k \left(P_k - \alpha_k\,\rho_k\,\frac{\partial B_k}{\partial \alpha_k} - \frac{\partial B_k}{\partial \nu_k}\right)\frac{\mathrm{D}\alpha_k}{\mathrm{D}t}\right] . \quad (2.13)$$

Now, for (2.11) and (2.13) to be in accordance to each other, it is sufficient to set :

$$P = \sum_k \alpha_k \left(P_k - \frac{\partial B_k}{\partial \nu_k}\right) , \quad (2.14)$$

and

$$P_k - \alpha_k\,\rho_k\,\frac{\partial B_k}{\partial \alpha_k} - \frac{\partial B_k}{\partial \nu_k} = P_j - \alpha_j\,\rho_j\,\frac{\partial B_j}{\partial \alpha_j} - \frac{\partial B_j}{\partial \nu_j} , \forall\, k\,,\, j\,,\, k \neq j\ . \quad (2.15)$$

Equation (2.14) corresponds to the thermodynamic mixture pressure definition, while equation (2.15) represents the mechanical equilibrium condition. These two definitions are consecutive to the choice of the system energy definition subjected to the constraints (2.5)–(2.10).

Dependence on the phase compressibility is usually neglected during the compaction process. As a matter of fact, at moderate loading, each particle volume can be considered unchanged. When loading intensity increases, the bed porosity conversely decreases and the compressible effects become gradually important, typically for pressures greater than 100 MPa. It is therefore commonly assumed that

$$\frac{\partial B_k}{\partial \nu_k} = 0\ .$$

All these facts thus lead to the only dependence of B_k on α_k and consequently, the mechanical equilibrium condition reduces to

$$P_k - \alpha_k\,\rho_k\frac{\mathrm{d}B_k}{\mathrm{d}\alpha_k} = P_j - \alpha_j\,\rho_j\frac{\mathrm{d}B_j}{\mathrm{d}\alpha_j} , k \neq j\ . \quad (2.16)$$

We are now able to define the *granular* pressure, denoted by β_k by setting

$$\beta_k = \alpha_k\,\rho_k\,\frac{\mathrm{d}B_k}{\mathrm{d}\alpha_k}\ . \quad (2.17)$$

From this definition, we may deduce the configuration energy B_k :

$$B_k = \int_{\alpha_k^0}^{\alpha_k} \frac{\beta_k}{\alpha \rho_k} \, \mathrm{d}\alpha \ , \tag{2.18}$$

where α_k^0 is the initial value of α_k, the value from which compaction energy starts to be effective. Denote $\pi_k \stackrel{\text{def}}{=} P_k - \beta_k$, and the common value equilibrium pressure by Π, then the equilibrium condition (2.16) becomes

$$\pi_k = \pi_j = \Pi \ , \forall \, k \, , j \ , \quad k \neq j \ ; \tag{2.19}$$

and with $\beta \stackrel{\text{def}}{=} \sum_k (\alpha_k \beta_k)$ standing for the *mixture compaction pressure*, the thermodynamic mixture pressure P is given by :

$$P = \Pi + \beta = \sum_k \alpha_k \, P_k \ . \tag{2.20}$$

The granular pressure (2.17) expressed as a function of the volume fraction α_k can be determined quite easily by experimental means (see Kuo et al. (1980) [18], Elban and Chiarito (1986) [7]). It is then necessary to find a fitting curve. Example of such a fitting function is given in Bdzil et al. (1999) [4] :

$$\beta_s = -\tau \, (\alpha_s - \alpha_s^0) \, \frac{\log(1-\alpha_s)}{1-\alpha_s} \ ,$$

where the subscript s stands for the solid granular material, and α_s^0 and τ are two given positive constant numbers.

In section 4, we will adddress another option offering better properties regarding both granular energy and granular sound speed. At this point, we assume that such a granular equation of state is given.

2.2 Volume fraction equation

In order to determine the volume fraction evolution equation, the mechanical equilibrium condition ($k \neq j$) :

$$P_k(\rho_k, s_k) - \beta_k(\alpha_k, \rho_k) = P_j(\rho_j, s_j) - \beta_j(\alpha_j, \rho_j) \ ,$$

is differentiated along a trajectory, giving :

$$\begin{aligned} c_k^2 \, \frac{\mathrm{D}\rho_k}{\mathrm{D}t} + \rho_k \, \Gamma_k \, T_k \, \frac{\mathrm{D}s_k}{\mathrm{D}t} - \frac{\beta_k}{\rho_k} \, \frac{\mathrm{D}\rho_k}{\mathrm{D}t} - \left(\frac{\beta_k}{\alpha_k} + \alpha_k \, \rho_k \, \frac{\mathrm{d}^2 B_k}{\mathrm{d}{\alpha_k}^2} \right) \, \frac{\mathrm{D}\alpha_k}{\mathrm{D}t} = \\ c_j^2 \, \frac{\mathrm{D}\rho_j}{\mathrm{D}t} + \rho_j \, \Gamma_j \, T_j \, \frac{\mathrm{D}s_j}{\mathrm{D}t} - \frac{\beta_j}{\rho_j} \, \frac{\mathrm{D}\rho_j}{\mathrm{D}t} - \left(\frac{\beta_j}{\alpha_j} + \alpha_j \, \rho_j \, \frac{\mathrm{d}^2 B_j}{\mathrm{d}{\alpha_j}^2} \right) \, \frac{\mathrm{D}\alpha_j}{\mathrm{D}t} \ . \end{aligned}$$

From (2.7) and the mass evolution equations, the relation written above reduces to

$$\begin{aligned} \left(\frac{\rho_k \, c_k^2}{\alpha_k} + \alpha_k \, \rho_k \, \frac{\mathrm{d}^2 B_k}{\mathrm{d}{\alpha_k}^2} \right) \, \frac{\mathrm{D}\alpha_k}{\mathrm{D}t} + \left(\rho_k \, c_k^2 - \beta_k \right) \, \frac{\partial u}{\partial x} = \\ \left(\frac{\rho_j \, c_j^2}{\alpha_j} + \alpha_j \, \rho_j \, \frac{\mathrm{d}^2 B_j}{\mathrm{d}{\alpha_j}^2} \right) \, \frac{\mathrm{D}\alpha_j}{\mathrm{D}t} + \left(\rho_j \, c_j^2 - \beta_j \right) \, \frac{\partial u}{\partial x} \ . \end{aligned} \tag{2.21}$$

As the saturation constraints may be read as

$$\sum_k \frac{\mathrm{D}\alpha_k}{\mathrm{D}t} = 0 \,, \tag{2.22}$$

resolution of (2.22)–(2.21) results in the following expressions defining the evolution equations of the volume fractions α_k :

$$\frac{\mathrm{D}\alpha_k}{\mathrm{D}t} = -\frac{\alpha_k}{\rho_k\,\mathcal{C}_k^2}\left((\rho_k\,c_k^2-\beta_k)-\rho\,\mathcal{C}^2\sum_l\frac{\alpha_l}{\rho_l\,\mathcal{C}_l^2}\,(\rho_l\,c_l^2-\beta_l)\right)\frac{\partial u}{\partial x} \,, \tag{2.23}$$

with

$$\mathcal{C}_k^2 = c_k^2 + \alpha_k^2\,\frac{\mathrm{d}^2 B_k}{\mathrm{d}{\alpha_k}^2} \,, \tag{2.24}$$

and

$$\frac{1}{\rho\,\mathcal{C}^2} = \sum_l \frac{\alpha_l}{\rho_l\,\mathcal{C}_l^2} \,. \tag{2.25}$$

2.3 Equilibrium model summary

The mechanical equilibrium model can thus be expressed by the following system of equations $(k = 1\,,2)$:

$$\begin{aligned}
&\frac{\mathrm{D}\alpha_k}{\mathrm{D}t} = -\frac{\alpha_k}{\rho_k\,\mathcal{C}_k^2}\left((\rho_k\,c_k^2-\beta_k)-\rho\,\mathcal{C}^2\sum_l\frac{\alpha_l}{\rho_l\,\mathcal{C}_l^2}\,(\rho_l\,c_l^2-\beta_l)\right)\frac{\partial u}{\partial x} \,,\\
&\frac{\partial(\alpha_k\,\rho_k)}{\partial t}+\frac{\partial(\alpha_k\,\rho_k\,u)}{\partial x} = 0 \,,\\
&\frac{\partial(\rho\,u)}{\partial t}+\frac{\partial(\rho\,u^2+P)}{\partial x} = 0 \,,\\
&\frac{\partial(\rho\,E)}{\partial t}+\frac{\partial\left[(\rho\,E+P)\,u\right]}{\partial x} = 0 \,;
\end{aligned} \tag{2.26}$$

with the *granular pressure* β_k defined by (2.17), the mechanical equilibrium condition (2.19) and the mixture pressure P defined by (2.20). The mixture total energy is defined by

$$E = \mathcal{E} + \frac{1}{2}\,u^2 \,,\, \mathcal{E} = e + B = \sum_k Y_k\,\mathcal{E}_k \,,\, \mathcal{E}_k = e_k + B_k \,,$$

and definitions of $\mathcal{C}_k^2$ (resp. $\mathcal{C}^2$) as given by (2.24) (resp. by (2.25)).

2.4 Acoustic properties

We now focus our attention on the acoustic wave propagation in such material mechanical equilibrium mixtures. This is also an important point regarding the hyperbolic properties of the governing equations. In order to determine the wave propagation speed, let us write down the mixture pressure evolution equation :

$$\begin{aligned}\frac{\mathrm{D}P}{\mathrm{D}t} &= \frac{\mathrm{D}P_k}{\mathrm{D}t} - \frac{\mathrm{D}\beta_k}{\mathrm{D}t} + \sum_j \left(\beta_j \frac{\mathrm{D}\alpha_j}{\mathrm{D}t} + \alpha_j \frac{\mathrm{D}\beta_j}{\mathrm{D}t}\right) \\ &= c_k^2 \frac{\mathrm{D}\rho_k}{\mathrm{D}t} - \frac{\beta_k}{\rho_k}\frac{\mathrm{D}\rho_k}{\mathrm{D}t} - \left(\frac{\beta_k}{\alpha_k} + \alpha_k\,\rho_k\,\frac{\mathrm{d}^2 B_k}{\mathrm{d}{\alpha_k}^2}\right)\frac{\mathrm{D}\alpha_k}{\mathrm{D}t} \\ &\quad + \sum_j \left[\beta_j \frac{\mathrm{D}\alpha_j}{\mathrm{D}t} + \alpha_j \left(\frac{\beta_j}{\rho_j}\frac{\mathrm{D}\rho_j}{\mathrm{D}t} + \left(\frac{\beta_j}{\alpha_j} + \alpha_j\,\rho_j\,\frac{\mathrm{d}^2 B_j}{\mathrm{d}{\alpha_j}^2}\right)\frac{\mathrm{D}\alpha_j}{\mathrm{D}t}\right)\right] .\end{aligned}$$

Using now the mass equation and the volume fraction equation (2.23), we get

$$\frac{\mathrm{D}P}{\mathrm{D}t} + \left[\rho\,\mathcal{C}^2 \left(\sum_j \frac{\alpha_j}{\rho_j\,\mathcal{C}_j^2}\,\left(\rho_j\,c_j^2 - \beta_j\right)\right)^2 - \sum_j \left(\frac{\alpha_j\,\left(\rho_j\,c_j^2 - \beta_j\right)^2}{\rho_j\,\mathcal{C}_j^2} - \alpha_j\,\rho_j\,c_j^2\right)\right]\frac{\partial u}{\partial x} = 0 .$$

The sound speed square

$$\mathcal{C}_W{}^2 = \mathcal{C}^2 \left(\sum_j \frac{\alpha_j}{\rho_j\,\mathcal{C}_j^2}\,\left(\rho_j\,c_j^2 - \beta_j\right)\right)^2 - \frac{1}{\rho}\sum_j \left(\frac{\alpha_j\,\left(\rho_j\,c_j^2 - \beta_j\right)^2}{\rho_j\,\mathcal{C}_j^2} - \alpha_j\,\rho_j\,c_j^2\right) , \tag{2.27}$$

corresponds to the equilibrium sound speed square in the granular medium. In the absence of granular pressure ($\beta_j = 0$), (2.27) corresponds to the definition of the well known non-monotonic Wood sound speed [36]. System (2.26) is therefore hyperbolic with characteristic speeds u, $u + \mathcal{C}_W$, $u - \mathcal{C}_W$.

2.5 Thermodynamic closure

Using both the pure phase equations of state, the mixture energy and pressure definitions together with the mechanical equilibrium conditions, there is no difficulty to determine the mixture equation of state.

For sake of simplicity, we give what this mixture equation of state is, when all compressible materials are assumed to be governed by the stiffened gas equation of state (EOS). This EOS is quite accurate for description of gases, liquids and solids at high pressures. This method of defining the mixture EOS is not restricted to this particular example. Mie Grüneisen or any other convex EOS can be considered as well.

With the stiffened gas EOS, the energy, pressure and density are linked by the following relation

$$\rho_k\,e_k = \frac{P_k + \gamma_k\,P_{k,\infty}}{\gamma_k - 1} , \tag{2.28}$$

where γ_k and $P_{k,\infty}$ are positive constants, usually determined by using the reference curves of the materials. Hugoniot curves are usually used, but saturation curves may be used for special purposes (see [19]). Returning now to our example, the mixture total internal energy reads as ($\mathcal{E} = e + B$, $\mathcal{E}_k = e_k + B_k$)

$$\rho\,\mathcal{E} = \sum_k \alpha_k\,\rho_k\,\mathcal{E}_k\ . \tag{2.29}$$

Using (2.28) in (2.29), we get

$$\rho\,\mathcal{E} - \sum_k \frac{\alpha_k\,\gamma_k\,P_{k,\infty}}{\gamma_k - 1} - \sum_k \alpha_k\,\rho_k\,B_k = \sum_k \frac{\alpha_k\,P_k}{\gamma_k - 1}\ . \tag{2.30}$$

With the mixture pressure definition (2.20) and the mechanical equilibrium condition (2.19), we may thus write

$$P = \pi_k + \beta = P_k - \beta_k + \sum_j \alpha_j\,\beta_j\ .$$

Inserting the above relation in (2.30), we get

$$\rho\,e - \sum_k \frac{\alpha_k\,\gamma_k\,P_{k,\infty}}{\gamma_k - 1} = (P - \beta)\left(\sum_k \frac{\alpha_k}{\gamma_k - 1}\right) + \sum_k \frac{\alpha_k\,\beta_k}{\gamma_k - 1}\ ,$$

and the mixture equation of state reads as

$$\begin{aligned} P &= \frac{\rho\,e - \sum_k \left(\frac{\alpha_k}{\gamma_k - 1}\right)(\gamma_k\,P_{k,\infty} + \beta_k)}{\sum_k \left(\frac{\alpha_k}{\gamma_k - 1}\right)} + \beta\ , \\ &= \frac{\rho\,\mathcal{E} - \sum_k \left(\frac{\alpha_k}{\gamma_k - 1}\right)(\gamma_k\,P_{k,\infty} + \beta_k) - \sum_k \alpha_k\,\rho_k\,B_k}{\sum_k \left(\frac{\alpha_k}{\gamma_k - 1}\right)} + \beta\ . \end{aligned} \tag{2.31}$$

System (2.26) is now closed by (2.31). This mechanical equilibrium model is able to describe wave propagation in granular mixtures. However, it is unable to reproduce compaction irreversibility. To reach this aim, we are going to build a non-equilibrium model with relaxation that will tend in some limit to system (2.26). The mechanical equilibrium model will be used during the loading process only, while unloading will be treated by the non-equilibrium model presented below.

3 Non equilibrium model

The non-equilibrium model must involve two main features :

1. the non-equilibrium model must tend to the mechanical equilibrium one when mechanical relaxation effects are stiff;

2. the non-equilibrium sound speed must be greater than the equilibrium one, as it is usually the case for non-equilibrium models.

On this basis, we propose the following model, which is an extension of the model given by Saurel et al. (2009) in [34], for fluid-fluid interfaces, to the case of granular mixtures :

$$
\begin{aligned}
&\frac{\mathrm{D}\alpha_1}{\mathrm{D}t} = \mu\,\pi_r\ ,\\
&\frac{\partial(\alpha\rho)_k}{\partial t} + \frac{\partial\left((\alpha\rho)_k\,u\right)}{\partial x} = 0\ ,\\
&\frac{\partial\left((\alpha\rho\mathcal{E})_k\right)}{\partial t} + \frac{\partial\left((\alpha\rho\mathcal{E})_k\,u\right)}{\partial x} + (\alpha P)_k\,\frac{\partial u}{\partial x} = -\delta_k\,\pi_I\,\mu\,\pi_r\ ,\\
&\frac{\partial(\rho u)}{\partial t} + \frac{\partial(\rho u^2 + P)}{\partial x} = 0\ ,\\
&\frac{\partial(\rho E)}{\partial t} + \frac{\partial\left((\rho E + P)\,u\right)}{\partial x} = 0\ ;
\end{aligned}
\tag{3.1}
$$

where $\delta_k = k^{'} - k$, $k = 1\,,\,2$, $k^{'} = 2$ if $k = 1$, and $k^{'} = 1$ if $k = 2$. For any flow variable f, and in all that follows, f_r stands for the difference of the phase variables f_k : $f_r = f_1 - f_2$, hence, here $\pi_r = \pi_1 - \pi_2$. It is implicit in this formulation that $k = 1$ corresponds to the solid granular phase while $k = 2$ stands for the gas phase. We recall hereafter the definitions of the main variables involved in system (3.1) :

$$
\begin{aligned}
&\pi_k = P_k - \beta_k\ ,\\
&E_k = \mathcal{E}_k + \frac{1}{2}\,u^2\ ,\quad \mathcal{E}_k = e_k + B_k\ ,\\
&E = \sum_k Y_k E_k\ ,\quad P = \sum_k \alpha_k P_k\ ,\\
&\pi_I = \frac{Z_2\,\pi_1 + Z_1\,\pi_2}{Z_1 + Z_2}\ ,\quad Z_k = \rho_k c_k\ ,\quad c_k^2 = \frac{\dfrac{P_k}{\rho_k^2} - \left.\dfrac{\partial e_k}{\partial \rho_k}\right|_{P_k}}{\left.\dfrac{\partial e_k}{\partial P_k}\right|_{\rho_k}}\ .
\end{aligned}
$$

The generalized interfacial pressure π_I given above, has been determined through the Riemann problem solution as given by Saurel et al. (2003) in [32].
The main point of this model relies on the relaxation parameter μ

$$
\mu = \begin{cases} +\infty\ , & \text{if } \pi_1 > \pi_2\ ,\\ 0\ , & \text{otherwise}\ . \end{cases}
\tag{3.2}
$$

Thus, during loading, the weak compressibility of the solid will imply $\pi_1 > \pi_2$, and a stiff pressure relaxation coefficient will be used. As it is shown in appendix A, such a treatment is equivalent to the

direct resolution of the equilibrium model (2.26). During unloading, vanishing relaxation coefficient will be used.
This non-equilibrium model (3.1) thus contains two limit models :

1. the mechanical equilibrium model (2.26), when the relaxation parameter μ tends to infinity,
2. a *frozen* model when this parameter is set to zero.

It is now necessary to analyze these two models, as it is also important to examine the physical meaning of the relaxation parameter μ as a function of π_1 and π_2. This is addressed in a specific section 7, after validation of this non-equilibrium model against experimental results. Let us check before, the accordance of this model with the fundamental principles of thermodynamics.

3.1 Energy conservation

System (3.1) contains three energy conservation equations : two of them are addressed to the evolution of each phase total internal energy $\mathcal{E}_k$, while the last one stands for the total mixture energy conservation. Consequently, this system is over-determined but is still compatible. Numerical resolution of interface problems with fluid-fluid and fluid-granular mixture interfaces requires compatible over-determined system, in particular for wave transmission. The fundamental reason is that the phase energy equations are not in conservative form. The total mixture energy equation, being conservative, ensures a proper treatment of the two non-conservative internal energy equations in the single phase limit, i.e. on both sides of a material interface, even in the presence of shocks. This justifies why the total mixture energy is needed for numerical reasons, as shown by Saurel et al. (2009), in [34].
For both theoretical and numerical reasons, let us first check the compatibility of these three energy equations. With the notation conventions given previously, $k = 1\,,2$, the equation of the total internal energy $\mathcal{E}_k$ may be written by

$$\rho \frac{\mathrm{D}}{\mathrm{D}t} \left(Y_k \mathcal{E}_k\right) + (\alpha P)_k \frac{\partial u}{\partial x} = -\delta_k \, \pi_I \, \mu \, \pi_r \; ; \tag{3.3}$$

now summing the equations (3.3), for $k = 1\,,\,2$ and adding the kinetic energy obtained from the mixture equation lead to the following resulting equation

$$\rho \frac{\mathrm{D}}{\mathrm{D}t} \left(Y_1 \mathcal{E}_1 + Y_2 \mathcal{E}_2 + \frac{1}{2} u^2 \right) + \frac{\partial \left(P u\right)}{\partial x} = 0 \; ,$$

which corresponds to the total mixture equation of system (3.1).

3.2 Entropy inequality

Let us show now that the non-equilibrium model is in agreement with the entropy inequality requirement. An equivalent form of equation (3.3) is

$$(\alpha \rho)_k \frac{\mathrm{D} e_k}{\mathrm{D}t} + (\alpha P)_k \frac{\partial u}{\partial x} = -\delta_k \left(\pi_I + \beta_k\right) \mu \, \pi_r \; .$$

With the help of the volume fraction equation and the mass conservation equation of phase k, the velocity divergence can be expressed by

$$\frac{\partial u}{\partial x} = -\frac{1}{\alpha_k}\frac{\mathrm{D}\alpha_k}{\mathrm{D}t} - \frac{1}{\rho_k}\frac{\mathrm{D}\rho_k}{\mathrm{D}t} = -\frac{\delta_k}{\alpha_k}\mu\,\pi_r - \frac{1}{\rho_k}\frac{\mathrm{D}\rho_k}{\mathrm{D}t}\ ,$$

and the internal energy equation now reads as

$$(\alpha\rho)_k\frac{\mathrm{D}e_k}{\mathrm{D}t} - \frac{(\alpha P)_k}{\rho_k}\frac{\mathrm{D}\rho_k}{\mathrm{D}t} = \delta_k(\pi_k - \pi_I)\,\mu\,\pi_r\ .$$

With the help of the Gibbs identity for phase k, we get

$$(\alpha\rho T)_k\frac{\mathrm{D}s_k}{\mathrm{D}t} = -\delta_k(\pi_I - \pi_k)\,\mu\,\pi_r\ .$$

Now replacing π_I by its definition, we get

$$\pi_I - \pi_k = -\frac{Z_k}{Z_1 + Z_2}\,(\pi_k - \pi_{k'}) = -\delta_k\frac{Z_k}{Z_1 + Z_2}\,\pi_r\ ,$$

and the entropy equation of phase k becomes

$$(\alpha\rho T)_k\frac{\mathrm{D}s_k}{\mathrm{D}t} = \frac{Z_k}{Z_1 + Z_2}\,\mu\,\pi_r^2\ ,$$

which shows a non negative entropy production for each phase k, and therefore ensures the mixture entropy production to be non negative as well.

3.3 Frozen model

During the unloading stage, the relaxation parameter is set to zero ($\mu = 0$). It is interesting to examine the acoustic properties of the corresponding model, as the hesteresis phenomenon, shown in figure 1.1, is expected to be reproduced due to the change in the acoustic behaviour when μ varies from $+\infty$ to 0.

The frozen limit model corresponds to the system (3.1), when $\mu = 0$. An alternative formulation of this system may be expressed by

$$\frac{\partial \mathbf{W}}{\partial t} + \mathbf{A}(W)\,\frac{\partial \mathbf{W}}{\partial x} = 0\ ,$$

with the vector of variables $\mathbf{W}$ and the matrix $\mathbf{A}(\mathbf{W})$ defined by

$$\mathbf{W} = \begin{pmatrix} \alpha_1 \\ s_1 \\ s_2 \\ u \\ P_1 \\ P_2 \end{pmatrix} , \quad \mathbf{A}(\mathbf{W}) = \begin{pmatrix} u & 0 & 0 & 0 & 0 & 0 \\ 0 & u & 0 & 0 & 0 & 0 \\ 0 & 0 & u & 0 & 0 & 0 \\ P_r/\rho & 0 & 0 & u & \alpha_1/\rho & \alpha_2/\rho \\ 0 & 0 & 0 & \rho_1 c_1^2 & u & 0 \\ 0 & 0 & 0 & \rho_2 c_2^2 & 0 & u \end{pmatrix} .$$

The eigenvalues of this matrix correspond to the following wave speeds

$$\begin{cases} \lambda_0 & = u \ , \\ \lambda_1 & = u - c_f \ , \\ \lambda_2 & = u + c_f \ . \end{cases}$$

Here, the frozen sound speed c_f is defined by

$$c_f^2 = Y_1 c_1^2 + Y_2 c_2^2 \ . \tag{3.4}$$

This sound speed is much greater than the mechanical equilibrium sound speed $\mathcal{C}_W$ given by (2.27), as shown in appendix B. Moreover, this result guarantees the hyperbolicity of the non-equilibrium model (3.1).

3.4 Limit system when $\mu \to +\infty$

During compression, the relaxation parameter is assumed to be stiff ($\mu \to +\infty$). It is important to show that the asymptotic limit of the non equilibrium model (3.1), when $\mu \to +\infty$, corresponds to the mechanical equilibrium model (2.26). This is detailed in appendix A.

It is now clear that formulation (3.1) contains two limit models, each one being hyperbolic and having its own mixture sound speed definition. Closure of this model is ensured by finally defining appropriate equations of state and relaxation parameter μ. The first point is the objective of the following section. Justification of the relaxation parameter setting is examined in section 7.

4 Equations of state

Since powder compaction situations involve two thermodynamic phases (solid and gas), three equations of state are needed. As a matter of fact, and since each material is considered as being compressible, we need an equation of state for each of the two phases, in order to express its thermodynamic behaviour. A third equation of state is also needed to express the intergranular pressure linked to its corresponding configuration energy.

4.1 Thermodynamic equations of state

For the sake of simplicity, and not because it is restricted to, each material is assumed to obey the *stiffened gas* equation of state (EOS). This formulation is able to deal with both gas and condensed phases. It reads as

$$P_k = (\gamma_k - 1)\rho_k e_k - \gamma_k P_{k,\infty} \ . \tag{4.1}$$

γ_k and $P_{k,\infty}$ are characteristic positive parameters of a given material. They are generally determined from a given reference curve (mostly from the experimental Hugoniot curve), as detailed e.g. by Le Métayer et al. (2004) in [19]. Example of some material data are listed in table 1.

	ρ_0 (kg/m^3)	γ	P_∞ (Pa)
Air	1	1.4	0
Liquid water	1 000	4.4	6×10^8
HMX	1 903	5.5	31×10^8
NaCl (solid)	2 165	4.2	63×10^8

TAB. 1: *Stiffened gas EOS data of some materials under interest for powder compaction*

4.2 Granular equation of state

When dealing with solid-gas mixtures, only the solid phase is subjected to intergranular efforts and contains consequently configurational energy. The granular EOS is determined by quasi-static compression of powders. The system volume is measured, and the solid volume fraction of the granular bed is deduced, as a function of the applied stress. This type of experiment is described e.g. by Kuo et al. (1980) in [18], Elban and Chiarito (1986) in [7], and more recently by Jogi (2003) in [14], where successive loading-unloading cycles have been studied.

It is possible to fit corresponding curves (granular pressure β – solid volume fraction α) by the following function, defining the configuration energy (the granular pressure will be defined subsequently)

$$B(\alpha) = \begin{cases} B_a(\alpha) \ , & \text{if } \alpha_0 < \alpha < 1 \ , \\ 0 \ , & \text{otherwise} \ ; \end{cases} \tag{4.2}$$

where α_0 corresponds to the solid volume fraction when then granular pressure is zero, and

$$B_a(\alpha) = a[(1-\alpha)\ \log(1-\alpha) + (1 + \log(1-\alpha_0))\,(\alpha - \alpha_0) - (1-\alpha_0)\log(1-\alpha_0)]^n \ . \tag{4.3}$$

This volume fraction limit depends on the powder material, on its grain morphology or its granulometry and so on. It is clear from (4.2)–(4.3) that $B(\alpha_0) = 0$. a and n are also characteristic positive parameters of a given powder, and more precisely on its response during quasi-static loading.
For the present model, it is necessary to formulate the first and second derivatives of B_k given by

equivalent relations (4.2)–(4.3) defining B_k. The first derivative of B_k w.r.t. α_k is

$$\frac{\mathrm{d}B_k}{\mathrm{d}\alpha_k} = \begin{cases} {B_{a_k}}'(\alpha_k)\,, & \text{if } \alpha_{k,0} < \alpha_k < 1\,, \\ 0\,, & \text{otherwise}\,, \end{cases} \tag{4.4}$$

with

$${B_{a_k}}'(\alpha_k) = -a_k\, n_k\, (\log(1-\alpha_k)+1)\left(\frac{B_{a_k}(\alpha_k)}{a_k}\right)^{(n_k-1)/n_k}\,. \tag{4.5}$$

Obviously,

$$\frac{\mathrm{d}B_k}{\mathrm{d}\alpha_k}(\alpha_{k,0}) = 0\,, \quad \text{when} n_k > 1\,.$$

This ensures the tangency of the pressure curve with the volume fraction axis at $\alpha_k = \alpha_{k,0}$. We are now able to define the granular pressure β_k

$$\beta_k = (\alpha\rho)_k \frac{\mathrm{d}B_k}{\mathrm{d}\alpha_k}\,. \tag{4.6}$$

Since the second derivative of B_k is also needed in the definition of the solid granular speed of sound, we give its definition below :

$$\frac{\mathrm{d}^2 B_k}{\mathrm{d}{\alpha_k}^2} = \begin{cases} B''_{a_k}(\alpha_k)\,, & \text{if} \quad \alpha_{k,0} < \alpha_k < 1\,, \\ 0\,, & \text{otherwise}\,, \end{cases} \tag{4.7}$$

with

$$\begin{aligned} B''_{a_k}(\alpha_k) = a_k n_k \Bigg[\frac{1}{1-\alpha_k}\left(\frac{B_k(\alpha_k)}{a_k}\right)^{(n_k-1)/n_k} + \\ + (n_k-1)(\log(1-\alpha_k)+1)\left(\frac{B_k(\alpha_k)}{a_k}\right)^{(n_k-2)/n_k} \Bigg]\,. \end{aligned} \tag{4.8}$$

By using Jogi experimental data [14], based on granular HMX, with particle size around 100 μm, we have obtained the fitting curve in lines, shown on figure 4.1, on the basis of definition (4.6) and a configuration energy given by (4.2)–(4.3).

Using Duberg and Nyström experiments (1986) [6], based on solid granular NaCl, we have obtained the results shown in figure 4.2.

Now, all the data we need to validate our model are available, and we can therefore perform the numerical validation for wave dynamics tests in powder media and check how the compaction hysteresis phenomenon is reproduced.

Appropriate numerical schemes have been derived by Saurel et al. (2009), in [34] for a simplified situation of a fluid-fluid model. Extension to the present model of a similar algorithm can be used here, and we give in the following section the additional modifications of that algorithm in the granular compaction context.

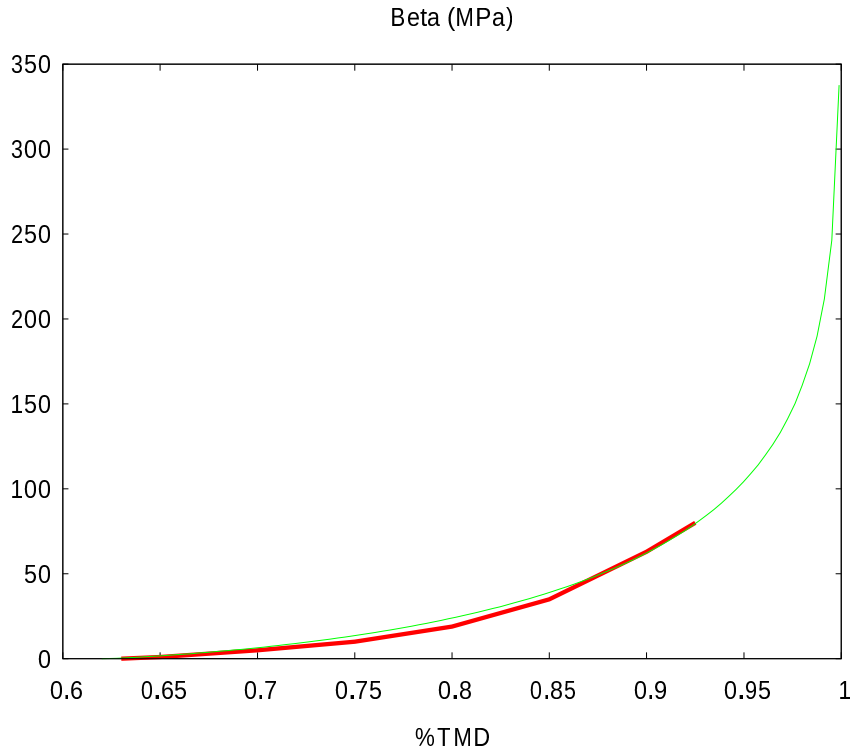

FIG. 4.1: *Approximation of the experimental compression curve (bold red lines) for granular HMX, following Jogi [14], by the granular equation of state (4.2)–(4.3) and (4.6), in thin green lines. The fitting parameters are determined in the zone where the curves are superimposed. Function behaviour for extrapolated data is shown when the solid volume fraction tends to one. Obviously, compressible effects involved in the thermodynamic equation of state become important in this range. Fitting parameters in the solid volume fraction* 0.63–0.93, *are :* $a = 3 \times 10^4$ Pa *and* $n = 1.1$. *The percentage of the theoretical maximum density is defined by :* $\%\mathrm{TMD} = (\alpha_s \rho_s)/\rho_{s,0}$.

5 Numerical method

The non-equilibrium model (3.1) is close to the two-phase model studied by Saurel et. al (2009), in [34]. The numerical method described in that reference paper proceeds in three main steps :

1. HYPERBOLIC STEP : solution of the non-equilibrium system without relaxation terms;
2. RELAXATION STEP : determination of the equilibrium pressure and corresponding volume fraction variables;

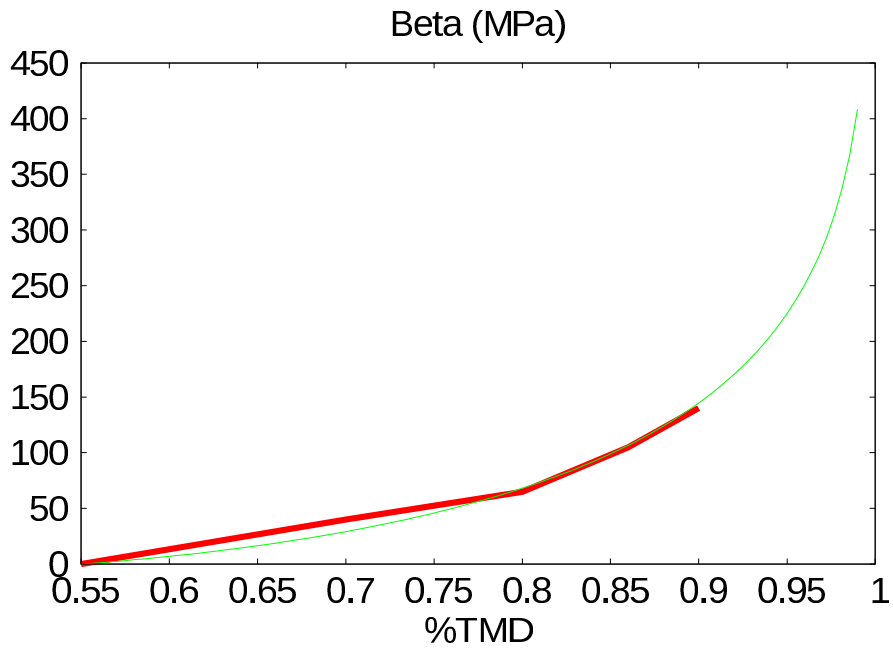

FIG. 4.2: *Approximation of the experimental compression curve (bold red lines) for granular NaCl, following Duberg and Nyström [6], by the granular equation of state (4.2)–(4.3) and (4.6) in thin green lines. The fitting parameters are determined in the zone where the curves are superimposed. Function behaviour for extrapolated data is shown when the solid volume fraction tends to one. Obviously, compressible effects involved in the thermodynamic EOS become important in this range. Fitting parameters in the solid volume fraction range* 0.55–0.9 *are :* $a = 5 \times 10^4 \mathrm{Pa}$ *and* $n = 1.02$ *(*$\%\mathrm{TDM} = (\alpha_s \rho_s)/\rho_{s,0}$ *).*

3. INTERNAL ENERGY RESET : use the equilibrium volume fraction in the mixture EOS, based on the mixture energy conservation (2.31), then determine the corrected equilibrium pressure and reset each corresponding phase internal energy.

In the present context of granular materials, the system of equations solved in the hyperbolic step is

stated as $(k = 1\,,\,2)$:

$$
\begin{aligned}
&\frac{\mathrm{D}\alpha_1}{\mathrm{D}t} = 0\,,\\
&\frac{\partial(\alpha\rho)_k}{\partial t} + \frac{\partial\left((\alpha\rho)_k u\right)}{\partial x} = 0\,,\\
&\frac{\partial\left((\alpha\rho)_k e_k\right)}{\partial t} + \frac{\partial\left((\alpha\rho)_k e_k u\right)}{\partial x} + \alpha_k P_k \frac{\partial u}{\partial x} = 0\,,\\
&\frac{\partial(\rho u)}{\partial t} + \frac{\partial(\rho u^2 + P)}{\partial x} = 0\,,\\
&\frac{\partial(\rho E)}{\partial t} + \frac{\partial\left((\rho E + P)u\right)}{\partial x} = 0\,;
\end{aligned}
\tag{5.1}
$$

where

$$
P = \sum_k \alpha_k P_k\,, \quad E = \mathcal{E} + \frac{1}{2}\,u^2\,, \quad \mathcal{E} = e + B\,.
$$

So the only difference with the formulation used in [34] for the hyperbolic step lies in the definition of the total mixture energy E, since it involves both a thermodynamic (e) and a granular (B) energy part. The internal phase energy equation formulation in (5.1) has been simplified from the formulation given by (3.1), using the granular Gibbs identity (2.17).
The third step of this method (that is, the internal phase energy reset), is also unchanged w.r.t. [34]. The only change lies in the mixture EOS formulation (2.31) that is used instead of its fluid variant mixture EOS formulation.
The second step (pressure relaxation), is however quite different, since the mechanical equilibrium condition is different as well. Note this relaxation step is performed only if $\pi_1 > \pi_2$.
Let us now detail the relaxation step. The system of differential equations that has to be solved is $(k = 1\,,\,2)$:

$$
\begin{aligned}
&\frac{\mathrm{d}\alpha_1}{\mathrm{d}t} = \mu\,\pi_r\,,\\
&\frac{\mathrm{d}(\alpha\rho)_k}{\mathrm{d}t} = 0\,,\\
&\frac{\mathrm{d}\left((\alpha\rho)_k \mathcal{E}_k\right)}{\mathrm{d}t} = -\delta_k \pi_I \mu \pi_r\,,\\
&\frac{\mathrm{d}(\rho u)}{\mathrm{d}t} = 0\,,\\
&\frac{\mathrm{d}(\rho E)}{\mathrm{d}t} = 0\,,
\end{aligned}
$$

in the limit $\mu \to +\infty$, and where

$$
\pi_I = \frac{Z_2\pi_1 + Z_1\pi_2}{Z_1 + Z_2}\,, \quad \mathcal{E}_k = e_k + B_k\,.
$$

Since only the equilibrium solution is required, the aim is to replace this sytem of ordinary differential equations by an algebraic system. After some manipulations, the internal phase energy equations become ($k = 1\,,\,2$) :

$$\frac{\mathrm{d}\mathcal{E}_k}{\mathrm{d}t} + \pi_I \frac{\mathrm{d}\nu_k}{\mathrm{d}t} = 0\ ,$$

with $\nu_k = 1/\rho_k$. The integral form of that system of two equations is

$$\mathcal{E}_k - \mathcal{E}_k^0 + \widehat{\pi}_{I,k}\,(\nu_k - \nu_k^0) = 0\ ,$$

where

$$\widehat{\pi}_{I,k} = \frac{1}{\nu_k - \nu_k^0} \int_0^{\Delta t} \pi_I\, \frac{\mathrm{d}\nu_k}{\mathrm{d}t} \mathrm{d}t\ .$$

Following Saurel et al. (2009) [34], a sufficiently accurate estimation of the interfacial pressure average may be obtained by setting :

$$\widehat{\pi}_{I,k} = \pi\ ,$$

which represents the equilibrium state pressure definition.
So the system of equations to be solved is

$$e_k(P,\nu_k) + B_k(\alpha_k,\rho_k) - e_k(P_k^0,\nu_k^0) - B_k(\alpha_k^0,\rho_k^0) + \pi\,(\nu_k - \nu_k^0) = 0\ ,\ \ k = 1\,,\,2\ . \tag{5.2}$$

Since the apparent densities $(\alpha\rho)_k$ remain constant during the relaxation step and the volume fractions may be expressed as $\alpha_k = (\alpha\rho)_k\,\nu_k$, system (5.2) may be reformulated by

$$e_k(P,\nu_k) + B_k(\nu_k) - e_k(P_k^0,\nu_k^0) - B_k(\nu_k^0) + \pi\,(\nu_k - \nu_k^0) = 0\ ,\ \ k = 1\,,\,2\ .$$

This system involves three unknowns : the specific phase volume variables ν_k, ($k = 1\,,\,2$), and the equilibrium pressure variable π. Its closure is ensured by the saturation constraint $\sum_k \alpha_k = 1$. This saturation condition can also be expressed more conveniently by

$$\sum_k (\alpha\rho)_k\,\nu_k = 1\ . \tag{5.3}$$

Let be more explicit by taking the example of materials governed by the *stiffened gas* EOS (4.1). Each internal phase energy e_k can therefore be replaced by a function of the thermodynamic pressure P_k and the specific volume ν_k :

$$e_k = \nu_k\,\frac{P_k + \gamma_k\,P_{k,\infty}}{\gamma_k - 1}\ .$$

Each phase pressure P_k can be expressed with the help of the equilibrium stress as a function of π :

$$P_k = \pi + \beta_k(\alpha_k,\rho_k)\ .$$

In that specified context, system (5.2) becomes

$$\frac{\pi + \beta_k + \gamma_k P_{k,\infty}}{\gamma_k - 1}\,\nu_k + B_k - \frac{P_k^0 + \gamma_k P_{k,\infty}}{\gamma_k - 1}\,\nu_k^0 - B_k^0 + \pi\,(\nu_k - \nu_k^0) = 0\ .$$

Note that in state "0", corresponding to the state reached at the end of the hyperbolic state, the equilibrium pressure π has not been used, since that state is out of mechanical equilibrium. Rearranging terms after some manipulations, allows us to write that

$$\nu_k = \frac{\left(P_k^0 + \gamma_k P_{k,\infty} + (\gamma_k - 1)\,\pi\right)\nu_k^0 + (\gamma_k - 1)\left(B_k^0 - B_k\right)}{\beta_k + \gamma_k\left(\pi + P_{k,\infty}\right)} \,. \tag{5.4}$$

We recall that the variables B_k and β_k, both functions of the pair (α_k,ρ_k) may be rewritten as functions of ν_k only, so the equation (5.4) is finally expressed as a function of the specific volume variable ν_k to be determined. For a given estimate of the equilibrium pressure π, specific volumes ν_k are solution of (5.4). This pressure estimate is correct if the constraint relation (5.3) is fulfilled. A Newton type algorithm is appropriate to solve this problem.

6 Test problems and validations

We recall that our model has been built to deal with the three main following features :

1. irreversibility of powder compaction,
2. wave dynamics (shock and expansion waves),
3. computational resolution of interfaces separating fluids and granular mixtures problems.

The goal of this section is therefore to check the ability of the model to simulate these various phenomena and to validate it through a panel of appropriate test problems.

6.1 Compaction of a powder sample

Let us consider a HMX powder sample (as used by Jogy in [14]) of 1.5 cm length, with an initial solid fraction set to 0.63 . The sample is pressed by a right moving piston at imposed velocity of 1 m/s . The right wall boundary is at rest ans is assumed to be undeformable. This is depicted in figure 6.1.

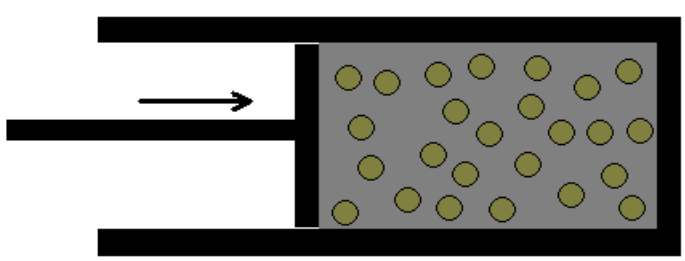

FIG. 6.1: *Schematic representation of a powder press process.*

The computational domain involves 100 cells. Here, the method described in section 5 has been used with an extended version on moving meshes. The corresponding solution is shown in figure 6.2 at times $t = 25.5\,\mu\text{s}$, $t = 51.0\,\mu\text{s}$, and $t = 76.4\,\mu\text{s}$.

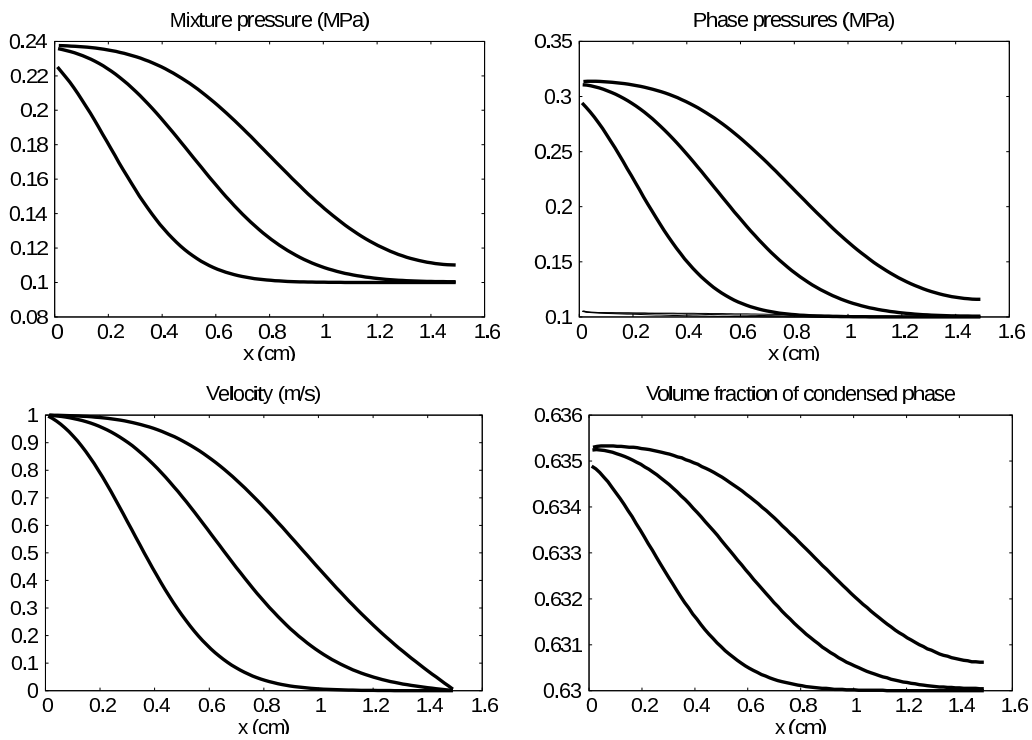

FIG. 6.2: *Propagation of a weak compaction wave in the mixture. Mixture pressure ($P = \alpha_1 P_1 + \alpha_2 P_2$), phase pressures P_k , mixture velocity u and solid volume fraction α_1 profiles are shown at times $25.5\,\mu\text{s}$, $51.0\,\mu\text{s}$ and $76.4\,\mu\text{s}$. The compression wave is dispersed and produces a weak solid volume fraction increase. The phase pressure difference between the gas phase (dashed lines) and the solid phase (solid lines), due to the granular pressure, is visible on the top right graph. The compaction wave reflects on the tube end wall at the last instant. Stiff pressure relaxation is used, corresponding to the mechanical equilibrium model.*

The propagation mechanism shown in figure 6.2, is very fast, compared to the piston motion velocity. Multiple reflexions occur between the two boundaries during the slow piston motion, rendering the various variable fields quasi-uniform, and therefore only functions of the time.
With the same piston velocity, the same powder sample is pressed again up to a solid volume fraction of 0.80; then, the piston is removed back slowly (with a velocity set at -0.01 m/s), until the mixture

pressure reaches the atmospheric pressure value. At this time, the piston motion is stopped. Flow variables being uniform in space, only their time evolution is shown in figure 6.3.

The first top left graph of figure 6.3 shows the time evolution of the piston velocity. That velocity is initially positive, then it becomes negative for about $1.5\,\mathrm{ms}$, and is zero when the mixture pressure value reaches the atmospheric pressure one. The piston trajectory is depicted in the top right graph. The mixture pressure increases during compression, then decreases rapidly when the piston velocity is negative, even if this value is close to zero. This is a consequence of the change in the mixture speed of sound in our model, that ranges from the mechanical equilibrium one when $\mu \to +\infty$ to the frozen one, when $\mu = 0$. The solid volume fraction increases during compression and remains unchanged during expansion. Thus, the granular medium stays compact. The thermodynamic solid pressure P_1 has the same time evolution behaviour than the mixture pressure, that both decrease abruptly during expansion. The solid phase thus recovers the atmospheric pressure value at the end of the cycle. Conversely, the gas phase stays compressed in the granular pores, as shown in the right graph at the third row of figure 6.3. The graph related to the *total pressures* $(P_k - \beta_k)$, shows the stress equality during the compression stage, while enhancing disequilibrium creation during the expansion stage. That disequilibrium is not surprising : at the end of the cycle, the solid pressure has reached the atmospheric pressure value, but the *granular pressure* β_1, which represents the effect of the plastic stress at the granular scale is still present. At last, the most characteristic graph is the last bottom right graph of figure 6.3, where the mixture pressure is depicted as a function of the compression rate (we recall that $\%\mathrm{TDM} = (\alpha\rho)_1/\rho_{1,0}$, where $\rho_{1,0}$ represents the standard density of the solid phase). The compression rate exhibits a slight decrease during the expansion stage, due to the mixture compressibility. Indeed, the expansion curve around $80\%\mathrm{TDM}$ is not strictly vertical. This last graph clearly shows the ability of the model to predict/reproduce the hysteresis phenomenon of powder compaction.

We now address the same experiment tests of Jogi [14], with 3 successive loading–unloading cycles. In these examples, the solid volume fraction has been recorded at the end of each unloading stage. For the first cycle, the powder sample is pressed up to the solid volume fraction value of 0.75, then the stress is relaxed. In the second cycle, the same sample is compressed again, until the solid volume fraction value attains 0.809, and the stress is relaxed again. In the last third cycle, the mixture is pressed now up to a solid volume fraction value of 0.938, then the stress is relaxed again once more. Results of the full series of the three cycles are given in figure 6.4, and compared to Jogi's experimental data results.

Similar agreement of results have been obtained by Gonthier (2003, 2004), in [10, 11], with his model compared to Jogi's experimental results. However, the two-phase flow model of Gonthier contains explicitly an extra function corresponding to the unloaded solid volume fraction. This additional function needs extra experimental efforts for its model's calibration and this is not what we are looking for with our model.

To end with our validation tests concerning the powder compaction irreversibility feature, we want to show the ability of the present model to deal with different kinds of powder materials. So let us consider a NaCl powder sample, as studied by Duberg and Nyström (1986) in [6]. EOS parameters are given in table 1 and in figure 4.2. The comparison between model predictions and experiments is shown in figure 6.5.

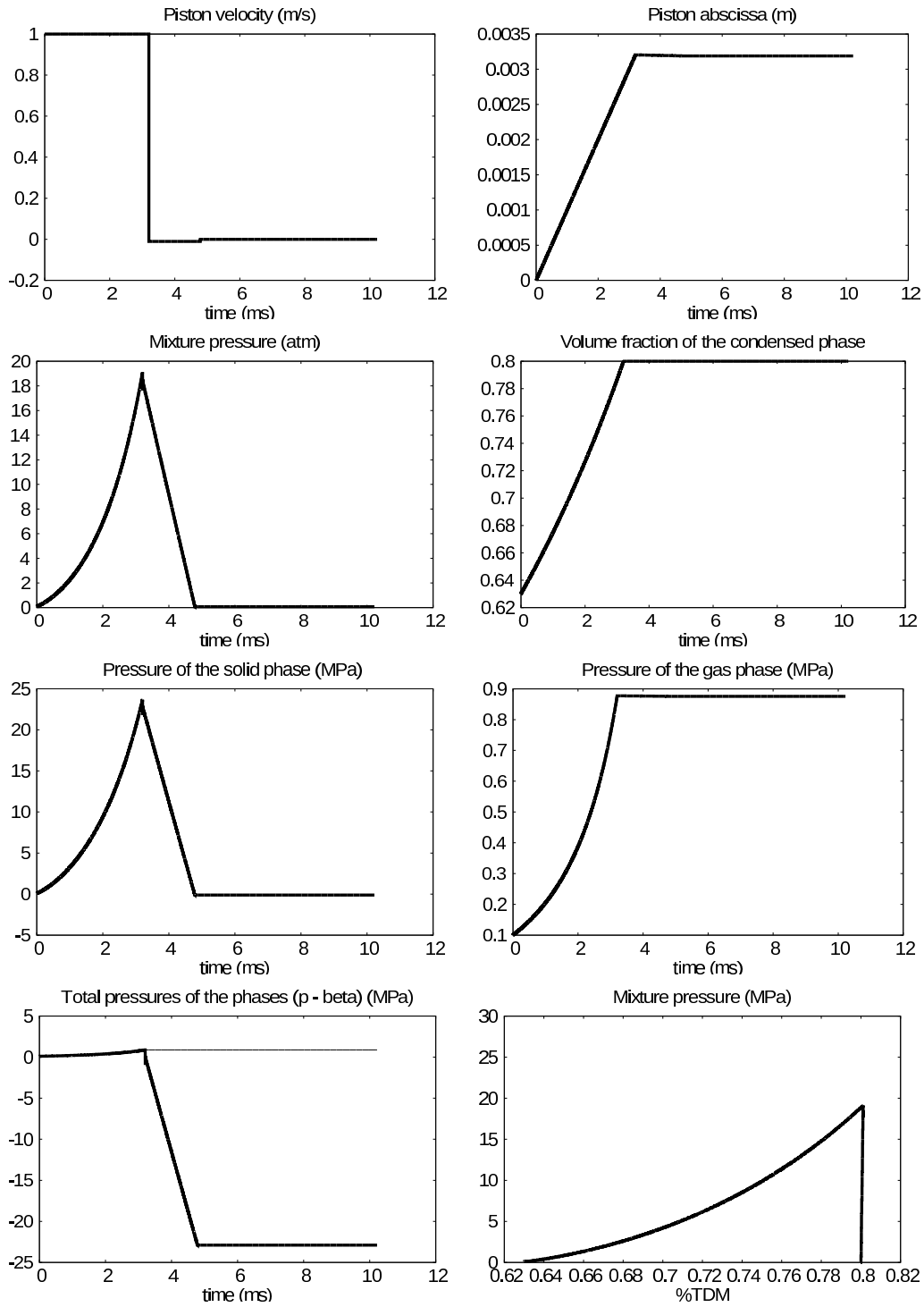

FIG. 6.34 *Time evolution of the main flow variables for a loading–unloading cycle with HMX powder sample. The maximum value of the solid volume fraction set to* $80\,\%$*, is reached at time* $t = 3\,\mathrm{ms}$*, and remains unchanged during the unloading stage. The hesteresis cycle is shown on the last right bottom graph.*

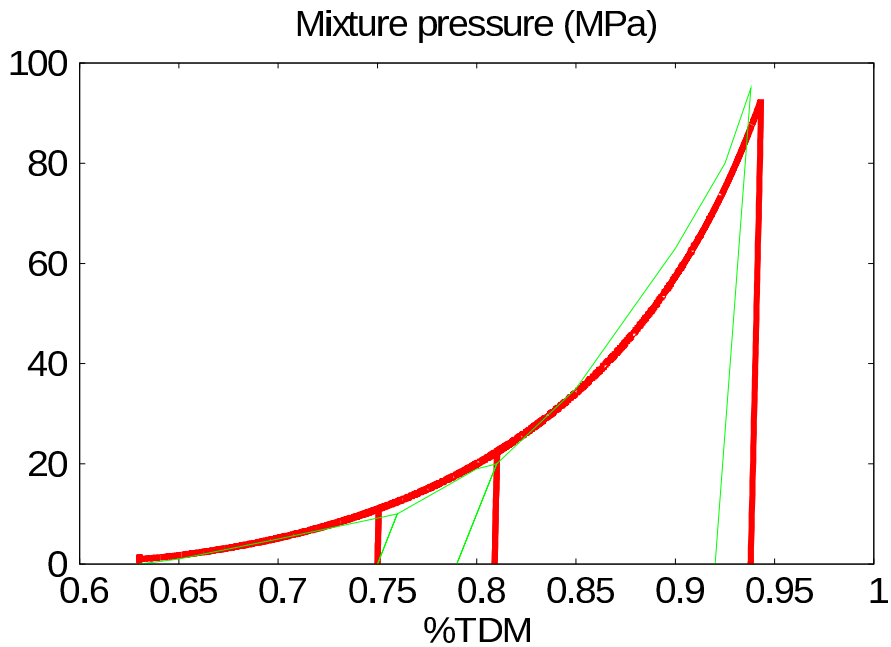

FIG. 6.4: *Mixture pressure evolution as a function of the compression rate ($\%\mathrm{TDM} = (\alpha\rho)_1/\rho_{1,0}$), for three successive loading–unloading cycles of HMX powder sample. Experimental data are shown in thin green lines and numerical results in bold red lines. The agreement is very good for a model free of any adjustable parameter.*

Figure 6.5 shows up a good agreement between the model's numerical results and the experimental ones.
In the following subsection, we examine the ability of the model to deal with large amplitude wave propagation, as well as interfaces separating pure fluids to granular mixtures.

6.2 Wave and interface dynamics validation tests

In all the following tests, the granular material corresponds to a HMX powder sample with its corresponding EOS parameters as given by table 1 and figure 4.1.
So, let us consider a *shock tube* of $1\,\mathrm{m}$ length, involving a high pressure chamber on the left, filled with a gas at the initial pressure value set to $0.1\,\mathrm{GPa}$, and a low pressure chamber on the right, filled with the same granular material as the one studied in figures 6.2–6.4, at a pressure set to the atmospheric pressure value. The gas is governed by the ideal gas EOS, with air polytropic coefficient. An initial volume fraction discontinuity is therefore present in the tube at the abscissa $0.5\,\mathrm{m}$. In order to prevent division by zero in the flow model, the initial solid fraction in the left chamber is set to 10^6; in the right chamber, the solid volume fraction is set to 0.63. The initial solid phase density

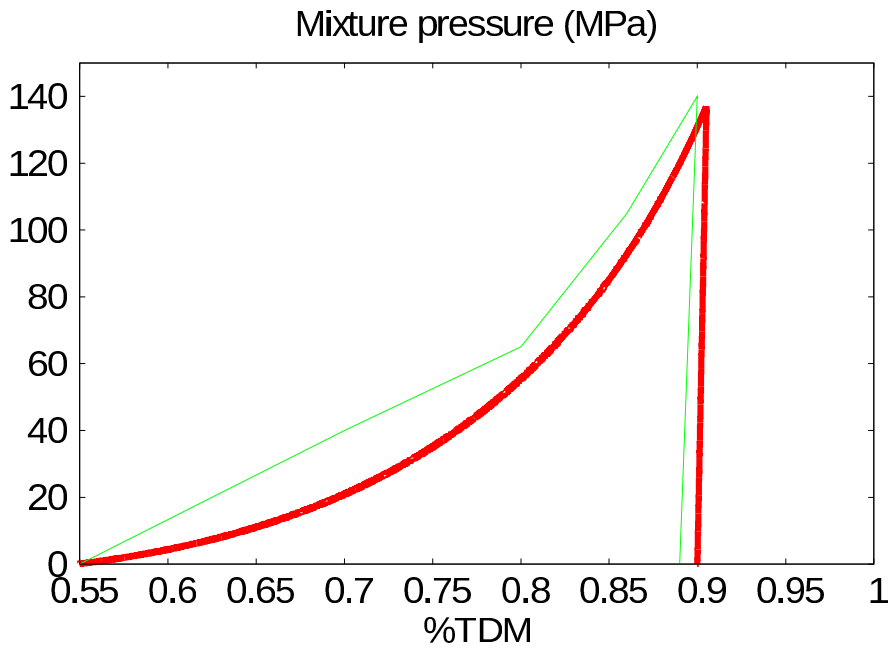

FIG. 6.5: *Mixture pressure evolution as a function of the compression rate for a NaCl powder sample. Experimental data are depicted in thin green lines and numerical results in bold red lines.*

is set constant in the whole domain and is equal to $1\,903\,\mathrm{kg/m^3}$. Both initial states are assumed to be at rest. The aim of this test problem is to evaluate the ability of the model to compute right facing shock and associated bed compaction, left facing expansion wave and the interface evolution separating the nearly pure gas phase from the solid powder mixture. Results are given in figure 6.6 at time $t = 0.38\,\mathrm{ms}$. The mesh contains $1\,000$ computational cells.

On the left top graph of figure 6.6, the left facing expansion wave and right facing shock are clearly visible. At the interface location, visible on the bottom right graph, both pressure and velocity are perfectly continuous. The phase pressure graph shows the solid pressure evolution in lines and the gas pressure one in dashed lines. The pressure difference between the two phase pressures is due to the granular pressure effect. On the left, the solid pressure reaches a very low level and is not in equilibrium with the gas phase pressure, as the left part of the domain corresponds to an expansion process. This has no consequence since the solid volume fraction in this region is very small.
The same test is rerun with an increased initial gas pressure value in the left chamber by a factor of 100 (i.e. $10\,\mathrm{GPa}$), in order to simulate conditions close to detonation product contact with granular media. Corresponding computational results are shown in the different graphs of figure 6.7, at time $t = 36\,\mu\mathrm{s}$.

This test shows the ability of the model to deal with interfaces separating fluids to solid granular mixtures in severe conditions, where the fluid behaviour of granular materials is recovered as a limit.

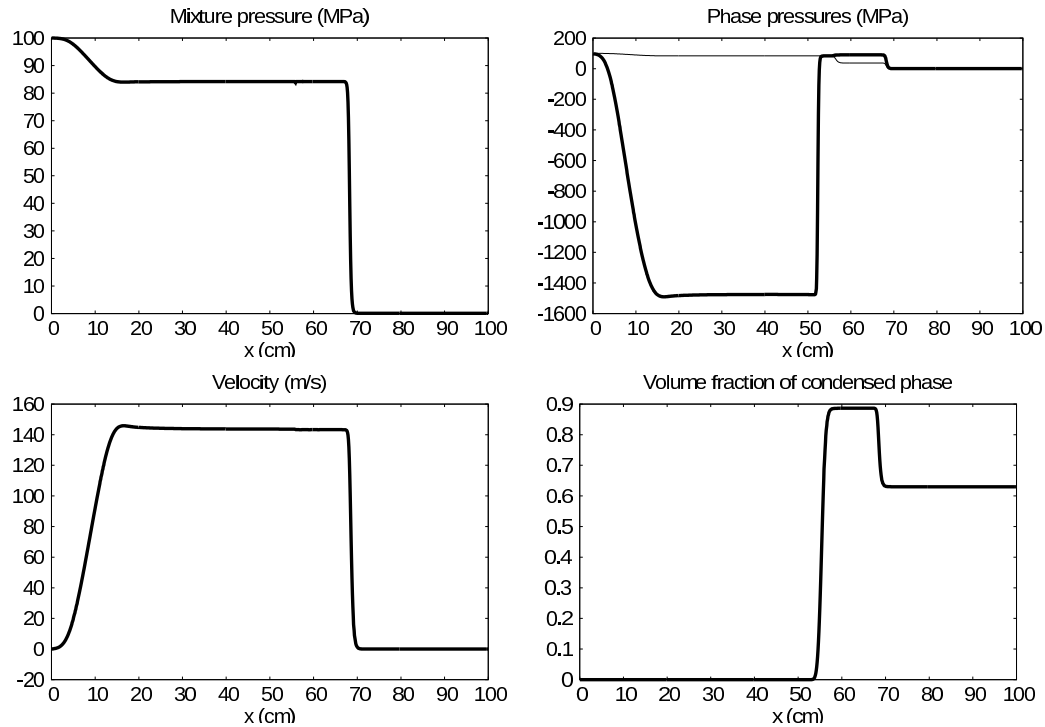

FIG. 6.6: Shock tube *test with high gas pressure on the left and solid granular mixture on the right. Interface conditions of equal mixture pressure and equal velocities are perfectly matched. The granular mixture is compacted by the shock wave.*

The phase pressure difference under such conditions in the granular bed becomes insignificant.
Let us consider now the symmetric situation with the expansion of a high pressure solid granular bed. In the left chamber, the granular bed is at the initial pressure value of $10\,\mathrm{GPa}$. On the right, gas is present and at the atmospheric pressure. In these conditions, the model uses now a zero relaxation parameter ($\mu = 0$), and we want to demonstrate its numerical ability of solving these interfaces. This is the aim of the results shown in the four graphs of figure 6.8.

All these various tests presented in this subsection show the capabilities of the model to deal with various kinds of interface problems:

1. when the granular bed is under compression, which corresponds to using the model with stiff relaxation in compaction zones ($\mu \to +\infty$),
2. when the granular bed is under expansion, which relates to the use of the frozen non-equilibrium model, ($\mu = 0$), to express the irreversible character of powder compaction.

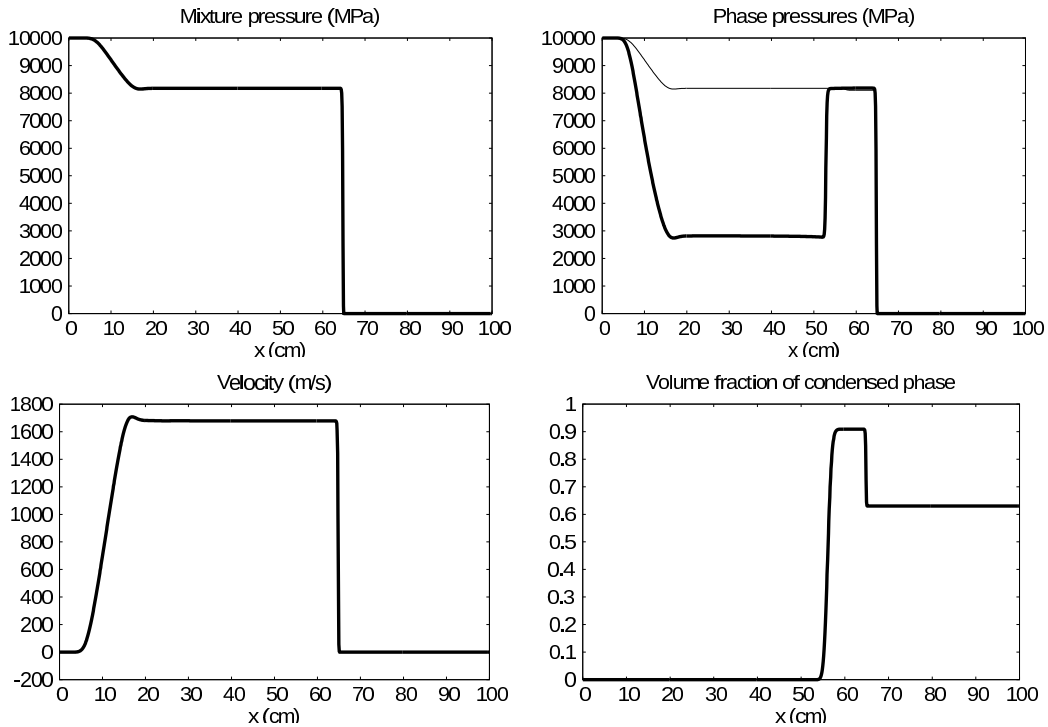

FIG. 6.7: Shock tube *test with high gas pressure on the left ans solid granular mixture on the right. Interface conditions of equal mixture pressure and equal velocities are once more prefectly matched. The pressure difference between the phase pressures in the compacted zone in the right chamber now vanishes, showing the negligible effects of granular pressure in such high gas pressure conditions, at least regarding wave dynamics. The fluid limit is recovered.*

Both limit models are suitable for solving interface problem simulations.

6.3 Two–dimensional example test

The goal of this subsection is to show that both model and numerical method are able to deal with complex multidimensional phenomena, as such appearing during the impact and penetration of a projectile into a solid granular bed. This is illustrated by an example given in figure 6.9, where a solid projectile (considered as non-deformable), impacts a solid granular mixture. That solid projectile is made of copper ($\rho_{\mathrm{Cu}} = 8\,900\,\mathrm{kg/m^3}$), and moves to the right at the initial velocity set to $10\,\mathrm{m/s}$. The copper projectile has an initial radius length of $0.1\,\mathrm{m}$. The other problem dimensions are given in figure 6.9.

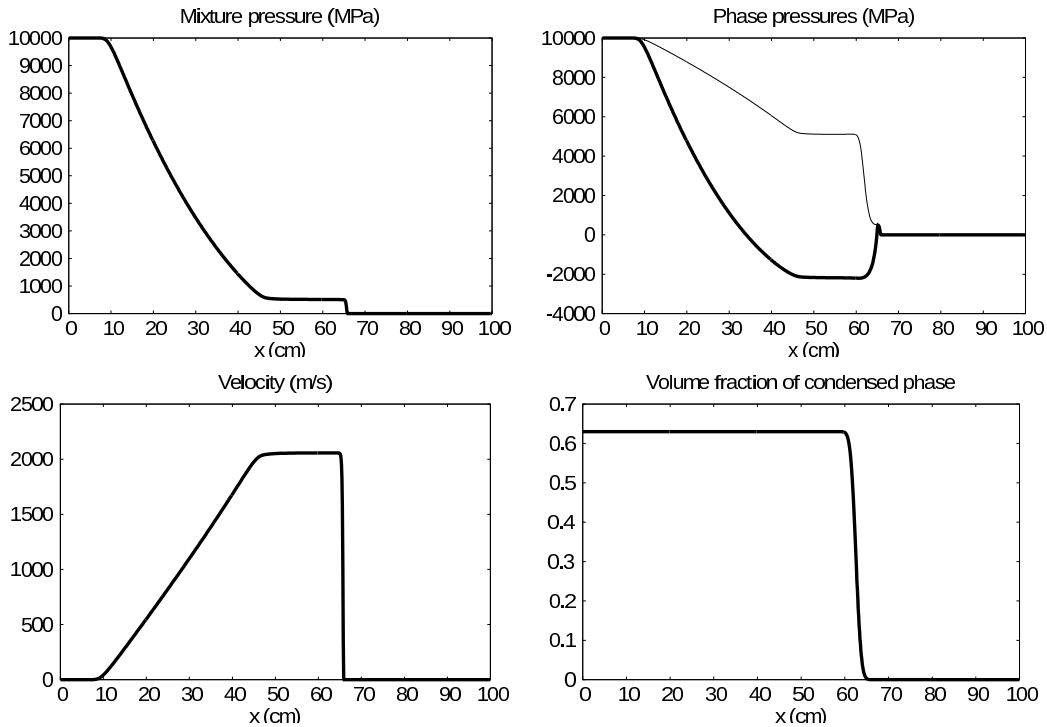

FIG. 6.8: Shock tube *test with high solid granular mixture pressure on the left and low gas pressure on the right. Interface conditions of equal mixture pressure and equal phase velocities are again perfectly matched, even in the absence of relaxation effects ($\mu = 0$).*

Here again, the HMX powder considered for this simulation is the same as previously used in the tests presented in the previous subsections, the initial HMX density is equal to $1\,903\,\mathrm{kg/m^3}$. The granular bed has an initial solid volume fraction value of 0.63 . The surrounding air, as well as the air contained in the powder mixture, has the initial density value equal to $1\,\mathrm{kg/m^3}$.

The flow behaviour is clearly different in figure 6.10, when irreversibility is accounted for, especially in the projectile wake. This can be important for example when determining the amount of ejected powder due to the projectile impact.

This type of computation involves 3 materials : the air, the granular powder, and the solid projectile. Model and numerical method extension to an arbitrary number of phases is straightforward. The non-deformable character of the solid projectile is solved with the correction procedure detailed in Petitpas et al. (2009), [26].

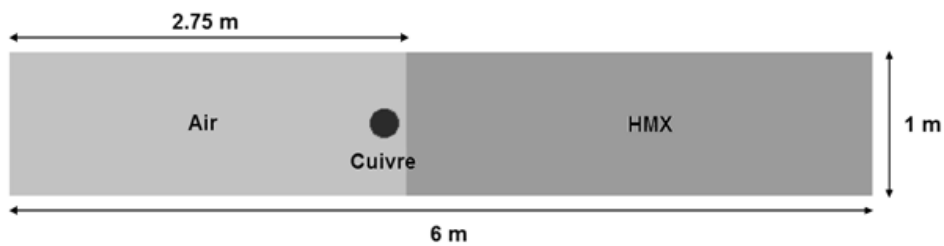

FIG. 6.9: *Schematic representation of the initial conditions during the impact of a copper projectile into a granular mixture made of HMX powder and with an initial solid volume fraction value set to* 0.63 .

6.4 Shock induced powder compaction test

We now finally examine the ability of the model against experimental data for shock propagation in powder samples. Corresponding experiments have been done by Sandusky and Liddiard (1985), [30]. In the following test case, the granular material corresponds to a HMX powder with the following granular EOS parameters :

$$\alpha_{s,0} = 0.73 \,, \quad a = 10^4 \,, \quad n = 1.05 \,.$$

The thermodynamic HMX parameters are those given in table 1. We assume the porosity to be filled with air with a density $\rho = 1.2\,\mathrm{kg/m^3}$, and $\gamma = 1.4$. At the initial time, the HMX-air mixture is assumed to be at rest, and a piston impacts the granular bed at various velocities. In figure 6.11, we compare experimental data (cross symbols) with numerical results (lines). The shock wave speed, shock wave pressure and the percent theoretical maximum density after compaction, for various piston velocities, are presented. As shown in the different graphs of figure 6.11, the results show an excellent agreement.

7 Relaxation parameter switch discussion

The non-equilibrium model (3.1) is able to link, in an unique formulation, the *frozen model* with the corresponding sound speed $c_f^2 = Y_1 c_1^2 + Y_2 c_2^2$, when $\mu = 0$, and the *mechanical equilibrium model* (2.26), when $\mu \to +\infty$. The irreversible powder compaction cycle depicted in figure 1.1, has

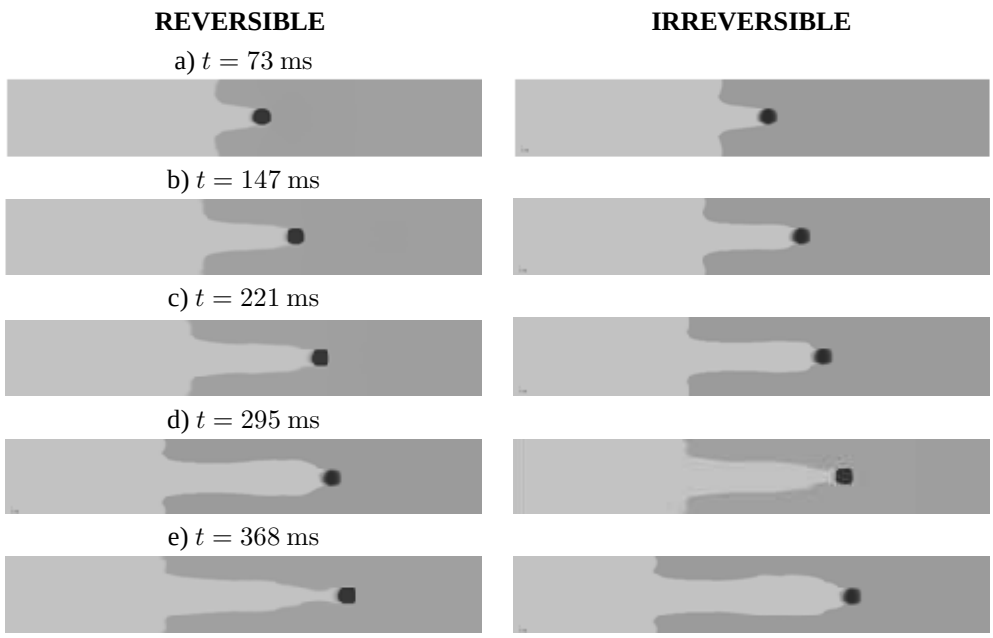

FIG. 6.10: *Qualitative flow behaviour during the impact of a solid projectile into a granular bed. On the left graph column, the mechanical equilibrium model has been solved by the help of the non-equilibrium one, which corresponds to using stiff relaxation parameter everywhere ($\mu \rightarrow +\infty$). On the right graph column, the switch (3.2) is used, which corresponds to irreversible compaction. Computed results are shown at times a)* $t = 73$ ms, *b)* $t = 147$ ms , *c)* $t = 221$ ms, *d)* $t = 295$ ms *and e)* $t = 368$ ms.

indeed been successfully reproduced, as shown in figures 6.4 and 6.5, with the following relaxation parameter switch setting :

$$\mu = \begin{cases} +\infty \,, & \text{if } \pi_1 > \pi_2 \,, \\ 0 \,, & \text{otherwise} \,. \end{cases} \tag{7.1}$$

Before explaining this *switch* procedure, it is first important to agree with the assumption this function μ is a simplified analogue of a certainly much more sophisticated function, which still remains to be determined, but this is not the aim of the present report.

Powder compaction may be considered as involving at least four different physical stages :

1. *Stress accumulation*: during the early events of granular bed compaction, acoustic waves propagate and reflect on both the solid piston and wall boundaries, making the mixture pressure to increase, in particular those acoustic waves related to the solid phase. Elastic deformations appear but are of low amplitude, due to the high resistance of elastic bodies to deformation.

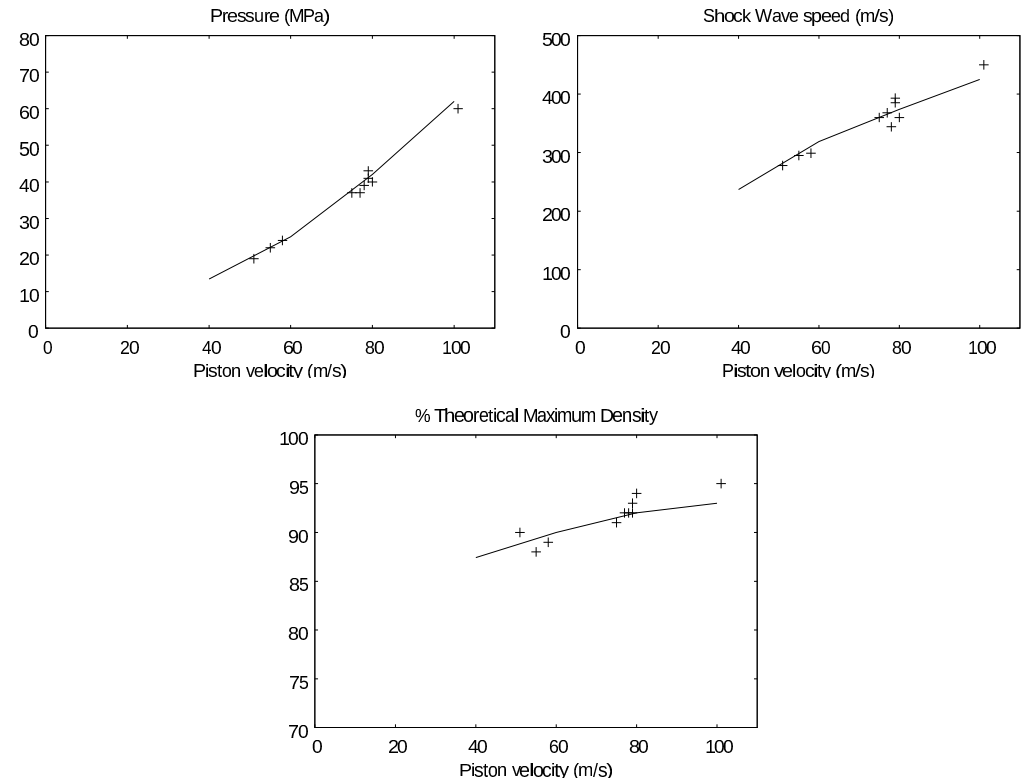

FIG. 6.11: *Comparison between numerical (lines), and experimental (cross symbols) results for wave speeds, pressure and theoretical maximum density in the shocked state, for various piston impact velocities.*

During that stage, the solid volume fraction is nearly constant, and therefore the right hand side of the solid volume fraction evolution equation is close to zero, so that the relaxation parameter might be considered as being close to zero as well. Even with a small compression rate (e.g. a little few percent), the stress phase differential $(\pi_1 - \pi_2)$, exceeds the plastic limit Y_P. For HMX, that limit is of the order of 100 MPa (see Khasainov et al., 1981, [17]). Then, the process undergoes plastic deformation.

2. *Plastic deformation*: plastic deformations result in stress relaxation, i.e. $\pi_1 = \pi_2$, at the end of the relaxation process. That process obviously occurs at a finite rate, but if the details of this relaxation process are not of interest, and if only the equilibrium state is in concern, then the relaxation parameter μ can be set to be stiff, ($\mu \to +\infty$). During that stage, plastic stresses increase, as well as the granular bulk pressure β_s, that summarizes their effects. It is important to recall that this relaxation process occuring during this plastic regime is irreversible.

3. *Frozen unloading*: plastic stresses aroung gas pores are now present and summarized by the bulk pressure β_s. Is the piston is removed, the solid pressure rapidly adjusts to the external pressure (e.g. the atmospheric pressure), while the plastic stresses at the pore scale remain present and unchanged. As plastic deformation is irreversible, both pore volumes and solid volume fraction are unchanged. This corresponds to considering the *frozen model* ($\mu = 0$), and the granular bed remains compacted and out of equilibrium.
4. *Long time relaxation*: if the compacted granular solid bed is left by its own under those non-equilibrium conditions for a very long time (say, several months or even years), stress relaxation will occur, resulting in compact solid dislocation production.

Our aim is not to model stages 1. and 4. To illustrate stages 1. and 2., let us consider once more the same granular HMX sample, under *frozen* compression, corresponding to the so called *stress accumulation* stage, followed by the finite rate relaxation step, corresponding to the *plastic deformation* stage. During the second stage, the relaxation parameter is arbitrarily set to $\mu = 10^{-6}\,\mathrm{Pa}^{-1}\,\mathrm{s}^{-1}$. The powder sample is compressed by a relative volume of 1 % only. In order to illustrate the scale of this transformation, stages 1. and 2. are both depicted in the same graph together with experimental data as shown in the figure 7.1.

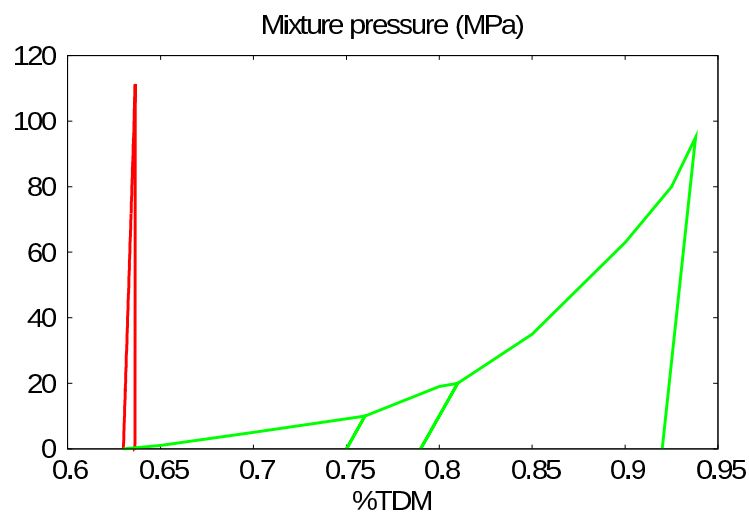

FIG. 7.1: *Decomposition of stages 1. (left side of red curve $\mu = 0$) and 2. (right side of red curve μ is finite) of the compaction process for an HMX sample. The plastic limit is exceeded during stage 1. Those events are shown in red lines. The end state of the relaxation path belongs to the equilibrium curve of the considered material (experimental results are represented by green lines).*

During stage 1., the mixture pressure increases dramatically, since the solid volume fraction is frozen and the solid medium is weakly compressible. Considering $\mu = 0$ in stage 1, is certainly excessive, and yet shows that the plastic limit of $100\,\mathrm{MPa}$ for HMX can be overpassed easily (stress

differential at the spike value is $\pi_1 - \pi_2 = 180$ MPa). Then plastic relaxation occurs and the mixture pressure decreases dramatically, to finally reach the equilibrium curve.
Since the equilibrium curve has been attained after plastic deformations, which are obviously irreversible, the unloading stage 3. will occurat constant solid volume fraction. This justifies the use of the setting $\mu = 0$, during the unloading stage 3.
In most of the partical applications we are interested in, there is no need to model nor describe the detailed phenomena occuring in stages 1. and 2. Only the final equilibrium relaxed state of stage 2. is needed. This is achieved by considering the $\mu \to +\infty$ setting in place of both stage 1.–2. full description. This justifies the *switch* (7.1). Note that this switch procedure renders the model free of any adjustable parameter.
Nevertheless, the model presented in this report has one limited aspect relying on the single velocity restriction, that is assumed in the description of multiphase mixtures. In some applications, gas (or liquid) permeation in granular beds or media may have significant effects. Obviously, those effects cannot be represented by the present model. For those effects to be accounted for, we need to extend the present model in order to restore the velocity drift effects. This is the goal of the following section : we will propose a full non equilibrium model (two velocities, two pressures), from which we will show all the sub-models presented in this report are derived.

8 A compaction model with velocity drift effects

The compaction model (3.1), is a temperature non-equilibrium two-phase flow model with a single velocity. In some specific situations, fluid permeation in granular beds may have significant effects that have therefore to be accounted for. Following the work of Guillard and Duval (2007), [12], a Darcy type law can be obtained to model drifts effects. This Darcy law has been obtained on the basis of asymptotic analysis of the velocity non-equilibrium Baer and Nunziato model (1986), [3], in the barotropic case. We extend here that approach to non-barotropic fluids in the presence of granular effects.

8.1 The full non-equilibrium model

The Baer and Nunziato model, [3], considers each phase to be compressible and evolving with its own velocity, temperature and pressure. The system is hyperbolic and involves 7 partial differential equations for two phases in one space dimension. Its natural generalization to the case of granular mixtures and in absence of both heat and mass transfers may be stated as (notations and index

conventions are the same as stated previously, $k = 1\,,\,2)$:

$$
\begin{aligned}
&\frac{\partial \alpha_1}{\partial t} + u_I \frac{\partial \alpha_1}{\partial x} = \mu\, \pi_r \;, \\
&\frac{\partial (\alpha\rho)_k}{\partial t} + \frac{\partial (\alpha\rho)_k u_k}{\partial x} = 0 \;, \\
&\frac{\partial (\alpha\rho u)_k}{\partial t} + \frac{\partial \left(\alpha_k (\rho u^2 + P)_k\right)}{\partial x} = \delta_k \left(\pi_I \frac{\partial \alpha_1}{\partial x} - \lambda u_r \right) \;, \\
&\frac{\partial (\alpha\rho E)_k}{\partial t} + \frac{\partial \left(\alpha(\rho E + P)\, u\right)_k}{\partial x} = \delta_k \left(\pi_I\, u_I \frac{\partial \alpha_1}{\partial x} - \lambda\, u_I{}'\, u_r - \mu\, \pi_I{}'\, \pi_r \right) \;.
\end{aligned}
\tag{8.1}
$$

We recall that $\pi_r = \pi_1 - \pi_2$ and $u_r = u_1 - u_2$ and are associated to stress and velocity relaxation parameters μ and λ respectively. $\delta_k = k^{'} - k$, with $k = 1\,,\,2$ and $k^{'} = 2$ if $k = 1$ and $k^{'} = 1$ if $k = 2$. The total phase energy E_k is defined with the help of the generalized total internal energy $\mathcal{E}_k$ involving the granular configuration energy B_k and the usual phase internal energy e_k, by

$$
E_k = \mathcal{E}_k + \frac{1}{2}\, u_k^2 \;, \quad \mathcal{E}_k = e_k + B_k \;.
$$

Following the work of Saurel et al. (2003), [32], the interfacial variables are defined by

$$
\begin{aligned}
u_I &= u_I{}' - \mathrm{sgn}\left(\frac{\partial \alpha_1}{\partial x}\right) \frac{\pi_r}{Z_1 + Z_2} \;, \qquad u_I{}' = \frac{Z_1 u_1 + Z_2 u_2}{Z_1 + Z_2} \;; \\
\pi_I &= \pi_I{}' - \mathrm{sgn}\left(\frac{\partial \alpha_1}{\partial x}\right) \frac{Z_1 Z_2}{Z_1 + Z_2}\, u_r \;, \qquad \pi_I{}' = \frac{Z_2 \pi_1 + Z_1 \pi_2}{Z_1 + Z_2} \;.
\end{aligned}
\tag{8.2}
$$

Here, $Z_k = \rho_k c_k$ is the acoustic impedance of phase k.
The Darcy type law, responsible for gas penetration, is obtained from an asymptotic analysis of the flow model (8.1), in the limit of stiff mechanical relaxation. To perform that analysis, it is more convenient to express the system (8.1) in terms of physical primitive variables (density, velocity, pressure). Denoting

$$
\frac{\mathrm{D}_k}{\mathrm{D}t} \stackrel{\text{def}}{=} \frac{\partial}{\partial t} + u_k \frac{\partial}{\partial x} \;,
$$

the corresponding primitive equations are summarized hereafter:

$$
\begin{aligned}
&\frac{\mathrm{D}_k \alpha_k}{\mathrm{D}t} = \delta_k \left[\left(\frac{Z_{k'}}{Z_1 + Z_2} - Y_{k'} \right) u_r \frac{\partial \alpha_k}{\partial x} + \mu^{'}\, \pi_r \right] \;, \\
&\alpha_k \left[\frac{\mathrm{D}_k \rho_k}{\mathrm{D}t} + \rho_k \frac{\partial u_k}{\partial x} \right] = -\rho_k \frac{\mathrm{D}_k \alpha_k}{\mathrm{D}t} \;, \\
&\alpha_k \left[\rho_k \frac{\mathrm{D}_k u_k}{\mathrm{D}t} + \frac{\partial P_k}{\partial x} \right] = -\delta_k \left[\left(\beta_k + \delta_k \frac{Z_k}{Z_1 + Z_2}\, \pi_r \right) \frac{\partial \alpha_1}{\partial x} + \lambda^{'}\, u_r \right] \;, \\
&\alpha_k \left[\frac{\mathrm{D}_k P_k}{\mathrm{D}t} - c_k^2 \frac{\mathrm{D}_k \rho_k}{\mathrm{D}t} \right] = \Gamma_k \left[\frac{Z_{k'}}{Z_1 + Z_2}\, \lambda^{'}\, u_r^2 + \frac{Z_k}{Z_1 + Z_2}\, \mu^{'}\, \pi_r^2 + 2\, \frac{Z_1 Z_2}{(Z_1 + Z_2)^2}\, \pi_r\, u_r \frac{\partial \alpha_k}{\partial x} \right] \;;
\end{aligned}
\tag{8.3}
$$

where

$$\left.\frac{\partial e_k}{\partial P_k}\right|_{\rho_k} = \frac{1}{\rho_k \Gamma_k}\ , \quad \left.\frac{\partial e_k}{\partial \rho_k}\right|_{P_k} = \frac{P_k}{\rho_k^2} - \frac{c_k^2}{\rho_k\,\Gamma_k}\ ,$$

$$\mu^{'} = \mu + \frac{1}{Z_1+Z_2}\left|\frac{\partial \alpha_1}{\partial x}\right|\ , \qquad \lambda^{'} = \lambda + \frac{Z_1 Z_2}{Z_1+Z_2}\left|\frac{\partial \alpha_1}{\partial x}\right|\ .$$

Noticing that the left hand side of the last equation of system (8.3) is exactly equal to

$$\alpha_k \rho_k \Gamma_k T_k \frac{\mathrm{D}_k s_k}{\mathrm{D}t}\ ,$$

we easily derive the entropy evolution equation for phase k :

$$\alpha_k \rho_k T_k \frac{\mathrm{D}_k s_k}{\mathrm{D}t} = \frac{Z_{k'}}{Z_1+Z_2}\,\lambda\, u_r^2 + \frac{Z_k}{Z_1+Z_2}\,\mu\,\pi_r^2 + \frac{Z_k}{(Z_1+Z_2)^2}\left|\frac{\partial \alpha_k}{\partial x}\right|\left(Z_{k'}\,u_r + \mathrm{sgn}\left(\frac{\partial \alpha_k}{\partial x}\right)\pi_r\right)^2\ ,$$

which clearly shows that non negative entropy production is ensured for each phase k. Obviously, non negative entropy production of the mixture is consequently guaranteed.

8.2 Supplementary important equations

8.2.1 Equation for u_r

Combining the phase velocity equations of system (8.3), results in the following equation for $u_r = u_1 - u_2$:

$$\frac{\partial u_r}{\partial t} + \frac{\partial\left[u_r\left(u - \frac{Y_r}{2}\,u_r\right)\right]}{\partial x} = \frac{1}{\rho\, Y_1 Y_2}\left(Y_1\,\frac{\partial(\alpha_2 P_2)}{\partial x} - Y_2\,\frac{\partial(\alpha_1 P_1)}{\partial x} + \pi_I{}^{'} - \lambda^{'}\,u_r\right)\ . \tag{8.4}$$

This last relation, which has been obtained without any assumption, is important for the determination of the Darcy type law, that will be determined around the mechanical equilibrium limit.

8.2.2 Mixture equations

From system (8.1), we can esily derive the following mixture equations for mass ρ, momentum $(\rho\, u)$ and total energy E, in a conservative form :

$$\begin{aligned}
&\frac{\partial \rho}{\partial t} + \frac{\partial(\rho\, u)}{\partial x} = 0\ ,\\
&\frac{\partial(\rho\, u)}{\partial t} + \frac{\partial\left(\rho\, u^2 + P + \rho\, Y_1 Y_2 u_r^2\right)}{\partial x} = 0\ ,\\
&\frac{\partial(\rho\, E)}{\partial t} + \frac{\partial\left[(\rho\, E + P)\ u + \rho\, Y_1 Y_2 u_r H_r\right]}{\partial x} = 0\ ,
\end{aligned} \tag{8.5}$$

where

$$\left\{\begin{array}{l}
\rho = \alpha_1\rho_1 + \alpha_2\rho_2 \ , \quad P = \alpha_1 P_1 + \alpha_2 P_2 \ , \\[2ex]
u = Y_1 u_1 + Y_2 u_2 \ , \quad Y_k = \dfrac{(\alpha_k\rho_k)}{\rho} \ , \\[2ex]
E = \mathcal{E} + \dfrac{1}{2}\left(u^2 + Y_1 Y_2 u_r^2\right) \ , \ \mathcal{E} = e + B \ , \\[2ex]
e = Y_1 e_1 + Y_2 e_2 \ , \quad B = Y_1 B_1 + Y_2 B_2 \ , \\[2ex]
H_r = H_1 - H_2 \ , \quad H_k = E_k + \dfrac{P_k}{\rho_k} \ ,
\end{array}\right. \tag{8.6}$$

respectively define the mixture mass, pressure, velocity, phase k mass fraction, mixture total energy, mixture total internal energy, mixture internal energy, mixture compaction energy, total phase enthalpy difference and phase k total enthalpy. Note that because of the mixture and phase mass conservations, and for any flow variable f, we have

$$\left\{\begin{array}{l}
\dfrac{\partial(\rho\, f)}{\partial t} + \dfrac{\partial\left((\rho\, f)\, u\right)}{\partial x} = \rho\, \dfrac{\mathrm{D}f}{\mathrm{D}t} \ , \\[2ex]
\dfrac{\partial(\alpha_k\rho_k f)}{\partial t} + \dfrac{\partial\left((\alpha_k\rho_k f\, u_k)\right)}{\partial x} = (\alpha_k\rho_k)\, \dfrac{\mathrm{D}_k f}{\mathrm{D}t} \ ,
\end{array}\right. \tag{8.7}$$

and in the particular case $f = Y_1 f_1 + Y_2 f_2$, we get

$$\begin{array}{c}
\dfrac{\partial(\alpha\rho f)_1 + (\alpha\rho f)_2}{\partial t} + \dfrac{\partial\left((\alpha\rho f u)_1 + (\alpha\rho f u)_2\right)}{\partial x} = (\alpha\rho)_1\, \dfrac{\mathrm{D}_1 f_1}{\mathrm{D}t} + (\alpha\rho)_2\, \dfrac{\mathrm{D}_2 f_2}{\mathrm{D}t} = \\[2ex]
\dfrac{\partial(\rho\, f)}{\partial t} + \dfrac{\partial\left(\rho\, f\, u + \rho\, Y_1 Y_2 u_r f_r\right)}{\partial x} \ .
\end{array} \tag{8.8}$$

Relations (8.7)–(8.8) are written down here because they will be used many times in this report.

The term

$$\frac{1}{2}\, Y_1 Y_2 u_r^2 \,,$$

represents a *turbulent energy* due to the relative motion, while the term

$$\rho\, Y_1 Y_2 u_r^2 \,,$$

represents the corresponding associated *turbulent pressure*. Note that those *turbulent* terms appear *naturally* as just a consequence of accounting for the relative velocity u_r. The mass equation of phase k can therefore be rewritten equivalently either by ($k = 1\,,\,2$) :

$$\frac{\partial(\alpha_k \rho_k)}{\partial t} + \frac{\partial\left(\alpha_k \rho_k\, u + \delta_k \rho\, Y_1 Y_2 u_r\right)}{\partial x} = 0 \,, \tag{8.9}$$

or in terms of the mass fraction $Y_k = (\alpha\,\rho)_k/\rho$ $(Y_1 + Y_2 = 1)$ by

$$\rho\, \frac{\mathrm{D}Y_k}{\mathrm{D}t} = -\delta_k\, \frac{\partial\left(\rho\, Y_1 Y_2 u_r\right)}{\partial x} \,. \tag{8.10}$$

We can deduce the mixture total internal energy equation, from the mixture total energy equation given in (8.5) :

$$\rho\, \frac{\mathrm{D}\mathcal{E}}{\mathrm{D}t} + P\, \frac{\partial u}{\partial x} + \frac{\partial\left(\rho\, Y_1 Y_2 u_r \mathcal{H}_r\right)}{\partial x} = -\rho\, Y_1 Y_2 u_r \left\{ \frac{\partial u_r}{\partial t} + \frac{\partial\left(u_r\left[u - \frac{Y_r}{2}\, u_r\right]\right)}{\partial x} \right\} \,, \tag{8.11}$$

where

$$\mathcal{H}_r = \mathcal{H}_1 - \mathcal{H}_2 \,, \qquad \mathcal{H}_k = h_k + B_k \,, \qquad h_k = e_k + \frac{P_k}{\rho_k} \,.$$

8.2.3 Entropy equations

With the notations used before, it can be shown that the entropy equation for phase k can be rewritten by ($k = 1\,,\,2$) :

$$\frac{\partial(\alpha\rho s)_k}{\partial t} + \frac{\partial\left((\alpha\rho s)_k u + \delta_k \rho\, Y_1 Y_2 u_r s_k\right)}{\partial x} =$$
$$\frac{1}{T_k}\left(\frac{Z_{k'}}{Z_1 + Z_2}\, \lambda\, u_r^2 + \frac{Z_k}{Z_1 + Z_2}\, \mu\, \pi_r^2 + \frac{Z_k}{(Z_1 + Z_2)^2} \left|\frac{\partial \alpha_k}{\partial x}\right| \left(Z_{k'}\, u_r + \mathrm{sgn}\left(\frac{\partial \alpha_k}{\partial x}\right) \pi_r \right)^2 \right) \,. \tag{8.12}$$

and the mixture entropy equation by ($s = Y_1 s_1 + Y_2 s_2$) :

$$\frac{T_m}{2}\left[\frac{\partial(\rho\, s)}{\partial t} + \frac{\partial\left[\rho\, \left(s\, u + Y_1 Y_2 u_r s_r\right)\right]}{\partial x} \right] =$$
$$\left(\bar{\tau}\, \lambda'\, u_r^2 + (1 - \bar{\tau})\, \mu'\, \pi_r^2 \right) - 2\, \frac{Z_1 Z_2}{(Z_1 + Z_2)^2}\, u_r \pi_r \tau_r \frac{\partial \alpha_1}{\partial x} \,, \tag{8.13}$$

where

$$T_m = 2\left(\frac{1}{T_1}+\frac{1}{T_2}\right)^{-1} ,$$
$$\tau_k = \frac{T_k}{T_1+T_2} , \quad \tau_r = \tau_1 - \tau_2 , \tag{8.14}$$
$$\bar{\tau} = \frac{\bar{T}}{\bar{T}+\tilde{T}} , \quad \bar{T} = \frac{Z_1T_1+Z_2T_2}{Z_1+Z_2} , \quad \tilde{T} = \frac{Z_2T_1+Z_1T_2}{Z_1+Z_2} ,$$

respectively represent a global mixture temperature (T_m), an average coefficient (τ_k) defined from the phase temperatures T_k , the average coefficient difference τ_r , a mixture average coefficient ($\bar{\tau}$) defined from the mixture temperatures $\bar{T}$ and $\tilde{T}$ themselves defined as averaging the phase temperatures T_k with the averaging impedance coefficients $Z_k/(Z_1+Z_2)$. Note that

$$\bar{T}+\tilde{T} = T_1+T_2 , \qquad \bar{\tau} = \frac{Z_1\tau_1+Z_2\tau_2}{Z_1+Z_2} , \qquad 2\,\frac{\bar{\tau}}{T_m} = \frac{Z_2}{Z_1+Z_2}\,\frac{1}{T_1} + \frac{Z_1}{Z_1+Z_2}\,\frac{1}{T_2} . \tag{8.15}$$

Those entropy equations, as written above, and again obtained without any sort of approximation, will be usefull for expressing the volume fraction evolution equation of the reduced model resulting from the asymptotic analysis presented in the following subsection.

8.2.4 Internal energy equations

In this subsection, we give the formulations of the phase internal energy equations since they will be needed later and also because their expressions will differ according to the approach chosen to determine the RHS of $\mathrm{D}(\alpha_1)/\mathrm{D}t$.
From the phase total energy equations in (8.1), after some calculations, it can be shown that the phase internal energy equations may be expressed under the following form ($k=1\,,2$) :

$$\frac{\partial(\alpha\rho e)_k}{\partial t} + \frac{\partial\left((\alpha\rho e)_k u\right)}{\partial x} + \delta_k\frac{\partial}{\partial x}\left(\rho\, Y_1Y_2u_re_k\right) + (\alpha P)_k\frac{\partial u}{\partial x} + \delta_k P_k\frac{\partial}{\partial x}\left(\frac{\rho\, Y_1Y_2u_r}{\rho_k}\right) =$$
$$\frac{Z_{k'}}{Z_1+Z_2}\,\lambda'\,u_r^2 - \delta_k\left(P_k - \delta_k\frac{Z_k}{Z_1+Z_2}\,\pi_r\right)\frac{\mathrm{D}\alpha_1}{\mathrm{D}t} + \frac{Z_k}{Z_1+Z_2}\left(Y_{k'} + \frac{Z_{k'}}{Z_1+Z_2}\right)\pi_r u_r\frac{\partial\alpha_k}{\partial x} . \tag{8.16}$$

8.3 Asymptotic analysis

The asymptotic analysis presented hereafter mainly follows the lines of Kapila et al. [15]. Each flow variable f is assumed to be smooth enough to possess the following stable asymptotic expansion

$$f = \bar{f} + \mathrm{o}(\epsilon^2) , \;\; \bar{f} = f^{(0)} + \epsilon\, f^{(1)} ,$$

where $f^{(0)}$ represent the mechanical equilibrium state of f and $f^{(1)}$ a small perturbation close around that equilibrium state. Conversely, the mechanical relaxation parameters are assumed to be stiff,

namely :

$$\mu^{'} = \frac{\mu_0}{\epsilon} \quad , \; 0 < \mu_0 = \text{cste} < +\infty \; ,$$
$$\lambda^{'} = \frac{\lambda_0}{\epsilon} \quad , \; 0 < \lambda_0 = \text{cste} < +\infty \; .$$

With these assumptions and notations, we get that, for the asymptotic expansion to be stable, and since $\mathrm{o}(\epsilon^{-1})$ term appears when inserting in (8.3), the following mechanical equilibrium constraints have to be held :

$$\left\{ \begin{array}{l} \pi_1^{(0)} = \pi_2^{(0)} = \pi^{(0)} \; , \\ u_1^{(0)} = u_2^{(0)} = u^{(0)} \; , \text{ or equivantly } u_r^{(0)} = 0 \; , \end{array} \right. \tag{8.17}$$

where $\pi^{(0)} = (\alpha_1 \pi_1)^0 + (\alpha_2 \pi_2)^0$.
The Darcy type law is obtained from the zero expansion of the relative velocity equation (8.4) :

$$\lambda_0 \, u_r^{(1)} = Y_1^{(0)} \, \frac{\partial (\alpha_2 P_2)^{(0)}}{\partial x} - Y_2^{(0)} \, \frac{\partial (\alpha_1 P_1)^{(0)}}{\partial x} + \pi^{(0)} \, \frac{\partial \alpha_1^{(0)}}{\partial x} \; . \tag{8.18}$$

With the help of (8.17) and the mixture pressure definition, (8.18) may be rewritten as

$$u_r^{(1)} = \frac{1}{\lambda_0} \left((\alpha_1 - Y_1)^{(0)} \, \frac{\partial P^{(0)}}{\partial x} - \alpha_2^{(0)} \, \frac{\partial (\alpha_1 \beta_1)^{(0)}}{\partial x} + \alpha_1^{(0)} \, \frac{\partial (\alpha_2 \beta_2)^{(0)}}{\partial x} \right) \; .$$

The first order expansion of the relative velocity $\bar{u}_r$ may therefore be expressed by

$$\bar{u}_r = u_r^{(0)} + \epsilon \, u_r^{(1)} = \frac{1}{\lambda^{'}} \left((\alpha_1 - Y_1)^{(0)} \, \frac{\partial P^{(0)}}{\partial x} - \alpha_2^{(0)} \, \frac{\partial (\alpha_1 \beta_1)^{(0)}}{\partial x} + \alpha_1^{(0)} \, \frac{\partial (\alpha_2 \beta_2)^{(0)}}{\partial x} \right) \; , \tag{8.19}$$

with $\lambda^{'} = \dfrac{\lambda_0}{\epsilon}$. Note that relation (8.19) has another equivalent expression, which will be used later and written down hereafter (we omit the (0) index and set $u_r = \bar{u}_r$) :

$$u_r = \frac{1}{\lambda^{'}} \left((Y_1 - \alpha_1) \, \frac{\partial \pi}{\partial x} - Y_2 \frac{\partial (\alpha_1 \beta_1)}{\partial x} + Y_1 \frac{\partial (\alpha_2 \beta_2)}{\partial x} \right) \; . \tag{8.20}$$

Finally, neglecting all $\mathrm{o}(\epsilon^2)$ terms, we can formulate the following reduced flow model accounting for permeation effects, which is obtained from solving for the first order expansion of the flow variables (here, no overlined variables are written to enlight the notations; $k = 1 \, , \, 2$) :

$$\begin{array}{l} \dfrac{\partial (\alpha \rho)_k}{\partial t} + \dfrac{\partial \left((\alpha \rho)_k \, u \right)}{\partial x} + \delta_k \, \dfrac{\partial \left(\rho \, Y_1 Y_2 u_r \right)}{\partial x} = 0 \; , \\ \dfrac{\partial (\rho \, u)}{\partial t} + \dfrac{\partial \left(\rho \, u^2 + P \right)}{\partial x} = 0 \; , \\ \dfrac{\partial (\rho \, E)}{\partial t} + \dfrac{\partial \left[(\rho \, E + P) \, u + \rho \, Y_1 Y_2 u_r H_r \right]}{\partial x} = 0 \; , \end{array} \tag{8.21}$$

with

$$\left\{\begin{array}{l} u_r = \dfrac{1}{\lambda'}\left((\alpha_1 - Y_1)\dfrac{\partial P}{\partial x} - \alpha_2\dfrac{\partial(\alpha_1\beta_1)}{\partial x} + \alpha_1\dfrac{\partial(\alpha_2\beta_2)}{\partial x}\right) , \\ \pi_1 = \pi_2 , \\ E = \mathcal{E} + \dfrac{1}{2}u^2 , \quad P = \alpha_1 P_1 + \alpha_2 P_2 , \\ \mathcal{E} = Y_1\mathcal{E}_1 + Y_2\mathcal{E}_2 , \quad \mathcal{E}_k = e_k + B_k . \end{array}\right. \tag{8.22}$$

Remark 8.1 *Note that both the* turbulent pressure $\left(\rho\, Y_1 Y_2 u_r^2\right)$ *and* turbulent energy $\left((Y_1 Y_2 u_r^2)/2\right)$ *are absent in the above system; this is due to the mechanical equilibrium constraint* $u_r^{(0)} = 0$ *and the relation* $(u_r^2)^{(1)} = 2\, u_r^{(1)}\, u_r^{(0)} = 0$ *, leading to* $\overline{u_r^2} = (u_r^2)^{(0)} + \epsilon\,(u_r^2)^{(1)} = 0$ *.*

Remark 8.2 *The above reduced model is the result of considering first order velocity, zero order pressure state variables in the full non–equilibrium* parent *model (8.1), (8.5).*

System (8.21)–(8.22) is not closed as temperature disequilibrium is present. Closure of that system requires the determination of an appropriate volume fraction equation, that should be in accordance with the entropy inequality requirement. We will show in the following section that this can be done consistently w.r.t. the full disequilibrium *parent* model (8.1), (8.5). Before that, we write down the following mixture entropy equation directly deduced from (8.13) which becomes, with the same asymptotic analysis and mechanical equilibrium constraints :

$$\begin{array}{c} \dfrac{T_m}{2}\left[\dfrac{\partial(\rho s)}{\partial t} + \dfrac{\partial\left((\rho\, s\, u) + \rho\, Y_1 Y_2 u_r s_r\right)}{\partial x}\right] = \dfrac{T_m}{2}\left[\rho\,\dfrac{\mathrm{D}s}{\mathrm{D}t} + \dfrac{\partial(\rho\, Y_1 Y_2 u_r s_r)}{\partial x}\right] = \\ \dfrac{T_m}{2}\left[(\alpha_1\rho_1)\,\dfrac{\mathrm{D}_1 s_1}{\mathrm{D}t} + (\alpha_2\rho_2)\,\dfrac{\mathrm{D}_2 s_2}{\mathrm{D}t}\right] = \overline{\tau}\,\lambda'\, u_r^2 \; ; \end{array} \tag{8.23}$$

the phase entropy equation, initially derived from (8.12), becomes

$$(\alpha_k\rho_k)\,\frac{\mathrm{D}_k s_k}{\mathrm{D}t} = \frac{1}{T_k}\,\frac{Z_{k'}}{Z_1 + Z_2}\,\lambda'\, u_r^2 \; . \tag{8.24}$$

8.4 Volume fraction and entropy equations

Determination of the volume fraction equation as done by Saurel et al. [33], consists in deriving the (phase and mixture) entropy equations from a system made of

- the mixture total internal energy equation expressed in terms of both phase entropy and volume fraction evolution equations, which is directly deduced from the system of conservation laws of the reduced model (8.21);
- the differentiation of the mechanical equilibrium constraint, $\pi_1 = \pi_2$, along a trajectory, which is also expressed in terms of phase entropy and volume fraction equations.

We then end up with a system of two phase entropy evolution equations that can be solved and expressed in terms of the volume fraction equation. Once this is done, we are able to write down the mixture entropy equation, the terms of which are analyzed to be in accordance to the mixture entropy production requirement. This physical constraint naturally leads us to an admissible definition of the volume fraction evolution equation. This admissible definition is therefore deduced from a sufficient condition. In the present report, determination of that evolution equation is done by adding the mixture entropy equation which is directly derived from the previous asymptotic analysis, that is equation (8.23).

8.4.1 Energy conservation constraint

We get the following mixture total internal energy equation from either asymptotic development as previously defined (droping all $\mathrm{o}(\epsilon^2)$ terms in the *parent* equation (8.11)), or directly from the total energy equation and mass and momentum equations in the reduced model with permeation (8.21):

$$\rho\,\frac{\mathrm{D}\mathcal{E}}{\mathrm{D}t} + P\,\frac{\partial u}{\partial x} + \frac{\partial\left(\rho\,Y_1Y_2u_r\mathcal{H}_r\right)}{\partial x} = 0\,. \tag{8.25}$$

Using configuration energy definition (2.18), and reduced equation for Y_1 which has the same form as given by (8.10), to find the evolution equation for $B = Y_1B_1 + Y_2B_2$, and definition of $e = Y_1e_1 + Y_2e_2$ with relations ($k = 1\,,\,2$) :

$$\mathrm{d}e_k = \frac{P_k}{\rho_k^2} + T_k\mathrm{d}s_k\ ,$$

and equations

$$\alpha_k\left(\frac{\mathrm{D}\rho_k}{\mathrm{D}t} + \rho_k\,\frac{\partial u}{\partial x}\right) = -\delta_k\left[\rho_k\frac{\mathrm{D}\alpha_1}{\mathrm{D}t} + \frac{\partial\left(\rho\,Y_1Y_2u_r\right)}{\partial x}\right]\ ,$$

with definition $P = \alpha_1P_1 + \alpha_2P_2 = \pi + \beta$, to find the evolution equation for e, we have

$$\left\{\begin{array}{l}\rho\,\dfrac{\mathrm{D}B}{\mathrm{D}t} = \beta_r\dfrac{\mathrm{D}\alpha_1}{\mathrm{D}t} - B_r\dfrac{\partial\left(\rho\,Y_1Y_2u_r\right)}{\partial x}\ ,\\[2ex] \rho\,\dfrac{\mathrm{D}e}{\mathrm{D}t} = -P\dfrac{\partial u}{\partial x} - P_r\dfrac{\mathrm{D}\alpha_1}{\mathrm{D}t} - h_r\dfrac{\partial\left(\rho\,Y_1Y_2u_r\right)}{\partial x} + (\alpha\rho T)_1\dfrac{\mathrm{D}s_1}{\mathrm{D}t} + (\alpha\rho T)_2\dfrac{\mathrm{D}s_2}{\mathrm{D}t}\ ;\end{array}\right. \tag{8.26}$$

where $h_r = h_1 - h_2$, $h_k = e_k + \dfrac{P_k}{\rho_k}$. So we get, for $\mathcal{E}$, the following additional equation

$$\rho\,\frac{\mathrm{D}\mathcal{E}}{\mathrm{D}t} = -P\,\frac{\partial u}{\partial x} - \pi_r\frac{\mathrm{D}\alpha_1}{\mathrm{D}t} - \mathcal{H}_r\frac{\partial\left(\rho\,Y_1Y_2u_r\right)}{\partial x} + (\alpha\rho T)_1\frac{\mathrm{D}s_1}{\mathrm{D}t} + (\alpha\rho T)_2\frac{\mathrm{D}s_2}{\mathrm{D}t}\ ; \tag{8.27}$$

using now the mechanical equilibrium relation $\pi_r = 0$ and equations (8.25) and (8.27) leads us to the following relation, linking together the phase entropy evolution equations :

$$(\alpha\rho T)_1\frac{\mathrm{D}s_1}{\mathrm{D}t} + (\alpha\rho T)_2\frac{\mathrm{D}s_2}{\mathrm{D}t} = -\rho\,Y_1Y_2u_r\frac{\partial\mathcal{H}_r}{\partial x}\ . \tag{8.28}$$

Noticing now that

$$\frac{\partial \mathcal{H}_r}{\partial x} = \frac{\partial h_r}{\partial x} + \left(\frac{\beta_1}{(\alpha\rho)_1} + \frac{\beta_2}{(\alpha\rho)_2} \right) \frac{\partial \alpha_1}{\partial x} \ ,$$

and that

$$\frac{\mathrm{D} s_k}{\mathrm{D} t} = \frac{\mathrm{D}_k s_k}{\mathrm{D} t} - \delta_k Y_{k'} u_r \frac{\partial s_k}{\partial x} \ ,$$

allow us to write

$$\begin{aligned} (\alpha\rho T)_1 \frac{\mathrm{D}_1 s_1}{\mathrm{D} t} + (\alpha\rho T)_2 \frac{\mathrm{D}_2 s_2}{\mathrm{D} t} = & - \left(Y_2 \beta_1 + Y_1 \beta_2 \right) \, u_r \frac{\partial \alpha_1}{\partial x} \\ & + \rho \, Y_1 Y_2 u_r \left[\left(T_1 \frac{\partial s_1}{\partial x} - \frac{\partial h_1}{\partial x} \right) - \left(T_2 \frac{\partial s_2}{\partial x} - \frac{\partial h_2}{\partial x} \right) \right] \ . \end{aligned} \tag{8.29}$$

Using now again the mechanical equilibrium $\pi_1 = \pi_2 = \pi$ and relation

$$T_k \frac{\partial s_k}{\partial x} - \frac{\partial h_k}{\partial x} = - \frac{1}{\rho_k} \, \frac{\partial P_k}{\partial x} \ ,$$

in (8.29), and noticing $\alpha_1 Y_2 - \alpha_2 Y_1 = \alpha_1 - Y_1$, we finally get

$$(\alpha\rho T)_1 \frac{\mathrm{D}_1 s_1}{\mathrm{D} t} + (\alpha\rho T)_2 \frac{\mathrm{D}_2 s_2}{\mathrm{D} t} = u_r \left[\left(Y_1 - \alpha_1 \right) \frac{\partial \pi}{\partial x} - Y_2 \frac{\partial (\alpha_1 \beta_1)}{\partial x} + Y_1 \frac{\partial (\alpha_2 \beta_2)}{\partial x} \right] \ ;$$

but since u_r is defined by (8.20), equation (8.29) is finally equivalent to the following relation

$$(\alpha\rho T)_1 \frac{\mathrm{D}_1 s_1}{\mathrm{D} t} + (\alpha\rho T)_2 \frac{\mathrm{D}_2 s_2}{\mathrm{D} t} = \lambda' \, u_r^2 \ . \tag{8.30}$$

8.4.2 Mechanical equilibrium constraint

The mechanical equilibrium constraint reads as

$$P_1(\rho_1, s_1) - \beta_1(\alpha_1, \rho_1) = P_2(\rho_2, s_2) - \beta_2(\alpha_2, \rho_2) \ .$$

Differentiating this relation along the trajectory line $\mathrm{d}x/\mathrm{d}t = u$, and since, for all $k = 1 \, , \, 2$ we have

$$\frac{\mathrm{D}\pi_k}{\mathrm{D} t} = \frac{\mathrm{D} P_k}{\mathrm{D} t} - \frac{\mathrm{D}\beta_k}{\mathrm{D} t} = \left(\beta_k - \rho_k c_k^2 \right) \frac{\partial u}{\partial x} + \frac{\delta_k}{(\alpha\rho)_k} \left(\rho_k c_k^2 - \beta_k \right) \rho \, \frac{\mathrm{D} Y_1}{\mathrm{D} t} - \delta_k \frac{\rho_k}{\alpha_k} \, \mathcal{C}_k^2 \, \frac{\mathrm{D}\alpha_1}{\mathrm{D} t} + \rho_k \Gamma_k T_k \frac{\mathrm{D} s_k}{\mathrm{D} t} \ ,$$

with

$$c_k^2 = \left. \frac{\partial P_k}{\partial \rho_k} \right|_{s_k} \ , \qquad \left. \frac{\partial P_k}{\partial s_k} \right|_{\rho_k} = \rho_k \Gamma_k T_k \ , \qquad \mathcal{C}_k^2 = c_k^2 + \alpha_k^2 \, \frac{\mathrm{d}^2 B_k}{\mathrm{d}{\alpha_k}^2} \ ,$$

we get

$$(\rho \, \Gamma T)_1 \frac{\mathrm{D} s_1}{\mathrm{D} t} - (\rho \, \Gamma T)_2 \frac{\mathrm{D} s_2}{\mathrm{D} t} = \mathbb{A} \, \frac{\mathrm{D}\alpha_1}{\mathrm{D} t} - \mathbb{B} \ , \tag{8.31}$$

with

$$\left\{\begin{array}{l} \mathbb{A} = \dfrac{\rho_1 \mathcal{C}_1^2}{\alpha_1} + \dfrac{\rho_2 \mathcal{C}_2^2}{\alpha_2} \ , \\ \mathbb{B} = \left(\displaystyle\sum_{k=1}^{2} \delta_k (\beta_k - \rho_k c_k^2) \right) \dfrac{\partial u}{\partial x} + \left(\displaystyle\sum_{k=1}^{2} \dfrac{\rho_k c_k^2 - \beta_k}{\alpha_k \rho_k} \right) \rho \, \dfrac{\mathrm{D} Y_1}{\mathrm{D} t} \ . \end{array}\right. \tag{8.32}$$

Relation (8.31) may be equivalently expressed in terms of $\mathrm{D}_k(s_k)/\mathrm{D}t$, as done for relation (8.28) to (8.29), which is :

$$(\rho \, \Gamma T)_1 \frac{\mathrm{D}_1 s_1}{\mathrm{D}t} - (\rho \, \Gamma T)_2 \frac{\mathrm{D}_2 s_2}{\mathrm{D}t} = \mathbb{A} \, \frac{\mathrm{D}\alpha_1}{\mathrm{D}t} - \mathbb{B}^{'} \ , \tag{8.33}$$

with

$$\mathbb{B}^{'} = \mathbb{B} - \rho \, Y_1 Y_2 u_r \left(\frac{\Gamma_1}{\alpha_1} T_1 \frac{\partial s_1}{\partial x} + \frac{\Gamma_2}{\alpha_2} T_2 \frac{\partial s_2}{\partial x} \right) \ . \tag{8.34}$$

We have therefore got a second relation (8.33) with definitions of $\mathbb{A}$ and $\mathbb{B}$ given by (8.32), and definition of $\mathbb{B}^{'}$ given by (8.34), linking again the two phase entropy evolution equations together.

8.4.3 Resolution of system (8.30)–(8.33), with definitions (8.32) and (8.34)

We are now given the following system

$$\left\{\begin{array}{l} (\alpha \rho T)_1 \dfrac{\mathrm{D}_1 s_1}{\mathrm{D}t} + (\alpha \rho T)_2 \dfrac{\mathrm{D}_2 s_2}{\mathrm{D}t} = \lambda^{'} u_r^2 \ , \\ (\rho \, \Gamma T)_1 \dfrac{\mathrm{D}_1 s_1}{\mathrm{D}t} - (\rho \, \Gamma T)_2 \dfrac{\mathrm{D}_2 s_2}{\mathrm{D}t} = \mathbb{A} \, \dfrac{\mathrm{D}\alpha_1}{\mathrm{D}t} - \mathbb{B}^{'} \ , \end{array}\right. \tag{8.35}$$

with definitions of $\mathbb{A}$, $\mathbb{B}$ and $\mathbb{B}^{'}$ given by (8.32) and (8.34). Since $\alpha_2 \Gamma_1 + \alpha_1 \Gamma_2 \neq 0$, system (8.35) possesses a unique solution which is

$$\left\{\begin{array}{l} (\alpha \rho)_1 \dfrac{\mathrm{D}_1 s_1}{\mathrm{D}t} = \dfrac{\alpha_1}{\Gamma_1} \dfrac{\Gamma}{T_1} \left(\lambda^{'} \, u_r^2 + \dfrac{\alpha_2}{\Gamma_2} \left(\mathbb{A} \, \dfrac{\mathrm{D}\alpha_1}{\mathrm{D}t} - \mathbb{B}^{'} \right) \right) \ , \\ (\alpha \rho)_2 \dfrac{\mathrm{D}_2 s_2}{\mathrm{D}t} = \dfrac{\alpha_2}{\Gamma_2} \dfrac{\Gamma}{T_2} \left(\lambda^{'} \, u_r^2 - \dfrac{\alpha_1}{\Gamma_1} \left(\mathbb{A} \, \dfrac{\mathrm{D}\alpha_1}{\mathrm{D}t} - \mathbb{B}^{'} \right) \right) \ , \end{array}\right. \tag{8.36}$$

where

$$\Gamma = \left(\frac{\alpha_1}{\Gamma_1} + \frac{\alpha_2}{\Gamma_2} \right)^{-1} \ . \tag{8.37}$$

8.4.4 Volume fraction evolution equation

In the previous subsection, we have expressed the s_k's evolution equations in terms of $\mathrm{D}\alpha_1/\mathrm{D}t$ that remains to be determined. The usual way to do so, is to write down the equation for the mixture

entropy equation. Since no mass nor heat transfers are assumed in this framework, we know, using property (8.8) for $s = Y_1 s_1 + Y_2 s_2$, that

$$\frac{\partial(\rho\, s)}{\partial t} + \frac{\partial\left(\rho\, s\, u + \rho\, Y_1 Y_2 u_r s_r\right)}{\partial x} = \alpha_1 \rho_1 \frac{\mathrm{D}_1 s_1}{\mathrm{D}t} + \alpha_2 \rho_2 \frac{\mathrm{D}_2 s_2}{\mathrm{D}t} \ ,$$

therefore, using the expressions given by (8.36), we obtain the following equation for s

$$\frac{\partial(\rho\, s)}{\partial t} + \frac{\partial\left(\rho\, s\, u + \rho\, Y_1 Y_2 u_r s_r\right)}{\partial x} = \Gamma \left[\left(\frac{\alpha_1}{(\Gamma T)_1} + \frac{\alpha_2}{(\Gamma T)_2} \right) \lambda^{'} u_r^2 - \frac{\alpha_1}{(\Gamma T)_1} \frac{\alpha_2}{(\Gamma T)_2} T_r \left(\mathbb{A} \frac{\mathrm{D}\alpha_1}{\mathrm{D}t} - \mathbb{B}^{'} \right) \right] . \tag{8.38}$$

We give in what follows two ways of defining $\mathrm{D}\alpha_1/\mathrm{D}t$.

1. A SUFFICIENT CONDITION TO DEFINE $\dfrac{\mathrm{D}\alpha_1}{\mathrm{D}t}$

   The usual way to determine $\mathrm{D}\alpha_1/\mathrm{D}t$ is to ensure positivity of the right hand side (RHS) of the above equation (8.38). Since the first term of this RHS is obviously non negative, positivity is preserved under the sufficient condition defined by assuming the second term of this RHS to be zero. In that case, we ensure a physically acceptable sub-model, (non negative entropy production), while defining at the same time $\mathrm{D}\alpha_1/\mathrm{D}t$, therefore ending and closing the sub-model with permeation derived from asymptotic analysis of the full non equilibrium model (8.1), (8.5). As a matter of fact, annihilating the second term of the RHS of (8.38), gives us the following definition for the volume fraction evolution equation :

$$\begin{aligned} \frac{\mathrm{D}\alpha_1}{\mathrm{D}t} &= \frac{\mathbb{B}^{'}}{\mathbb{A}} \ , \\ &= \frac{\displaystyle\sum_{k=1}^{2} \left[\delta_k \left(\beta_k - \rho_k c_k^2 \right) \frac{\partial u}{\partial x} - \frac{\rho_k c_k^2 - \beta_k}{\alpha_k \rho_k} \frac{\partial\left(\rho\, Y_1 Y_2 u_r\right)}{\partial x} - \rho\, Y_1 Y_2 u_r \frac{(\Gamma T)_k}{\alpha_k} \frac{\partial s_k}{\partial x} \right]}{\dfrac{\rho_1 \mathcal{C}_1^2}{\alpha_1} + \dfrac{\rho_2 \mathcal{C}_2^2}{\alpha_2}} \ . \end{aligned} \tag{8.39}$$

   Defining the generalized Wood speed of sound $\mathcal{C}_W$ by

$$\frac{1}{\rho\, \mathcal{C}_W^2} = \frac{\alpha_1}{\rho_1 \mathcal{C}_1^2} + \frac{\alpha_1}{\rho_1 \mathcal{C}_1^2} = \frac{\alpha_1 \alpha_2}{\rho_1 \mathcal{C}_1^2\, \rho_2 \mathcal{C}_2^2} \left(\frac{\rho_1 \mathcal{C}_1^2}{\alpha_1} + \frac{\rho_2 \mathcal{C}_2^2}{\alpha_2} \right) \ , \tag{8.40}$$

   equation (8.39), has the following alternative writing

$$\begin{aligned} \frac{\mathrm{D}\alpha_1}{\mathrm{D}t} = \rho\, \mathcal{C}_W^2 \frac{\alpha_1 \alpha_2}{\rho_1 \mathcal{C}_1^2\, \rho_2 \mathcal{C}_2^2} \Bigg\{ & \left[\sum_{k=1}^{2} \delta_k \left(\beta_k - \rho_k c_k^2 \right) \right] \frac{\partial u}{\partial x} - \left(\sum_{k=1}^{2} \frac{\rho_k c_k^2 - \beta_k}{\alpha_k \rho_k} \right) \frac{\partial\left(\rho\, Y_1 Y_2 u_r\right)}{\partial x} \\ & - \rho\, Y_1 Y_2 u_r \left(\sum_{k=1}^{2} \frac{\Gamma_k T_k}{\alpha_k} \frac{\partial s_k}{\partial x} \right) \Bigg\} \ . \end{aligned} \tag{8.41}$$

2. A CONSISTENT WAY TO DEFINE $\dfrac{\mathrm{D}\alpha_1}{\mathrm{D}t}$

We present here another way to define the volume fraction evolution equation by using another equation which is in fact already available. As a matter of fact, equation (8.23) is the expression of the mixture entropy equation directly derived from asymptotic analysis. So, to preserve consistency, it should coincide to equation (8.38), that is, the RHS of (8.23) has to be equal to the one of (8.38) :

$$2\,\frac{\bar{\tau}}{T_m}\,\lambda^{'}u_r^2 = \Gamma\,\left[\left(\frac{\alpha_1}{\Gamma_1 T_1}+\frac{\alpha_2}{\Gamma_2 T_2}\right)\lambda^{'}u_r^2 - \frac{\alpha_1}{\Gamma_1 T_1}\,\frac{\alpha_2}{\Gamma_2 T_2}\,T_r\,\left(\mathbb{A}\frac{\mathrm{D}\alpha_1}{\mathrm{D}t}-\mathbb{B}^{'}\right)\right]\,. \tag{8.42}$$

Noticing that

$$2\,\frac{\bar{\tau}}{T_m} = \frac{Z_2}{Z_1+Z_2}\,\frac{1}{T_1}+\frac{Z_1}{Z_1+Z_2}\,\frac{1}{T_2}\,,$$

and since $T_r \neq 0$, we finally get a relation that can be written by

$$\mathbb{A}\,\frac{\mathrm{D}\alpha_1}{\mathrm{D}t}-\mathbb{B}^{'} = \left(\frac{Z_2}{Z_1+Z_2}\,\frac{\Gamma_1}{\alpha_1}-\frac{Z_1}{Z_1+Z_2}\,\frac{\Gamma_2}{\alpha_2}\right)\lambda^{'}u_r^2\,, \tag{8.43}$$

and we therefore get

$$\frac{\mathrm{D}\alpha_1}{\mathrm{D}t} = \frac{\mathbb{B}^{''}}{\mathbb{A}} \tag{8.44}$$

with

$$\mathbb{B}^{''} = \mathbb{B}^{'} + \left(\frac{Z_2}{Z_1+Z_2}\,\frac{\Gamma_1}{\alpha_1}-\frac{Z_1}{Z_1+Z_2}\,\frac{\Gamma_2}{\alpha_2}\right)\lambda^{'}u_r^2\,, \tag{8.45}$$

where $\mathbb{B}^{'}$ and $\mathbb{A}$ are defined by (8.34) and (8.32). If we fully replace these expressions by their value, we get

$$\begin{aligned}\frac{\mathrm{D}\alpha_1}{\mathrm{D}t} &= \rho\,\mathcal{C}_W^2\,\frac{\alpha_1\alpha_2}{\rho_1\mathcal{C}_1^2\,\rho_2\mathcal{C}_2^2}\left(\sum_{k=1}^{2}\delta_k(\beta_k-\rho_k c_k^2)\right)\frac{\partial u}{\partial x}\\ &+\rho\,\mathcal{C}_W^2\,\frac{\alpha_1\alpha_2}{\rho_1\mathcal{C}_1^2\,\rho_2\mathcal{C}_2^2}\left(\sum_{k=1}^{2}\frac{\rho_k c_k^2-\beta_k}{\alpha_k\rho_k}\right)\rho\,\frac{\mathrm{D}Y_1}{\mathrm{D}t}\\ &+\rho\,\mathcal{C}_W^2\,\frac{\alpha_1\alpha_2}{\rho_1\mathcal{C}_1^2\,\rho_2\mathcal{C}_2^2}\sum_{k=1}^{2}\frac{\Gamma_k}{\alpha_k}\left(-\rho\,Y_1Y_2u_rT_k\frac{\partial s_k}{\partial x}+\delta_k\,\frac{Z_{k'}}{Z_1+Z_2}\,\lambda^{'}u_r^2\right)\,.\end{aligned} \tag{8.46}$$

8.5 Some remarks

Remark 8.3 *If we compare definition (8.44) to definition (8.39), we see that the source term has been augmented by a term which is proportional to $\lambda^{'}u_r^2$, this term may be interpreted by being a dissipative entropy term difference due to friction, and is therefore not negligible when friction occurs.*

Remark 8.4 *Note that with this approach of defining the volume fraction evolution equation, which is unique w.r.t. to consistency with the* parent *model (8.1), (8.5), we end up with a reduced model which automatically preserves non negativity of (phase and mixture) entropy productions. As a matter of fact, it is easy to check that the phase-entropy equation of the sub-model as defined by (8.36), coincides with the reduced by asymptotic analysis equation obtained from the* parent *model equation (8.12), which reads*

$$\alpha_k \rho_k \frac{\mathrm{D}_k s_k}{\mathrm{D}t} = \frac{1}{T_k} \frac{Z_{k'}}{Z_1 + Z_2} \lambda^{'} u_r^2 \geq 0 \, , \forall \, k = 1 \, , 2 \, .$$

Remark 8.5 *It is interesting to compare the RHS of either equation (8.41) or equation (8.46), to the RHS of the volume fraction equation presented by Saurel et al. in [33]. In that equation, granular effects are not considered but we have (for two phases)*

- *mass transfer, denoted by $\dot{m}_1$ ($\dot{m}_2 = -\dot{m}_1$);*
- *heat transfers, between the interface (at temperature T_I) and the phases. Those terms are denoted by $\mathbb{H}_k \, (T_I - T_k)$, for $k = 1 \, , 2$, where the $\mathbb{H}_k$'s stand for the global heat transfer coefficients.*

We recall hereafter that volume fraction equation :

$$\begin{aligned} \frac{\mathrm{D}\alpha_1}{\mathrm{D}t} = \alpha_1 \alpha_2 \rho \, c_W^2 \left(\sum_{k=1}^{2} \frac{\delta_k}{\rho_k c_k^2} \right) \frac{\partial u}{\partial x} + \rho \, c_W^2 \, \frac{\alpha_1 \alpha_2}{\rho_1 c_1^2 \, \rho_2 c_2^2} \left(\sum_{k=1}^{2} \frac{\delta_k \Gamma_k}{\alpha_k} \, \mathbb{H}_k (T_I - T_k) \right) \\ + \frac{\rho \, c_W^2}{\rho_1 \rho_2} \left(\sum_{k=1}^{2} \frac{\alpha_k}{c_k^2} \right) \dot{m}_1 \, . \end{aligned} \tag{8.47}$$

Obviously, the first term of the RHS of each of the equations (8.41), (8.46) or (8.47), is similar. Two remaining terms in (8.41) and in (8.46) need additional interpretation, those are

- *the equivalent mass transfer term, which corresponds to the second term in the RHS of either (8.41) or (8.46),*
- *the equivalent heat transfer term, which corresponds to the third term in the RHS of either (8.41) or (8.46).*

Concerning the second term of the RHS of (8.41) or (8.46), it is similar to the third term in the RHS of (8.47), which represents the rate of volume fraction change in the presence of mass transfer and

$$\dot{m}_1 \equiv \rho \, \frac{\mathrm{D}Y_1}{\mathrm{D}t} = - \frac{\partial (\rho \, Y_1 Y_2 u_r)}{\partial x} \, .$$

Now if we compare the multiplying factor, we get that in each of these equations, that factor represents the inverse of an interfacial density. As a matter of fact, that factor which is identical in both the equations (8.41) and (8.46), can be rewritten under the following form :

$$\frac{\rho \, \mathcal{C}_W^2}{\rho_1 \rho_2} \left(\left(\frac{\rho_2 c_2^2 - \beta_2}{\rho_2 \mathcal{C}_2^2} \right) \frac{\alpha_1}{\mathcal{C}_1^2} + \left(\frac{\rho_1 c_1^2 - \beta_1}{\rho_1 \mathcal{C}_1^2} \right) \frac{\alpha_2}{\mathcal{C}_2^2} \right) \, ,$$

and has to be compared to

$$\frac{1}{\rho_I} = \frac{\rho\, c_W^2}{\rho_1 \rho_2} \left(\frac{\alpha_1}{c_1^2} + \frac{\alpha_2}{c_2^2} \right) .$$

As detailed in reference [33], in the context of phase transition modelling, the mechanical relaxation process that occurs during mass transfer is isentropic. Actually, mass transfer produces pressure fluctuations in each phase, provoking acoustic wave propagation responsible for pressure equilibration. Since those acoustic waves are isentropic, the corresponding volume fraction change is an isentropic process as well.
The third term of the RHS of either (8.41) :

$$\rho\, \mathcal{C}_W^2\, \frac{\alpha_1 \alpha_2}{\rho_1 \mathcal{C}_1^2\, \rho_2 \mathcal{C}_2^2} \left(\left(\frac{\Gamma_1}{\alpha_1} \left(-\rho\, Y_1 Y_2 u_r \right) T_1 \frac{\partial s_1}{\partial x} - \frac{\Gamma_2}{\alpha_2} \left(\rho\, Y_1 Y_2 u_r \right) T_2 \frac{\partial s_2}{\partial x} \right) \right) , \tag{8.48}$$

or (8.46) :

$$\begin{aligned} \rho\, \mathcal{C}_W^2\, \frac{\alpha_1 \alpha_2}{\rho_1 \mathcal{C}_1^2\, \rho_2 \mathcal{C}_2^2} \Bigg[& \frac{\Gamma_1}{\alpha_1} \left(-\rho\, Y_1 Y_2 u_r\, T_1 \frac{\partial s_1}{\partial x} + \frac{Z_2}{Z_1 + Z_2}\, \lambda'\, u_r^2 \right) \\ & - \frac{\Gamma_2}{\alpha_2} \left(\rho\, Y_1 Y_2 u_r\, T_2 \frac{\partial s_2}{\partial x} + \frac{Z_1}{Z_1 + Z_2}\, \lambda'\, u_r^2 \right) \Bigg] , \end{aligned} \tag{8.49}$$

has to be compared to the second term of the RHS of (8.47) :

$$\rho\, c_W^2\, \frac{\alpha_1 \alpha_2}{\rho_1 c_1^2\, \rho_2 c_2^2} \left(\frac{\Gamma_1}{\alpha_1}\, \mathbb{H}_1 (T_I - T_1) - \frac{\Gamma_2}{\alpha_2}\, \mathbb{H}_2 (T_I - T_2) \right) .$$

In the present context, the fluids are assumed to be inviscid and non heat conductive. Consequently, conventional heat exchanges are absent, but replaced by generalized heat fluxes as given above in (8.48) and (8.49). Terms in (8.48), that correspond to the heat transported by the relative motion and producing phase dilatation, also appear in (8.49) and are augmented by a phase friction term associated with each phase generalized heat flux. As for the mass transfer process, mechanical relaxation is also achieved by acoustic wave propagation. Therefore, that process is isentropic too.

8.6 Summary : a pressure equilibrium models with drift effects

We summarize hereafter the thermodynamically consistent pressure equilibrium model with drift effects

$$\left\{ \begin{array}{l} \dfrac{\mathrm{D}\alpha_1}{\mathrm{D}t} = \rho\, \mathcal{C}_W^2\, \dfrac{\alpha_1 \alpha_2}{\rho_1 \mathcal{C}_1^2\, \rho_2 \mathcal{C}_2^2}\, \mathcal{F} , \\ \dfrac{\partial (\alpha\, \rho)_k}{\partial t} + \dfrac{\partial \left((\alpha\, \rho)_k u \right)}{\partial x} + \delta_k \dfrac{\partial \left(\rho\, Y_1 Y_2 u_r \right)}{\partial x} = 0 , \qquad \forall\, k = 1\,,2 \qquad , \\ \dfrac{\partial (\rho\, u)}{\partial t} + \dfrac{\partial \left(\rho\, u^2 + P \right)}{\partial x} = 0 , \\ \dfrac{\partial (\rho E)}{\partial t} + \dfrac{\partial \left((\rho\, E + P)\, u \right)}{\partial x} + \dfrac{\partial \left(\rho\, Y_1 Y_2 u_r \mathcal{H}_r \right)}{\partial x} = 0 , \end{array} \right. \tag{8.50}$$

where

$$\left\{\begin{array}{l} u_r = \dfrac{1}{\lambda'}\left[(\alpha_1 - Y_1)\dfrac{\partial P}{\partial x} - \alpha_2 \dfrac{\partial(\alpha_1\beta_1)}{\partial x} + \alpha_1 \dfrac{\partial(\alpha_2\beta_2)}{\partial x}\right] , \\ E = \mathcal{E} + \dfrac{1}{2}u^2 , \qquad \mathcal{E} = e + B ; \\ e = \displaystyle\sum_k Y_k e_k , \qquad B = \sum_k Y_k B_k , \qquad P = \sum_k \alpha_k P_k , \end{array}\right. \tag{8.51}$$

and $\mathcal{F}$ is either defined by

$$\mathcal{F} = \left(\sum_{k=1}^{2} \delta_k(\beta_k - \rho_k c_k^2)\right)\frac{\partial u}{\partial x} + \left(\sum_{k=1}^{2} \frac{\rho_k c_k^2 - \beta_k}{\alpha_k \rho_k}\right)\rho\,\frac{\mathrm{D}Y_1}{\mathrm{D}t} - \sum_{k=1}^{2}\frac{\Gamma_k}{\alpha_k}\,\rho\, Y_1 Y_2 u_r T_k \frac{\partial s_k}{\partial x} ; \tag{8.52}$$

(see (8.41)), or by

$$\begin{aligned} \mathcal{F} = & \left(\sum_{k=1}^{2} \delta_k(\beta_k - \rho_k c_k^2)\right)\frac{\partial u}{\partial x} + \left(\sum_{k=1}^{2} \frac{\rho_k c_k^2 - \beta_k}{\alpha_k \rho_k}\right)\rho\,\frac{\mathrm{D}Y_1}{\mathrm{D}t} \\ & + \sum_{k=1}^{2}\frac{\Gamma_k}{\alpha_k}\left(-\rho\, Y_1 Y_2 u_r T_k \frac{\partial s_k}{\partial x} + \delta_k \frac{Z_{k'}}{Z_1 + Z_2}\lambda' u_r^2\right) ; \end{aligned} \tag{8.53}$$

see (8.46). Pressure equilibrium is expressed by

$$P = \pi + \sum_k \alpha_k \beta_k .$$

When stiffened gas EOS is assumed to be hold for each phase, the expression of the mixture (thermodynamic) pressure P or (generalized) pressure π can be easily obtained and is given by (2.31). System (8.50)–(8.51), with either (8.52) or (8.53), thus corresponds to the extension of the mechanical equilibrium model (2.26), in the limit of low velocity drift. It can also be considered as an extension of the Kapila et al. model (2001) model, [15], or as a reduction of the Baer and Nunziato (1986) model, [3], a modified version of which is (8.1). Compared to this last model (8.1), the present model (8.50)–(8.51) is free of interfacial variable (u_I or π_I), and free of pressure relaxation μ (or μ'). However, that new model is restricted to *low velocity drift*, around the mechanical equilibrium state.
The numerical method to solve this system is described in appendix C and is used in the following validation section.

9 Velocity drift effect validation

To validate the flow model (8.50)–(8.51), a basic experimental situation is considered, in which gas permeation through a dense granular bed plays a major role, in the presence of pressure waves.

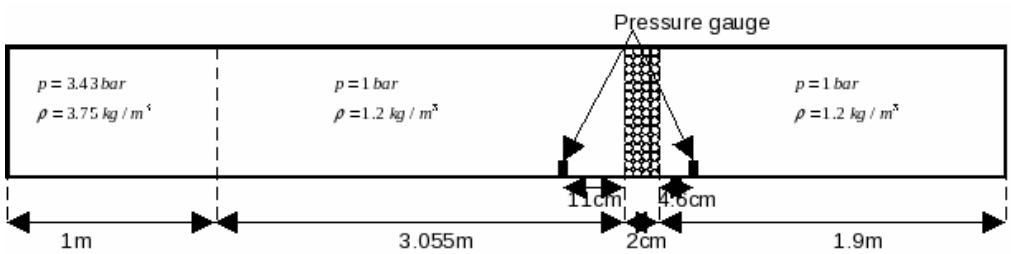

FIG. 9.1: *Experimental setup of shock induced particle fluidization facility (Rogue et al. (1998), [29]).*

Let us consider a vertical shock tube, filled with air ($\gamma_g = 1.4$). The initial configuaration is sketched in figure 9.1. In the high pressure chamber, the air pressure and density are initially set to

$$P_g = 3.43\,\mathrm{bar}\,, \qquad \rho_g = 3.75\,\mathrm{kg/m^3}\,.$$

The other chamber is filled with air at atmospheric pressure and with a density set to

$$\rho_g = 1.2\,\mathrm{kg/m^3}\,.$$

A membrane seperates the two chambers. In the low pressure chamber, a bed of small nylon solid particles is settled. Nylon particle density and volume fraction are set to

$$\rho_s = 1\,050\,\mathrm{kg/m^3}\,, \qquad \alpha_s = 0.65\,.$$

Stiffened gas EOS parameters for nylon are

$$\gamma_s = 4\,, \quad P_{s,\infty} = 600\,\mathrm{MPa}\,.$$

The granular EOS parameters are set to

$$a = 156\,\mathrm{kPa}\,, \qquad n = 1.02\,, \qquad \alpha_{s,0} = 0.65\,.$$

At the initial time, rupture of the membrane occurs and a supersonic shock wave propagates in the low pressure chamber, at Mach number 1.3 . Then, the shock interacts with the granular bed interface and a driffaction process appears. A weak shock is transmitted through the bed, while another shock is reflected. During the transmitted wave propagation, drag effects and pressure forces set the particle bed to motion. Gas permeation through the bed and drag effects produce shock weakening.
In order to examine gas permeation effects, two pressure gauges are settled : the first one at a distance of $11\,\mathrm{cm}$ before the particle bed, and the second one at a distance of $4.3\,\mathrm{cm}$ after the bed. The bed thickness is $2\,\mathrm{cm}$ (see figure 9.1). Corresponding experiments are reported in Rogue (1997) [28] and Rogue et al. (1998) [29].

The particles are modelled as compressible, with the EOS parameters given above. No irreversible compaction effect is considered here. The drag force coefficient is modelled by a simple formulation

$$\lambda = \frac{\lambda_0}{\epsilon} \,, \qquad \lambda_0 = \frac{1}{2}\,\frac{Z_1 Z_2}{Z_1 + Z_2} \,,$$

where λ_0 is the acoustic drag coefficient (see Saurel et al. (2003), [32]), and ϵ is a small positive parameter proportional to the inverse of the specific interfacial area ($\epsilon \simeq 1/A_I$). As for spherical particle beds the specific interfacial area A_I reads as

$$A_I = \frac{3\,\alpha_s}{r_p} \,,$$

where r_p is the radius of a particle, we use for the parameter ϵ an expression of the form

$$\epsilon = \frac{\epsilon_0}{\alpha_s} \,,$$

where, for the computations done in the present section

$$\epsilon_0 = 1.23\,10^{-2}\,\mathrm{m} \,.$$

In figure 9.2, the pressure evolution on the two gauges, in the case of no drift, is compared to experimental data records. Those experimental data records are depicted with thin lines and the numerical solution is drawn with thick lines. Many differences are clearly visible. When no drift is assumed, the transmitted shock is too weak while the reflected one is too strong.

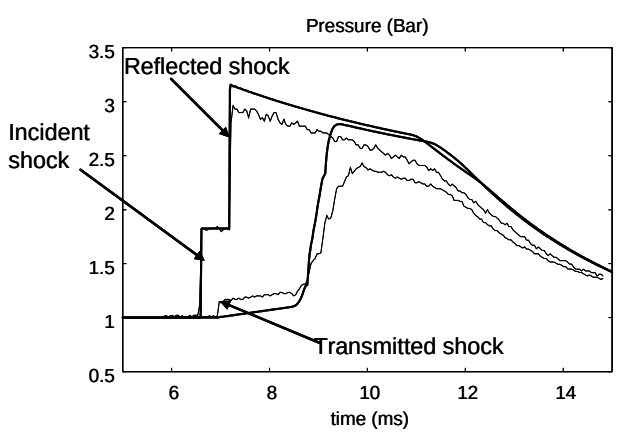

FIG. 9.2: *Comparison of recorded pressure signals (thin lines) with numerical computation results with the flow model (8.50)–(8.51), in the absence of velocity drift effects (thick lines). The reflected shock is too strong and the transmitted one is too weak.*

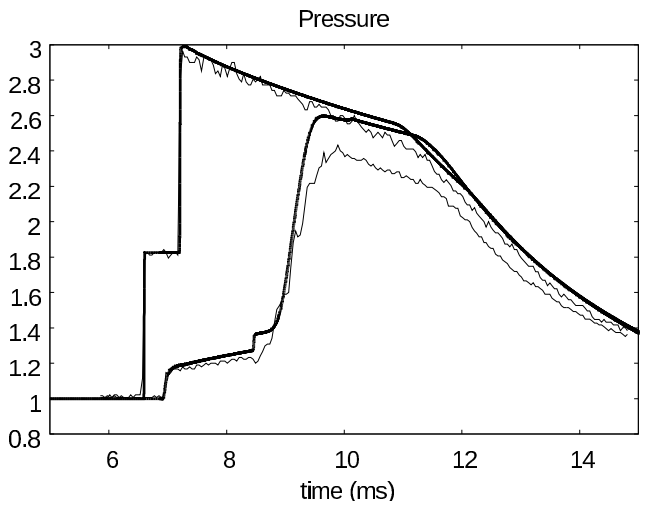

FIG. 9.3: *Comparison of recorded pressure signals (thin lines) with numerical computations with the flow model (8.50)–(8.51), when drift effects are accounted for. Both the reflected and transmitted shocks are of correct amplitude.*

In figure 9.3, the same comparison is made but now including drift effects. Computed results are reported with thick lines and compared with experimental data given with thin lines.

As shown in figure 9.3, both the reflected and transmitted waves have now the correct amplitude. It is only really at time $t = 9\,\mathrm{ms}$, that some differences appear. The level of the computed pressure on the second gauge is found to be higher than that got by experimentation. Those differences justly appear after the particle has passed by the second pressure gauge location. In figure 9.4, we give the time evolution of the volume fraction when drift effects are considered. When the particle bed has passed by the second gauge, ($t > 10\,\mathrm{ms}$), we should have got the same pressure level for both the gauges whereas they appear to be not equal on the experimental data records. Possible explanation might be due to some deviations of those two pressure gauges during the experiment.

10 Conclusion

A multiphase flow model for the irreversible compaction of powders has been built and validated. This resulting model is free of any adjustable parameter and is able to reproduce with fidelity loading–unloading cycles, as well as interface dynamics separating fluids and granular mixtures. Its numerical resolution has been achieved on the basis of simple extension of the method given in Saurel et al. (2009) [34]. Moreover, the model perfectly fits the frame of diffuse interface theory, used for

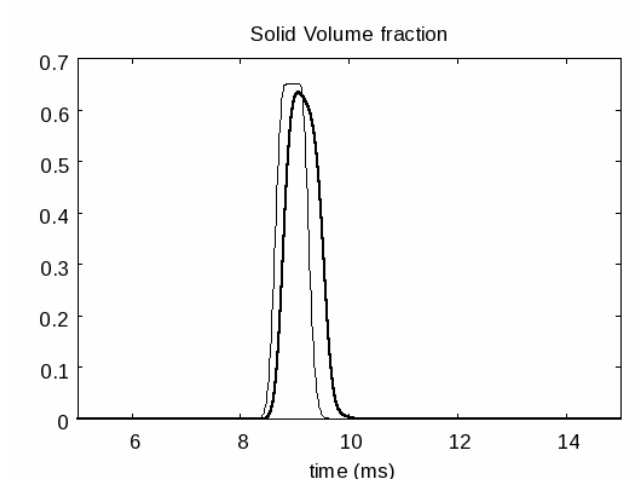

FIG. 9.4: *Time evolution of the volume fraction at the second gauge location. The solution in presence of drift is represented with thick lines and the solution without drift with thin lines. Drift effects make the particle bed slow down with more diffuse interfaces.*

different types of problems, ranging from material interfaces, cavitating flows [33], capillary fluids [25], to solid–fluid interfaces [8]. A lot of different types of physics may be introduced and inserted within this frame.

In this report, we have given another extension regarding gas permeation effects, resulting in a velocity non–equilibrium model. In this model, the only adjustable parameters are those related to the conventional drag force correlations. That corresponding model can also be considered as being a diffuse interface model with inter–penetration effects.

Acknowledgements

This work was partially supported by DGA-CEA Centre d'Études de Gramat. The authors are particularly grateful to Emmanuel Lapébie and Gérard Baudin.

Références

[1] R. Abgrall, *How to prevent pressure oscillations in multicomponent flow calculations : a quasi-conservative approach*, J. Comp. Phys., **125**, pp. 150–160, 1996.

[2] G. Alderborn and C. Nyström, *Pharmaceutical powder compaction technology*, Drugs and the Pharmaceutical Sciences, Marcel Dekker ed., New York, 1996.

[3] M.R. Baer, and J. W. Nunziato, *A two-phase mixture theory for the deflagration-to-detonation transition (DDT) in reactive granular materials*, Int. J. of Multiphase Flows, **12**, pp. 861-889, 1986.

[4] J.B. Bdzil, R. Menikoff, S.F. Son, A.K. Kapila and D.S. Stewart, *Two-phase modelling of DDT in granular materials : a critical examination of modelling issues*, Phys. Fluids, **11**, pp. 378–402, 1999.

[5] A. Chinnayya, E. Daniel and R. Saurel, *Modelling detonation waves in heterogeneous energetic materials*, Journal of Computational Physics, Vol. 196, 2, 2004.

[6] M. Duberg and C. Nyström, *Studies on direct compression of Tablets XVII. Porosity-pressure curves for the characterization of volume reduction mechanisms in powder compression*, Powder Technology, **46**, pp. 67-75, 1986.

[7] W.L. Elban and M.A. Chiarito, *Quasi-static compaction study of coarse HMX explosive*, Powder technology, **46**, (**2–3**), pp. 181–193, 1986.

[8] N. Favrie, S. Gavrilyuk and R. Saurel, *Diffuse solid–fluid interface model in cases of extreme deformations*, Journal of Computational Physics, **228**, **I. 16**, pp. 385–398, 2009.

[9] D.T. Gethin, D.V. Tran, A.K. Ariffin and R.W. Lewis, *An Investigation of Powder Compaction Processes*, Int. Journal of Powder Metallurgy, **30**, pp. 385–398, 1994.

[10] K.A. Gonthier, *Modelling and analysis of reactive compaction for granular energetic solids*, Combustion Science and Technology, **175**, (**9**), pp. 1679–1709.

[11] K.A. Gonthier, *Predictions for weak mechanical ignition of strain hardened granular explosive*, J. Applied Physics, **95**, (**7**), pp. 3482–3494.

[12] H. Guillard and F. Duval, *A Darcy law for the drift velocity in a two-phase flow model*, J. Comp. Phys., **224**, pp. 288–313, 2007.

[13] . Hermann, Constitutive equation for the dynamic compaction of ductile porous material, J. Applied Phys., **40**, pp. 2490–2499, 1969.

[14] V. Jogi, *Predictions for multi-scale shock heating of a granular energetic material*, Master thesis, Department of Science in Mechanical Engineering, Louisiana State University, December 2003.

[15] A.K. Kapila, R. Menikoff, J.B. Bdzil, S.F. Son and D.S. Stewart, *Two-phase modeling of deflagration to detonation transition in granular materials : Reduced equations*, Physics of Fluids, **13**, 10, pp. 3002–3024, 2001.

[16] S. Karni, *Multicomponent flow calculations by a consistent primitive algorithm*, Journal of Computational Physics, **112**, pp. 31–43, 1994.

[17] B. Khasainov, A. Borisov, B. Ermolaev, and A. Korotkov, *Two-phase visco-plastic model of shock initiation of detonation in high density pressed explosives*, Seventh International Symposium on Detonation, Naval Surface Weapons Center, Annapolis, pp. 435–447, 1981.

[18] K.K. Kuo, V. Yang and B.B. Moore, *Intergranular stress, particle-wall friction and speed of sound in granular propellant beds*, Journal of Balistics, **4**, pp. 697–730, 1980.

[19] O. Le Métayer, J. Massoni and R. Saurel, *Élaboration des lois d'état d'un liquide et de sa vapeur pour les modèles d'écoulements diphasiques*, Int. J. of Thermal Sciences, **43**, pp. 265–276, 2004 (in french).

[20] R.W. Lewis and A.R. Khoei, *A plasticity model for metal powder forming processes*, Int. J. of Plasticity, **17**, pp. 1659–1692, 2001.

[21] C.L. Martin, D. Bouvard and S. Shima, *Study of particle rearragement during powder compaction by the Dicrete Element Method*, J. of the Mechanics and Physics of Solids, **51**, (**4**), pp. 667–693, 2003.

[22] A. Murrone and H. Guillard, *A five equation reduced model for compressible two-phase flow computations*, J. Comput. Phys., **202**, 2, pp. 664–698, 2005.

[23] J. Oliver, S. Oller and J.C. Cante, *A plasticity model for simulation of industrial powder compaction processes*, Int. J. Solids Structures, **33**, pp. 3161–3178, 1996.

[24] S.L. Passman, J.W. Nunziato, E.K. Walsh, *A theory of multiphase mixtures*, in Rational Thermodynamics, C. Trusdell (ed.), Springer Verlag, 1984.

[25] G. Perigaud and R. Saurel, *A compressible flow model with capillary effects*, Journal of Computational Physics, **209**, pp. 139–178, 2005.

[26] F. Petitpas, R. saurel, E. Franquet and A. Chinnayya, *Modelling detonation waves in condensed materials : Multiphase CJ conditions and multidimensional computations*, Shock waves, **19**, **I. 5**, pp. 377–401, 2009.

[27] F. Petitpas, J. Massoni, R. Saurel, E. Lapebie and L. Munier, *Diffuse interface models for high speed cavitating underwater systems*, Int. J. Multiphase Flows, **35**, **I. 8**, pp. 747–759, 2009.

[28] X. Rogue, *Expériences et simulations d'écoulements diphasiques en tube à choc*, Ph.D. Thesis, Université de Provence, France, 1997.

[29] X. Rogue, G. Rodriguez, J.F. Haas and R. Saurel, *Experimental and numerical investigation of the shock-induced fluidization of a particle bed*, Shock Waves, **8**, pp. 29–45, 1998.

[30] H.W. Sandusky and T.P. Liddiard, *Dynamic compaction of porous beds*, Naval Surface Weapons Center, NSWC TR 83-246, 1985.

[31] R. Saurel and R. Abgrall, *A Multiphase Godunov method for compressible Multifluid and Multiphase flows*, J. Compu. Phys., **150**, (**2**), pp. 425–467, 1999.

[32] R. Saurel, S. Gavrilyuk and F. Renaud, *A multiphase model with internal degree of freedom : application to shock–bubble interaction*, Journal of Fluid Mechanics, **495**, pp. 283–321, 2003.

[33] R. Saurel, F. Petitpas and R. Abgrall, *Modeling phase transition in metastable liquids : application to cavitating ans flashing flows*, J. Fluid Mechanics, **607**, pp. 313–350, 2008.

[34] R. Saurel, F. Petitpas, and R.A. Berry, *Simple and efficient relaxation methods for interfaces separating compressible fluids, cavitating flows ans shocks in multiphase mixture*, J. Comp. Phys., **228**, pp. 1678–1712, 2009.

[35] R. Saurel, O. Le Métayer, J. Massoni and S. Gavrilyuk, *Shock jump relations for multiphase mixtures with stiff mechanical relaxation*, Int. J. Shock Waves, **16**, (3), pp. 209–232, 2007.

[36] A.B. Wood, *A textbook of sound*, G. Bell and Sons Ltd, London, 1930.

A Asymptotic limit of the pressure non-equilibrium model with stiff mechanical relaxation

Let us assume the pressure relaxation coefficient to be of the following form

$$\mu = \frac{\mu_0}{\epsilon} \text{ , with } \epsilon \to 0^+ \text{ .}$$

Each flow variable f is assumed to obey an asymptotic expansion

$$f = f^{(0)} + \epsilon\, f^{(1)} \text{ ,}$$

where $f^{(0)}$ and $f^{(1)}$ respectively represent the equilibrium state value and a small perturbated value around the equilibrium state of the flow variable f . We use the following notation
With these notations, the zero-order expansion of the volume fraction equation of the non equilibrium sytem (3.1)

$$\frac{\mathrm{D}\alpha_1}{\mathrm{D}t} = \mu\, \pi_r \text{ ,}$$

becomes

$$\frac{\mathrm{D}\alpha_1^{(0)}}{\mathrm{D}t} = \frac{\mu_0}{\epsilon}\, \pi_r^{(0)} + \mu_0\, \pi_r^{(1)} \text{ .}$$

This equation implies two new relations. The first one expresses evolution of the volume fraction at zero-order:

$$\frac{\mathrm{D}\alpha_1^{(0)}}{\mathrm{D}t} = \mu_0\, \pi_r^{(1)} \text{ ;} \tag{A1}$$

the second one expresses the evolution at ϵ^{-1} order:

$$\frac{\mu_0}{\epsilon}\, \pi_r^{(0)} = 0 \text{ ,}$$

which necessarily implies $\pi_r^{(0)} = 0$, i.e., the mechanical equilibrium condition is recovered:

$$\pi_1^{(0)} = \pi_2^{(0)} = \pi^{(0)} \text{ .} \tag{A2}$$

To define the RHS of the zero-order evolution equation of α_1 , it therefore remains to determine the pressure fluctuation difference π_r^1 . To do so, we need to express the evolution equations of the phase pressures π_k . This is done using the phase internal energy equations deduced from (3.1), since $\mathcal{E}_k = e_k + B_k$, which gives, after some calculations, the following evolution equation for the thermodynamic pressure P_k :

$$\frac{\mathrm{D}P_k}{\mathrm{D}t} + \rho_k c_k^2 \frac{\partial u}{\partial x} = \delta_k \left(-\frac{\rho_k c_k^2}{\alpha_k} + \delta_k \frac{\Gamma_k}{\alpha_k} \left(Y_{k'} + \frac{Z_{k'}}{Z_1 + Z_2} \right) \pi_r \right) \mu\, \pi_r \text{ ,} \tag{A3}$$

Now using (2.17) for defining β_k :

$$\beta_k = \alpha_k\, \rho_k\, \frac{\mathrm{d}B_k}{\mathrm{d}\alpha_k} \text{ ,}$$

and differentiating along the trajectory $\dfrac{\mathrm{d}x}{\mathrm{d}t} = u$ gives us

$$\frac{\mathrm{D}\beta_k}{\mathrm{D}t} = -\beta_k \frac{\partial u}{\partial x} + \delta_k \alpha_k \rho_k \frac{\mathrm{d}^2 B_k}{\mathrm{d}{\alpha_k}^2}\, \mu\, \pi_r \,. \tag{A4}$$

From (A3) and (A4), we easily derive the evolution equation for $\pi_k = P_k - \beta_k$:

$$\frac{\mathrm{D}\pi_k}{\mathrm{D}t} + (\rho_k c_k^2 - \beta_k)\, \frac{\partial u}{\partial x} = \delta_k \left(-\frac{\rho_k}{\alpha_k} \left(c_k^2 + \alpha_k^2 \frac{\mathrm{d}^2 B_k}{\mathrm{d}{\alpha_k}^2} \right) + \delta_k \frac{\Gamma_k}{\alpha_k} \left(Y_{k'} + \frac{Z_{k'}}{Z_1 + Z_2} \right) \pi_r \right) \mu\, \pi_r \,.$$

Denote

$$\mathcal{C}_k^2 = c_k^2 + \alpha_k^2 \frac{\mathrm{d}^2 B_k}{\mathrm{d}{\alpha_k}^2} \,,$$

then the evolution equation for π_k writes as :

$$\frac{\mathrm{D}\pi_k}{\mathrm{D}t} + (\rho_k c_k^2 - \beta_k)\, \frac{\partial u}{\partial x} = \delta_k \left(-\frac{\rho_k}{\alpha_k} \mathcal{C}_k^2 + \delta_k \frac{\Gamma_k}{\alpha_k} \left(Y_{k'} + \frac{Z_{k'}}{Z_1 + Z_2} \right) \pi_r \right) \mu\, \pi_r \,. \tag{A5}$$

Now looking at its zero-order expansion, using (A2), we get :

$$\frac{\mathrm{D}\pi_k^{(0)}}{\mathrm{D}t} + (\rho_k^{(0)}\, (c_k^{(0)})^2 - \beta_k^{(0)})\, \frac{\partial u^{(0)}}{\partial x} = \delta_k \left(-\frac{\rho_k^{(0)}}{\alpha_k^{(0)}} (\mathcal{C}_k^{(0)})^2 \right) \mu_0\, \pi_r^{(1)} \,.$$

Differentiation of (A2) finally leads us to the following relation :

$$\mu_0\, \pi_r^{(1)} = -\frac{\displaystyle\sum_{k=1}^{2} \delta_k \left(\rho_k^{(0)}\, (c_k^{(0)})^2 - \beta_k^{(0)} \right)}{\displaystyle\sum_{k=1}^{2} \frac{\rho_k^{(0)}\, (\mathcal{C}_k^{(0)})^2}{\alpha_k^{(0)}}}\, \frac{\partial u^{(0)}}{\partial x} \,.$$

The zero-order volume fraction equation is therefore expressed as

$$\frac{\mathrm{D}\alpha_1^{(0)}}{\mathrm{D}t} = -\frac{\displaystyle\sum_{k=1}^{2} \delta_k \left(\rho_k^{(0)}\, (c_k^{(0)})^2 - \beta_k^{(0)} \right)}{\displaystyle\sum_{k=1}^{2} \frac{\rho_k^{(0)}\, (\mathcal{C}_k^{(0)})^2}{\alpha_k^{(0)}}}\, \frac{\partial u^{(0)}}{\partial x} \,.$$

which is in perfect agreement with the first equation of the full equilibrium system (2.26). Note that (2.26) is also the zero-order expansion of the full non-equilibrium model (8.1), (8.5) in the limit of the one velocity, one pressure equilibrium condition :

$$\pi_1^{(0)} = \pi_2^{(0)} = \pi^{(0)} \,, \qquad u_1^{(0)} = u_2^{(0)} = u^{(0)} \,, \qquad u_1^{(1)} = u_2^{(1)} = u^{(1)} = 0 \,.$$

B Frozen and equilibrium mixture sound speed relations

Let us consider the full equilibrium (velocity and pressure) state of a granular mixture (index $k = 1$), with a gas (index $k = 2$). The mechanical equilibrium condition and the mixture pressure are respectively defined by the following relations :

$$\begin{cases} \pi_1 = P_1 - \rho\, Y_1 \dfrac{\mathrm{d}B_1}{\mathrm{d}\alpha_1} = \pi_2 = P_2 \ , \\ P = \rho^2 \dfrac{\partial e}{\partial \rho} = \displaystyle\sum_{k=1}^{2} \alpha_k P_k \ . \end{cases}$$

We aim to get the equilibrium mixture sound speed expression. Since full equilibrium is assumed, we have

$$\frac{\mathrm{D}s_k}{\mathrm{D}t} = 0 \ , \qquad \frac{\mathrm{D}Y_k}{\mathrm{D}t} = 0 \ ,$$

and therefore we have

$$\frac{\mathrm{D}P_k}{\mathrm{D}t} = c_k^2 \frac{\mathrm{D}\rho_k}{\mathrm{D}t} \ . \tag{B1}$$

Noticing that

$$\frac{\mathrm{D}\rho_k}{\mathrm{D}t} = -\frac{\rho\, Y_k}{\alpha_k^2} \frac{\mathrm{D}\alpha_k}{\mathrm{D}t} + \frac{Y_k}{\alpha_k} \frac{\mathrm{D}\rho}{\mathrm{D}t} \ ,$$

differentiation of the equilibrium condition leads us to the following expression

$$c_1^2 \left(-\frac{\rho\, Y_1}{\alpha_1^2} \frac{\mathrm{D}\alpha_1}{\mathrm{D}t} + \frac{Y_1}{\alpha_1} \frac{\mathrm{D}\rho}{\mathrm{D}t} \right) - \left(\rho\, Y_1 \frac{\mathrm{d}^2 B_1}{\mathrm{d}{\alpha_1}^2} \frac{\mathrm{D}\alpha_1}{\mathrm{D}t} + \frac{\beta_1}{\rho} \frac{\mathrm{D}\rho}{\mathrm{D}t} \right) = c_2^2 \left(-\frac{\rho\, Y_2}{\alpha_2^2} \frac{\mathrm{D}\alpha_2}{\mathrm{D}t} + \frac{Y_2}{\alpha_2} \frac{\mathrm{D}\rho}{\mathrm{D}t} \right) \ ,$$

so that (using $\alpha_1 + \alpha_2 = 1$)

$$\frac{\mathrm{D}\rho}{\mathrm{D}t} = \frac{1}{\rho} \left(\frac{\dfrac{Y_1 c_1^2}{\alpha_1} - \dfrac{Y_2 c_2^2}{\alpha_2} - \dfrac{\beta_1}{\rho}}{\dfrac{Y_1 c_1^2}{\alpha_1^2} + \dfrac{Y_2 c_2^2}{\alpha_2^2} + Y_1 \dfrac{\mathrm{d}^2 B_1}{\mathrm{d}{\alpha_1}^2}} \right) \frac{\mathrm{D}\alpha_1}{\mathrm{D}t} \ . \tag{B2}$$

Now if we differentiate the mixture pressure relation

$$\frac{\mathrm{D}P}{\mathrm{D}t} = P_r \frac{\mathrm{D}\alpha_1}{\mathrm{D}t} + \alpha_1 \frac{\mathrm{D}P_1}{\mathrm{D}t} + \alpha_2 \frac{\mathrm{D}P_2}{\mathrm{D}t} \ ,$$

and use (B2) and (B1), we get for P

$$\frac{\mathrm{D}P}{\mathrm{D}t} = \left(Y_1 c_1^2 + Y_2 c_2^2 - \frac{\left(\dfrac{P_r}{\rho} - \dfrac{Y_1 c_1^2}{\alpha_1} + \dfrac{Y_2 c_2^2}{\alpha_2} \right) \left(\dfrac{Y_1 c_1^2}{\alpha_1} - \dfrac{Y_2 c_2^2}{\alpha_2} - \dfrac{\beta_1}{\rho} \right)}{\dfrac{Y_1 c_1^2}{\alpha_1^2} + \dfrac{Y_2 c_2^2}{\alpha_2^2} + Y_1 \dfrac{\mathrm{d}^2 B_1}{\mathrm{d}{\alpha_1}^2}} \right) \frac{\mathrm{D}\rho}{\mathrm{D}t} \ .$$

But because of the mechanical equilibrium relation, we have

$$\beta_1 = P_r \ .$$

So finally, the above relation may be equivalently expressed by

$$\frac{\mathrm{D}P}{\mathrm{D}t} = c_W^2 \, \frac{\mathrm{D}\rho}{\mathrm{D}t} \ ,$$

where the equilibrium mixture sound speed is defined by

$$c_W^2 = c_f^2 - \frac{\left(\dfrac{Y_1 c_1^2}{\alpha_1} - \dfrac{Y_2 c_2^2}{\alpha_2} - \dfrac{\beta_1}{\rho} \right)^2}{\dfrac{Y_1 c_1^2}{\alpha_1^2} + \dfrac{Y_2 c_2^2}{\alpha_2^2} + Y_1 \dfrac{\mathrm{d}^2 B_1}{\mathrm{d}{\alpha_1}^2}} \ ,$$

with

$$c_f^2 = Y_1 c_1^2 + Y_2 c_2^2 \ ,$$

representing the frozen mixture speed of sound. Obviously :

$$c_f^2 > c_W^2 \ .$$

When only fluids are present, so in the absence of compaction effect, we recall that the conventional equilibrium mixture speed of sound, denoted by $c_{W,\mathrm{fluids}}$, is

$$c_{W,\mathrm{fluids}}^2 = \frac{\dfrac{Y_1 c_1^2 \, Y_2 c_2^2}{\alpha_1^2 \, \alpha_2^2}}{\dfrac{Y_1 c_1^2}{\alpha_1^2} + \dfrac{Y_2 c_2^2}{\alpha_2^2}} \ ,$$

or, equivalently written by

$$\frac{1}{c_{W,\mathrm{fluids}}^2} = \frac{\alpha_1^2}{Y_1 c_1^2} + \frac{\alpha_2^2}{Y_2 c_2^2} \ .$$

The difference between the (square of the) equilibrium mixture sound speed of Wood c_W^2 with granular effects, and the conventional one for fluid mixtures is

$$c_W^2 - c_{W,\mathrm{fluids}}^2 = \frac{1}{\rho} \left[\frac{(\rho_1 c_1^2 - \rho_2 c_2^2)^2}{\dfrac{\rho_1 c_1^2}{\alpha_1} + \dfrac{\rho_2 c_2^2}{\alpha_2}} - \frac{\left(\rho_1 c_1^2 - \rho_2 c_2^2 - \beta_1\right)^2}{\dfrac{\rho_1 c_1^2}{\alpha_1} + \dfrac{\rho_2 c_2^2}{\alpha_2} + \alpha_1 \rho_1 \dfrac{\mathrm{d}^2 B_1}{\mathrm{d}{\alpha_1}^2}} \right] \ .$$

Suppose now that

$$\rho_1 c_1^2 - \rho_2 c_2^2 > 0 \ , \qquad \rho_1 c_1^2 - \rho_2 c_2^2 - \beta_1 > 0 \ ; \tag{B3}$$

and that B_1 is monotone increasing and strictly convex w.r.t. α_1 :

$$\frac{\mathrm{d}B_1}{\mathrm{d}\alpha_1} > 0 \,, \qquad \frac{\mathrm{d}^2 B_1}{\mathrm{d}{\alpha_1}^2} > 0 \,. \tag{B4}$$

Note the inequalities (B3) are usually valid since the sound speed for the solid phase is dominant compared to the one related to the gas phase and the *configuration* sound speed. Inequalities (B4) are also verified with our definition of $B_1(\alpha_1)$. Consequently, we have

$$\begin{aligned} c_W^2 - c_{W,\text{fluids}}^2 &= \frac{\alpha_1\rho_1 \dfrac{\mathrm{d}^2 B_1}{\mathrm{d}{\alpha_1}^2}\left(\rho_1 c_1^2 - \rho_2 c_2^2 - \alpha_1\rho_1 \dfrac{\mathrm{d}B_1}{\mathrm{d}\alpha_1}\right)^2}{\rho\left(\dfrac{\rho_1 c_1^2}{\alpha_1} + \dfrac{\rho_2 c_2^2}{\alpha_2}\right)\left(\dfrac{\rho_1 c_1^2}{\alpha_1} + \dfrac{\rho_2 c_2^2}{\alpha_2} + \alpha_1\rho_1 \dfrac{\mathrm{d}^2 B_1}{\mathrm{d}{\alpha_1}^2}\right)} \\ &+ \frac{\alpha_1\rho_1 \dfrac{\mathrm{d}B_1}{\mathrm{d}\alpha_1}\left(\rho_1 c_1^2 - \rho_2 c_2^2 - \alpha_1\rho_1 \dfrac{\mathrm{d}B_1}{\mathrm{d}\alpha_1}\right)}{\rho\left(\dfrac{\rho_1 c_1^2}{\alpha_1} + \dfrac{\rho_2 c_2^2}{\alpha_2}\right)} \qquad > 0 \,. \end{aligned}$$

Therefore, the *granular* sound speed is always larger than the *conventional* one if (B3) holds and if $B_1(\alpha_1)$ is a monotone increasing and convex function of the variable α_1 .

C Numerical method to solve the equilibrium model with velocity drift terms

The system that has to be solved is the one defined by (8.50), with (8.51), and the RHS of the volume fraction equation defined by $\mathcal{F}$ as given either by (8.52), or by (8.53). $\mathcal{F}$ is rewritten under the following form

$$\mathcal{F} = \mathcal{F}_H + \mathcal{F}_D \,, \tag{C1}$$

with

$$\mathcal{F}_H = \left(\sum_{k=1}^{2} \delta_k(\beta_k - \rho_k c_k^2)\right) \frac{\partial u}{\partial x} \,, \tag{C2}$$

that term $\mathcal{F}_H$ will be used in the *hyperbolic* step. That step will be explained afterwards. The definition of the term $\mathcal{F}_D$ is

$$\mathcal{F}_D = \mathcal{F}_{D_1} + \mathcal{F}_{D_2} \,; \tag{C3}$$

that term will be used in the *drift* step. It is formed by two terms $\mathcal{F}_{D_1}$ and $\mathcal{F}_{D_2}$, where $\mathcal{F}_{D_2}$ is defined by

$$\mathcal{F}_{D_2} = \left(\sum_{k=1}^{2} \delta_k \frac{\Gamma_k}{\alpha_k} w_k\right) \lambda' \, u_r^2 \,. \tag{C4}$$

The definition of the factor term w_k depends on the definition of the evolution equation for α_1 (see subsection 8.4.4). When $\mathcal{F}$ is defined by (8.52), w_k is set as

$$w_k = \frac{\alpha_k}{\Gamma_k}\,\Gamma\ , \tag{C5}$$

with Γ is defined by (8.37). When $\mathcal{F}$ is defined by (8.53), w_k has the following formulation

$$w_k = \frac{Z_{k'}}{Z_1 + Z_2}\ . \tag{C6}$$

Note that when w_k is defined by (C5), $\mathcal{F}_{D_2} = 0$. At last, the term $\mathcal{F}_{D_1}$ is split into two terms

$$\mathcal{F}_{D_1} = \mathcal{F}_{D_1,1} + \mathcal{F}_{D_1,2}\ , \tag{C7}$$

with

$$\begin{aligned} \mathcal{F}_{D_1,1} &= \left(\sum_{k=1}^{2} \frac{\rho_k c_k^2 - \beta_k}{\alpha_k \rho_k}\right) \rho\,\frac{\mathrm{D}Y_1}{\mathrm{D}t}\ , \\ \mathcal{F}_{D_1,2} &= -\sum_{k=1}^{2} \frac{\Gamma_k}{\alpha_k}\,\rho\,Y_1 Y_2 u_r T_k \frac{\partial s_k}{\partial x}\ . \end{aligned} \tag{C8}$$

We recall that here,

$$\rho\,\frac{\mathrm{D}Y_1}{\mathrm{D}t} = -\frac{\partial}{\partial x}\left(\rho\,Y_1 Y_2 u_r\right)\ .$$

So the original system (8.50), with (8.51) is split into two subsystems :

- a *hyperbolic* subsystem,
- a *diffusive* subsystem.

The numerical method used to solve the original (unsplit) system therefore proceeds in three steps :

- a *hyperpolic* step, where the *hyperbolic* subsystem is solved;
- a *drift* step, where the *diffusive* subsystem is solved;
- a *reset–correction* step, where the predicted solution is corrected in such a way that the mixture total energy is preserved.

Each of these subsystems and steps is described in what follows.

C.1 Hyperbolic step

We aim to solve the following *hyperbolic* subsystem

$$\left\{\begin{array}{l} \dfrac{\mathrm{D}\alpha_1}{\mathrm{D}t} = \rho\,\mathcal{C}_W^2\,\dfrac{\alpha_1\alpha_2}{\rho_1\mathcal{C}_1^2\,\rho_2\mathcal{C}_2^2}\,\mathcal{F}_H\ , \\ \dfrac{\partial(\alpha\,\rho)_k}{\partial t} + \dfrac{\partial\left((\alpha\,\rho)_k u\right)}{\partial x} = 0\ ,\ k = 1\,,2\ , \\ \dfrac{\partial(\rho\,u)}{\partial t} + \dfrac{\partial\left(\rho\,u^2 + P\right)}{\partial x} = 0\ , \\ \dfrac{\partial(\rho\,E)}{\partial t} + \dfrac{\partial\left[(\rho\,E + P)\,u\right]}{\partial x} = 0\ , \end{array}\right. \tag{C9}$$

where

$$E = \mathcal{E} + \frac{1}{2}\,u^2\ , \quad \mathcal{E} = \sum_{k=1}^{2} Y_k \mathcal{E}_k\ , \quad \mathcal{E}_k = e_k + B_k\ , \quad P = \sum_{k=1}^{2} \alpha_k P_k\ , \tag{C10}$$

and $\mathcal{F}_H$ is defined by (C2). This subsystem is the one which has already been considered in section 5.

C.2 Velocity drift step

In this step, the aim is to solve the following (sub)system :

$$\left\{\begin{array}{l} \dfrac{\partial \alpha_1}{\partial t} = \rho\,\mathcal{C}_W^2\,\dfrac{\alpha_1\alpha_2}{\rho_1\mathcal{C}_1^2\,\rho_2\mathcal{C}_2^2}\,\mathcal{F}_D\ , \\ \dfrac{\partial(\alpha\,\rho)_k}{\partial t} + \delta_k \dfrac{\partial\,(\rho\,Y_1Y_2u_r)}{\partial x} = 0\ ,\ k = 1\,,2\ , \\ \dfrac{\partial(\rho\,u)}{\partial t} = 0\ , \\ \dfrac{\partial(\rho\,E)}{\partial t} + \dfrac{\partial\,(\rho\,Y_1Y_2u_r\mathcal{H}_r)}{\partial x} = 0\ ; \end{array}\right. \tag{C11}$$

where

$$E = \mathcal{E} + \frac{1}{2}\,u^2\ , \quad P = \sum_{k=1}^{2} \alpha_k P_k\ , \quad u_r = \frac{1}{\lambda'}\left((\alpha_1 - Y_1)\,\frac{\partial P}{\partial x} - \alpha_2\frac{\partial(\alpha\beta)_1}{\partial x} + \alpha_1\frac{\partial(\alpha\beta)_2}{\partial x}\right)\ ; \tag{C12}$$

and $\mathcal{F}_D$ is defined by relations (C3)–(C8). The two phase internal energy equations, directly derived from (8.36) can be considered too. They are ($k = 1\,,2$) :

$$\frac{\partial\,((\alpha\,\rho)_k e_k)}{\partial t} + \delta_k\left(\frac{\partial}{\partial x}\,(\rho\,Y_1Y_2u_re_k) + P_k\,\frac{\partial}{\partial x}\left(\frac{\rho\,Y_1Y_2u_r}{\rho_k}\right)\right) = -P_k\,\frac{\partial\alpha_k}{\partial t} + w_k\,\lambda'\,u_r^2\ , \tag{C13}$$

where w_k is defined by (C5) if $\mathcal{F}$ is defined by (8.52), and by (C6) if $\mathcal{F}$ is defined by (8.53).

The resolution method used to solve (C11) follows a three sub-step procedure which can be stated as :

1. DIFFUSION SUB-STEP :
   this sub-step is a solution prediction step where the various diffusion terms are considered, but where only a part of the volume fraction equation is solved :

   $$\frac{\partial\alpha_1}{\partial t} = \rho\,\mathcal{C}_W^2\,\frac{\alpha_1\alpha_2}{\rho_1\mathcal{C}_1^2\,\rho_2\mathcal{C}_2^2}\,\left(\mathcal{F}_{D_1,1} + \mathcal{F}_{D_2}\right)\ ,$$

   with $\mathcal{F}_{D_1,1}$ and $\mathcal{F}_{D_2}$ respectively defined by (C8) and (C4).
2. PRESSURE RELAXATION SUB-STEP :
   the remaining volume fraction equation terms in the RHS are addressed with a relaxation method.

3. RESET WITH CORRECTION SUB-STEP :
   in this sub-step, the updating is done by correcting the predicted solution in order to preserve the mixture total energy.

In the following, we describe sub-steps 1 and 2.

C.2.1 Diffusion sub-step

The sub-system considered during this step reads as

$$\left\{\begin{array}{l}
\dfrac{\partial \alpha_1}{\partial t} = \rho\, \mathcal{C}_W^2\, \dfrac{\alpha_1 \alpha_2}{\rho_1 \mathcal{C}_1^2\, \rho_2 \mathcal{C}_2^2}\, \left(\mathcal{F}_{D_1,1} + \mathcal{F}_{D_2}\right) \ , \\
\dfrac{\partial}{\partial t}\left((\alpha\rho)_k e_k\right) + \delta_k \left[\dfrac{\partial}{\partial x}\left(\rho\, Y_1 Y_2 u_r e_k\right) + P_k\, \dfrac{\partial}{\partial x}\left(\dfrac{\rho\, Y_1 Y_2 u_r}{\rho_k}\right)\right] = -\delta_k\, P_k\, \dfrac{\partial \alpha_1}{\partial t} + w_k\, u_r^2 \ , \ k = 1\,,2 \ , \\
\dfrac{\partial (\alpha\rho)_k}{\partial t} + \delta_k\, \dfrac{\partial}{\partial x}\left(\rho\, Y_1 Y_2 u_r\right) = 0 \ , \ k = 1\,,2 \ , \\
\dfrac{\partial (\rho\, u)}{\partial t} = 0 \ , \\
\dfrac{\partial (\rho\, E)}{\partial t} + \dfrac{\partial}{\partial x}\left(\rho\, Y_1 Y_2 u_r \mathcal{H}_r\right) = 0 \ ,
\end{array}\right.$$

with w_k defined by (C5)-(C6).

Mass equations

The following explicit scheme is used to solve the k-phase mass equation :

$$\frac{\partial (\alpha\rho)_k}{\partial t} + \delta_k\, \frac{\partial}{\partial x}\left(\rho\, Y_1 Y_2 u_r\right) \ .$$

Following the definition of u_r (C12), the mass flux $q = \rho Y_1 Y_2 u_r$ may be denoted by

$$q = q_1 + q_2 + q_3 \ ,$$

where, for $j = 1, 2, 3$:

$$q_j = \omega_j\, \frac{\partial p_j}{\partial x} \ ,$$

with

$$\left\{\begin{array}{ll}
p_1 = \pi \ , & \omega_1 = \dfrac{\rho\, Y_1 Y_2}{\lambda'}\left(\alpha_1 - Y_1\right) \ , \\[2ex]
p_2 = (\alpha\beta)_1 \ , & \omega_2 = -\dfrac{\rho\, Y_1 Y_2}{\lambda'}\, Y_2 \ , \\[2ex]
p_3 = (\alpha\beta)_2 \ , & \omega_3 = \dfrac{\rho\, Y_1 Y_2}{\lambda'}\, Y_1 \ .
\end{array}\right.$$

With these notations and definitions, the mass equation for phase k can be rewritten by

$$\frac{\partial(\alpha\rho)_k}{\partial t} + \delta_k \sum_{k=1}^{3} \frac{\partial q_m}{\partial x} = 0 \ .$$

Space and time integration of the mass equation is expressed by

$$(\alpha\rho)_{k,i}^{n+1} = (\alpha\rho)_{k,i}^{n} - \delta_k \frac{\Delta t}{\Delta x} \sum_{j=1}^{3} (q_{j,i+1/2}^{*} - q_{j,i-1/2}^{*}) \ , \tag{C14}$$

where the mass fluxes q_j^* ($j = 1, 2, 3$) remain to be determined at each cell boundary $i \pm 1/2$. To do so, we first use the continuity property of the mass fluxes at each cell boundary, i.e. ($l = i \pm 1/2$)

$$q_l^{*,-} = q_l^{*,+} = q_l^{*} \ .$$

Then, the diffusive character of the k-phase mass equation guarantees continuity of the generalized pressures p_j^* at each cell boundary $l = i \pm 1/2$:

$$p_{j,l}^{*,-} = p_{j,l}^{*,+} = p_{j,l}^{*} \ .$$

Expressed at the cell boundary $l = i - 1/2$, and using the notations $\omega_{j,L} = \omega_{j,i-1}$, $\omega_{j,R} = \omega_{j,i}$, we get, for $j = 1, 2, 3$:

$$\omega_{j,L} \left(p_j^* - p_{j,i-1}\right) = \omega_{j,R} \left(p_{j,i} - p_j^*\right) \ ,$$

and therefore we can define the $p_{j,l}^*$ for $l = i - 1/2$ and $j = 1,2,3$:

$$p_{j,l}^{*} = \frac{\omega_{j,L}\, p_{j,i-1} + \omega_{j,R}\, p_{j,i}}{\omega_{j,L} + \omega_{j,R}}.$$

The corresponding fluxes $q_{j,l}^*$ are consequently defined by the following relation

$$q_{j,l}^{*} = \frac{1}{2} \left[\omega_{j,L} \frac{p_{j,l}^{*} - p_{j,i-1}}{\Delta x/2} + \omega_{j,R} \frac{p_{j,i} - p_{j,l}^{*}}{\Delta x/2} \right] \ ,$$

which reduces to

$$q_{j,l}^{*} = \frac{2}{\Delta x} \frac{\omega_{j,L}\, \omega_{j,R}}{\omega_{j,L} + \omega_{j,R}} \left(p_{j,i} - p_{j,i-1}\right) \ .$$

Using (C14) with these definitions, the mass equations are updated for each phase $k = 1, 2$.

Energy equations

We recall that the energy equation to be considered for phase k reads as

$$\frac{\partial}{\partial t} \left((\alpha\rho)_k e_k\right) + \delta_k \left[\frac{\partial}{\partial x} \left(\rho\, Y_1 Y_2 u_r e_k\right) + P_k \frac{\partial}{\partial x} \left(\frac{\rho\, Y_1 Y_2 u_r}{\rho_k} \right) \right] = -P_k \frac{\partial \alpha_k}{\partial t} + w_k\, u_r^2 \ ,$$

where w_k is defined by (C5)–(C6). We recall that the phase entropy equation is written by

$$\frac{\partial s_k}{\partial t} + \delta_k \, \frac{\rho \, Y_1 Y_2 u_r}{(\alpha\rho)_k} \, \frac{\partial s_k}{\partial x} = \frac{1}{T_k} \, \frac{w_k}{(\alpha\rho)_k} \, \lambda' \, u_r^2 \, ,$$

which appears as a transport equation with a source term

$$\frac{\partial s_k}{\partial t} + v_k \, \frac{\partial s_k}{\partial x} = \mathcal{S}_k \, ,$$

where the *velocity* v_k is defined by (using definition of the mass flux q given previously):

$$v_k = \delta_k \frac{q}{(\alpha\rho)_k} \, ,$$

and the source term $\mathcal{S}_k$ defined by

$$\mathcal{S}_k = \frac{1}{T_k} \, \frac{w_k}{(\alpha\rho)_k} \, \lambda' \, \left(\frac{q}{\rho \, Y_1 Y_2} \right)^2 \, .$$

Since q can be determined at each cell boundary, the sign of v_k is determined too.
The following explicit scheme is used to update the solution of the transport equation of s_k

$$s_{k,i}^{n+1} = s_{k,i}^n - \frac{\Delta t}{\Delta x} \left(v_{k,i+1/2}^* \, s_{k,i+1/2}^* - v_{k,i-1/2}^* \, s_{k,i-1/2}^* \right) + \Delta t \, \mathcal{S}_{k,i}^n \, ,$$

where, for $l = i \pm 1/2$,

$$v_{k,l}^* = \delta_k \frac{q_{,l}^*}{(\alpha\rho)_{k,l}} \, , \qquad (\alpha\rho)_{k,l} = \frac{(\alpha\rho)_{k,l+1/2} + (\alpha\rho)_{k,l-1/2}}{2} \, ,$$

and

$$s_{k,l}^* = \begin{cases} s_{k,l-1/2} \quad , & \text{if } v_{k,l}^* \geq 0 \, , \\ s_{k,l+1/2} \quad , & \text{otherwise} \, . \end{cases} \tag{C15}$$

Therefore the phase entropies are known at each cell boundary $l = i \pm 1/2$.
At this stage, we know all cell boundary values of variables π^* , $(\alpha\beta)_k^*$, s_k^* , for $k = 1, 2$. It is now possible to determine the remaining values of variables ρ_k^* and P_k^* . When Stiffened Gas EOS is assumed to hold for each phase, we get the following relation

$$P_k + P_{k,\infty} = A_k \, \exp \left(\frac{s_k - s_{k,0}}{C_{V\,k}} \right) \, \rho_k^{\gamma_k} \, ,$$

where A_k , $s_{k,0}$ are non negative constants depending on phase k . We can therefore express ρ_k as

$$\rho_k = \left(\frac{P_k + P_{k,\infty}}{S_k} \right)^{1/\gamma_k} \, , \quad \text{with} \quad S_k = A_k \, \exp \left(\frac{s_k - s_{k,0}}{C_{V\,k}} \right) \, .$$

From (C15), we deduce that, at each cell boundary $l = i \pm 1/2$, and for $k = 1, 2$

$$\rho^*_{k,l} = \begin{cases} \rho_{k,l-1/2} \left(\dfrac{P^*_{k,l} + P_{k,\infty}}{P_{k,l-1/2} + P_{k,\infty}} \right)^{1/\gamma_k} & , \quad \text{if} \quad v^*_{k,l} \geq 0 \, , \\ \rho_{k,l+1/2} \left(\dfrac{P^*_{k,l} + P_{k,\infty}}{P_{k,l+1/2} + P_{k,\infty}} \right)^{1/\gamma_k} & , \quad \text{otherwise} \, . \end{cases} \tag{C16}$$

and, since

$$\pi_k = \pi^* = P^*_k - \frac{(\alpha\beta)^*_k}{\alpha^*_k} \, ,$$

we get, for all $k = 1, 2$

$$P^*_k = \pi^* + \frac{(\alpha\beta)^*_k}{\alpha^*_k} \, , \tag{C17}$$

and also

$$(\alpha\beta)^*_k = (\alpha^*_k)^2 \, \rho^*_k \frac{\mathrm{d}B_k}{\mathrm{d}\alpha_k}(\alpha^*_k) \, . \tag{C18}$$

Since π^* and $(\alpha\beta)^*_k$ are function of α^*_k only, so are the P^*_k 's: $P^*_k = P^*_k(\alpha^*_k)$. Inserted in (C16), the densities become also functions of the volume fraction: $\rho^*_k = \rho^*_k(\alpha^*_k)$. The volume fraction solution is the correct one if equation (C18) is satisfied. The Newton-Raphson method is used to solve system (C16)–(C18).
Once all cell boundary values have been defined for P_k and ρ_k , there is no difficulty to derive those remaining values of the thermodynamic variables $e^*_{k,l}$, and $h^*_{k,l}$, for $k = 1, 2$ and $l = i \pm 1/2$. The mixture total energy evolution equation is thus approximated by

$$(\rho\, E)^{n+1}_{,i} = (\rho\, E)^n_{,i} - \frac{\Delta t}{\Delta x} \left(q^*_{i+1/2} \, (h^*_{r,i+1/2} + B^*_{r,i+1/2}) - q^*_{i-1/2} \, (h^*_{r,i-1/2} + B^*_{r,i-1/2}) \right) \, ,$$

where $h_{r,l} = h_{1,l} - h_{2,l}$, $B_{r,l} = B_{1,l} - B_{2,l}$, for $l = i \pm 1/2$.
Note that the phase enternal energy equations contain extra terms that cannot be expressed under a conservative form, so their accurate integration is an issue. The same type of difficulty is also present during the hyperbolic step since the internal energy equations considered there contain also non-conservative terms. Since that step is a predicting step, the simplest approximation has been retained for these terms. That is the same strategy that has been adopted here, with the following simple approximation scheme, for all $k = 1, 2$, and all index cell i :

$$\begin{aligned} (\alpha\rho\, e)^{n+1}_{k,i} \quad &= (\alpha\rho\, e)^n_{k,i} - \delta_k \frac{\Delta t}{\Delta x} \left(q^*_{i+1/2} \, h^*_{k,i+1/2} - q^*_{i-1/2} \, h^*_{k,i-1/2} \right) \\ &+ \delta_k \frac{\Delta t}{\Delta x} \left(\frac{q}{\rho_k} \right)^n_i (P^*_{k,i+1/2} - P^*_{k,i-1/2}) \\ &- \delta_k \frac{\Delta t}{\Delta x} \left[\frac{\rho\, \mathcal{C}^2_W}{\rho_1 \mathcal{C}^2_1 \, \rho_2 \mathcal{C}^2_2} \, P_k \left(\sum_{m=1}^{2} \frac{\beta_m - \rho_m c^2_m}{(\alpha\rho)_m} \right) \right]^n_i (q^*_{i+1/2} - q^*_{i-1/2}) \\ &+ \Delta t \, \tilde{w}^n_{k,i} \, \lambda' \, (u^n_{r,i})^2 \, , \end{aligned}$$

where $\tilde{w}_k$ is defined by

$$\tilde{w}_k = w_k - \delta_k \frac{\rho\, \mathcal{C}_W^2}{\rho_1 \mathcal{C}_1^2\, \rho_2 \mathcal{C}_2^2}\, P_k\, \mathcal{F}_{D2}\ ,$$

with w_k defined by (C5) or (C6), and $\mathcal{F}_{D2}$ defined by (C4). For $u_{r,i}^n$ we use the following approximation

$$u_{r,i}^n = \frac{1}{\lambda_0}\left[(\alpha_{1,i}^n - Y_{1,i}^n)\, \frac{\pi_{i+1/2}^* - \pi_{i-1/2}^*}{\Delta x} + Y_{2,i}^n\, \frac{\alpha_{1,i+1/2}^*\, \beta_{1,i+1/2}^* - \alpha_{1,i-1/2}^*\, \beta_{1,i-1/2}^*}{\Delta x} \right.$$
$$\left. - Y_{1,i}^n\, \frac{\alpha_{2,i+1/2}^*\, \beta_{2,i+1/2}^* - \alpha_{2,i-1/2}^*\, \beta_{2,i-1/2}^*}{\Delta x} \right]$$

Stability criterion

The method is stable if the following stability criterion is fulfilled :

$$\Delta t \leq \frac{\Delta x^2}{\max\limits_i \left[\rho\, \mathcal{C}_W^2\, q \sum\limits_{m=1}^{2} \frac{\delta_m}{\rho_m}\, \frac{\beta_m - \rho_m c_m^2}{\rho_m \mathcal{C}_m^2} \right]_i}\ .$$

This criterion is deduced from the pressure evolution equation which reads as

$$\begin{aligned} \frac{\mathrm{D}\pi}{\mathrm{D}t} = \rho\, \mathcal{C}_W^2 \quad \Bigg\{ & \left(\sum_{k=1}^{2} \frac{\alpha_k}{\rho_k \mathcal{C}_k^2}\, \left(\beta_k - \rho_k c_k^2\right) \right) \frac{\partial u}{\partial x} \\ & + \left(\sum_{k=1}^{2} \frac{\delta_k}{\rho_k}\, \frac{\beta_k - \rho_k c_k^2}{\rho_k \mathcal{C}_k^2} \right) \frac{\partial}{\partial x}\, (\rho\, Y_1 Y_2 u_r) \\ & - \rho\, Y_1 Y_2 u_r \left(\sum_{k=1}^{2} \frac{\delta_k}{\rho_k \mathcal{C}_k^2}\, \Gamma_k T_k \frac{\partial s_k}{\partial x} \right) \\ & + \left(\sum_{k=1}^{2} \frac{\Gamma_k}{\rho_k \mathcal{C}_k^2}\, w_k \right) \lambda'\, u_r^2 \Bigg\} \end{aligned}$$

Note that when w_k is defined by (C5), the factor term of $\lambda'\, u_r^2$ reduces to Γ . During the diffusion step, only part of the volume fraction equation in (C11) has been considered. Consequently, constraints become out of equilibrium at the end of the diffusion step.

C.2.2 Pressure relaxation and reset/correction step

It now remains to solve the following system, under the constraint $\pi_1 = \pi_2$

$$\left\{ \begin{array}{l} \dfrac{\partial \alpha_1}{\partial t} = -\rho\, \mathcal{C}_W^2\, \dfrac{\alpha_1 \alpha_2}{\rho_1 \mathcal{C}_1^2\, \rho_2 \mathcal{C}_2^2}\, \rho\, Y_1 Y_2 u_r \left(\displaystyle\sum_{m=1}^{2} \dfrac{\Gamma_k}{\alpha_k}\, T_k\, \dfrac{\partial s_k}{\partial x} \right) , \\ \left\{ \begin{array}{l} (\alpha\rho)_k \dfrac{\partial e_k}{\partial t} = -\delta_k P_k \dfrac{\partial \alpha_1}{\partial t} , \\ \dfrac{\partial (\alpha\rho)_k}{\partial t} = 0 , \end{array} \right. \quad \text{for } k = 1{,}2 , \\ \dfrac{\partial (\rho\, u)}{\partial t} = 0 , \\ \dfrac{\partial (\rho\, E)}{\partial t} = 0 . \end{array} \right. \tag{C19}$$

Resolution of that system is done in a way similar to what has been done during the hyperbolic pressure relaxation step.

Table des matières

1 Introduction **4**

2 Mechanical equilibrium model **6**
2.1 Definitions of P and configuration pressures and energies . . . 8
2.2 Volume fraction equation . . . 10
2.3 Equilibrium model summary . . . 11
2.4 Acoustic properties . . . 12
2.5 Thermodynamic closure . . . 12

3 Non equilibrium model **13**
3.1 Energy conservation . . . 15
3.2 Entropy inequality . . . 15
3.3 Frozen model . . . 16
3.4 Limit system when $\mu \to +\infty$ . . . 17

4 Equations of state **17**
4.1 Thermodynamic equations of state . . . 18
4.2 Granular equation of state . . . 18

5 Numerical method **20**

6 Test problems and validations **24**
6.1 Compaction of a powder sample . . . 24
6.2 Wave and interface dynamics validation tests . . . 28
6.3 Two–dimensional example test . . . 31
6.4 Shock induced powder compaction test . . . 33

7 Relaxation parameter switch discussion **33**

8 A compaction model with velocity drift effects **37**
8.1 The full non-equilibrium model . . . 37
8.2 Supplementary important equations . . . 39
8.2.1 Equation for u_r . . . 39
8.2.2 Mixture equations . . . 39
8.2.3 Entropy equations . . . 41
8.2.4 Internal energy equations . . . 42
8.3 Asymptotic analysis . . . 42
8.4 Volume fraction and entropy equations . . . 44
8.4.1 Energy conservation constraint . . . 45
8.4.2 Mechanical equilibrium constraint . . . 46
8.4.3 Resolution of system (8.30)–(8.33), with definitions (8.32) and (8.34) . . . 47
8.4.4 Volume fraction evolution equation . . . 47

8.5 Some remarks 49
8.6 Summary : a pressure equilibrium models with drift effects 51

9 Velocity drift effect validation **52**

10 Conclusion **55**

A Asymptotic limit of the pressure non-equilibrium model with stiff mechanical relaxation **59**

B Frozen and equilibrium mixture sound speed relations **61**

C Numerical method to solve the equilibrium model with velocity drift terms **63**
C.1 Hyperbolic step 64
C.2 Velocity drift step 65
C.2.1 Diffusion sub-step 66
C.2.2 Pressure relaxation and reset/correction step 71

Unité de recherche INRIA Sophia Antipolis
2004, route des Lucioles - BP 93 - 06902 Sophia Antipolis Cedex (France)

Unité de recherche INRIA Futurs : Parc Club Orsay Université - ZAC des Vignes
4, rue Jacques Monod - 91893 ORSAY Cedex (France)
Unité de recherche INRIA Lorraine : LORIA, Technopôle de Nancy-Brabois - Campus scientifique
615, rue du Jardin Botanique - BP 101 - 54602 Villers-lès-Nancy Cedex (France)
Unité de recherche INRIA Rennes : IRISA, Campus universitaire de Beaulieu - 35042 Rennes Cedex (France)
Unité de recherche INRIA Rhône-Alpes : 655, avenue de l'Europe - 38334 Montbonnot Saint-Ismier (France)
Unité de recherche INRIA Rocquencourt : Domaine de Voluceau - Rocquencourt - BP 105 - 78153 Le Chesnay Cedex (France)

Éditeur
INRIA - Domaine de Voluceau - Rocquencourt, BP 105 - 78153 Le Chesnay Cedex (France)
http://www.inria.fr
ISSN 0249-6399